Diffusion of CO_2 in Fluids Relevant to Carbon Capture, Utilisation and Storage

Shane P. Cadogan

Supervised by:

Prof. J. P. Martin Trusler

Prof. G. C. Maitland

Imperial College London

Qatar Carbonates and Carbon Storage Research Centre

Submitted in partial fulfilment of the requirements for the degree of Doctorate of Philosophy

Abstract

In this work, molecular diffusion coefficients of carbon dioxide (CO_2) in liquids relevant to carbon capture, utilisation and sequestration and enhanced oil recovery are reported. These parameters are necessary for the accurate and optimal design and control of such processes. Knowledge of these values is required to fully describe the migration of CO_2 away from the injection wells and also for calculating the rate of absorption of CO_2 into the formation fluids. However, diffusion coefficients are amongst the least studied of thermophysical properties, especially at high pressure, high temperature conditions.

This work extended previous measurements where available, and produced new measurements where not, of diffusion coefficients at infinite dilution of CO_2 in H_2O, and several relevant brines and hydrocarbons at high temperatures (< 423 K) and high pressures (< 69 MPa). The Taylor dispersion method was used to determine diffusion coefficients for CO_2 in water and selected hydrocarbons. The hydrocarbons chosen as representative of major crude oil components were *n*-heptane, *n*-hexadecane, squalane, cyclohexane, and toluene. A technique based on nuclear magnetic resonance was used to measure effective diffusion coefficients of CO_2 in several brines, encompassing monovalent and divalent salts, and a mixed brine.

The diffusion coefficients of CO_2 in water were correlated using the Stokes-Einstein equation in which the Stokes-Einstein number was assigned a value of 4 and the hydrodynamic radius was treated as a linear function of temperature. No relationship between brine salinity and the hydrodynamic radius was found. The results indicated pressure did not have an observable impact on the diffusivity in aqueous systems. The experimental uncertainty was found to be 2.3% with a coverage factor of 2 for the CO_2-water system and 1.5% with a coverage factor of 2 for the CO_2-brine systems.

In contrast to aqueous systems, the diffusion coefficient of CO_2 in hydrocarbons was found to be strongly dependent on pressure. At a given temperature the diffusion coefficient decreased by up to 50% over the pressure range investigated (1 to 69 MPa). A correlation based on the Stokes-Einstein equation and a two-parameter correlation based on the rough hard sphere theory was used to model the experimental results. The experimental uncertainty was found to be 1.5% with a coverage factor of 2.

Acknowledgements

Firstly, I would like to thank and acknowledge Prof. J. P. Martin Trusler and Prof. Geoffrey C. Maitland for their time and critical oversight. It is redundant to say that any work of merit herein has arisen due to their attention to detail and technical insight.
I must also take time to thank Dr. Tina Secuianu for putting the main experimental rig together and introducing me to the equipment and Gavin Barnes for his help with mechanical modifications that were needed over the years.

I would also like to express my gratitude to my colleagues in ACEX424, Rayane, Claudio, Geraldine, Tine, and Hao for their companionship. I also owe a great deal to Mario, Naveed and Ivan, with who I have spent what feels like an eternity. The time spent outside the lab with these gentlemen has certainly made the time inside the lab more productive.

Finally, I must thank my parents, family, and Kwok Lai whose constant patience and reassurance were often an invaluable balance to all the little niggles that arose during this process.

I gratefully acknowledge funding from the Qatar Carbonates and Carbon Storage Research Centre (QCCSRC), provided jointly by Qatar Petroleum, Shell, and Qatar Science & Technology Park.

Contents

Table of Figures

1. Introduction

Diffusion is a transport process relevant to many fields in the natural sciences and engineering. It can be the main transport process in systems where mixing is low or absent. It is due to its small magnitude, e.g. relative to advection over length scales of fractions of centimetres, that diffusion is often the rate-determining step in many processes. It is also an important parameter in predicting the rate of absorption of a solute into a solvent. Industrial instances where diffusion is relevant include, but are not limited to, biotechnology, distillation, solvent-solvent extraction, heterogeneous catalysis, and membrane based processes. The sequestration of carbon dioxide, CO_2, in saline aquifers and depleted oil and gas reservoirs is another example of where accurate values of the diffusion coefficient are valuable.

The dispersion of CO_2, in saturated heterogeneous porous media, such as saline aquifers, can be described as a function of the Peclet number [1]. The Peclet number is defined as the ratio of advection, $L \cdot v$, to the diffusion coefficient, D, where L is a characteristic length and v is the appropriate average velocity [2]. For flow in a capillary of radius R, the Peclet number, Pe, = $2Rv/D$ and v is the linear flow velocity averaged over the cross-section of the capillary. Diffusion is the dominant mechanism of dispersion in porous media when $Pe \leq 5$, and is significant up to $Pe \approx 300$ [3], which corresponds to fluid velocities on the order of $cm \cdot s^{-1}$ in micro-porous media with pore radius R of order 10^{-6} m and D of order 10^{-9} $m^2 \cdot s^{-1}$. Along with strongly influencing the transport of CO_2 in the heterogeneous media in which it may be sequestered, at low Peclet numbers [3-7], the rate of diffusion of CO_2 in the reservoir fluids will also impact the rate at which the plume of injected supercritical CO_2 will dissolve into these fluids [8]. The storage security of CO_2 is far greater after the gas has been dissolved in these fluids, due to both buoyancy and mineralisation effects [9]. However, despite its relevance, diffusion and diffusion coefficients are amongst the least studied thermophysical properties.

Industrial Instance of the Requirement for Accurate Diffusion Coefficients

According to the International Energy Agency (IEA) the combustion of fossil-fuel based hydrocarbons produces 80% of the world's energy (see Figure 1-1) and approximately 31.6 Gt of carbon dioxide (CO_2) per year in the process. This amounts to 42% of the annual anthropogenic release of this gas. This use of fossil fuel for energy production produces 86% more CO_2 than the next largest contributor, transport.

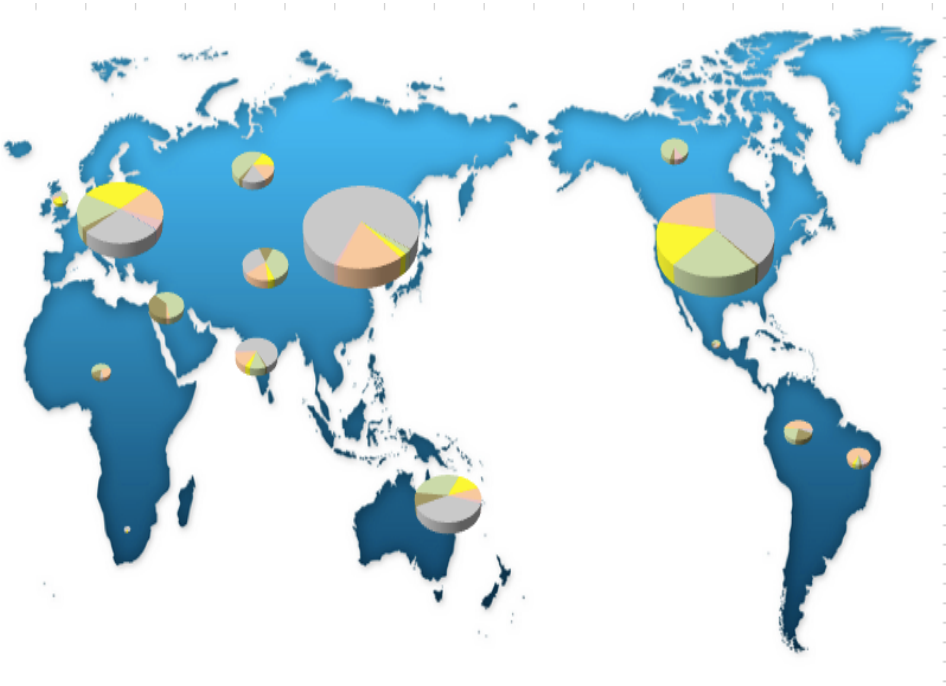

Figure 1-1. Global electricity production by source.
Sources considered were; grey, coal and peat; brown, oil; green, gas; yellow, nuclear; orange, renewables; pink, biofuel and waste; and blue, other. The area of the pie-charts show the relative amount of electricity produced; normalised to the amount of electricity produced by the USA (4.85 million GWh).
The collated data [10] was arbitrarily associated to geographic region [11].

The contribution of fossil fuels to the global energy portfolio is likely to continue increasing past the year 2030 [12]. It has been proposed that the CO_2 emitted in fossil fuel combustion has the potential to alter the delicate composition of chemicals that compose the earth's atmosphere. This may have detrimental effects to climate patterns. This theory of "man-made climate change" is now widely accepted among academics, policy makers and society in general.

There are many studies and techniques which have been proposed to mitigate this effect. The Princeton CO_2 stabilisation wedges propose a collection of approaches to

reduce CO_2 emissions [13]. These techniques range from decarbonisation of fuels and electricity to increased energy efficiency and conservation. While non-fossil fuel based sources of energy, such as solar power and nuclear fission, are attractive long-term alternatives, fossil fuels are undoubtedly set to remain a large contributor to the energy landscape for the foreseeable future [12]. Due to the infrastructure currently in place to consume fossil fuels for energy production and the intermittent nature of many renewable energy sources, carbon capture, utilisation and sequestration (CCUS) is an attractive short to medium term solution to the problem posed. It is possible that as much as 35% of the required reduction in anthropogenic emissions of CO_2 could be provided by the capture and sequestration of CO_2 in subsurface formations. Carbon dioxide can be most efficiently captured from high density sources, e.g. coal or gas fuelled power plants, steel manufacture plants, cement manufacture plants, etc. There is a large body of work available discussing the various ways in which CO_2 can be captured and the interested reader is directed to the following sources [14-26].

Among the carbon sinks being considered are depleted oil and gas fields, unminable coal seams, and saline aquifers, thought to have the world's largest capacity. Of special interest are the latter, in particular carbonate formations. Carbonate reservoirs differ from sandstone reservoirs due to the presence of chemical interactions between CO_2-enriched reservoir fluids and minerals composing the formation. Another issue with the saline aquifers primarily under investigation is that, unlike depleted oil and gas reservoirs, these systems are not proven geological and geochemical traps and their injectivity is not as well characterised as their hydrocarbon counterparts. It is for this reason that there is a large body of research being carried out on both the geophysical and chemical behaviour in these formations.

From the time at which the injected species and the reservoir fluids are in intimate contact, the CO_2 will dissolve into the reservoir fluids. The less dense super-critical CO_2 ($scCO_2$) will migrate upwards towards the geological barrier [27]. It has been stated that it is only at this point that the CO_2 can be thought of as being sequestered [28]. The (CO_2 + brine) solution is known to be denser than the brine [29] and sink in the reservoir. Hence the risk of buoyant migration and escape would be reduced. This results in an increased theoretical capacity in the formation [30]. This dissolution process can be thought of as acting in the presence of three resistances. When two immiscible phases are in contact an interface is formed. On either side of this interface is a stagnant boundary layer in which convective flow is essentially

negligible, providing two of the mentioned resistances. CO_2 must transverse these stagnant layers on both sides of the interface. The third resistance to dissolution is at the interface, however, it is often assumed that the interface is at all times saturated with the gas being absorbed. This assumption of instant equilibrium across the interface is usually sufficient when long contact times are realized [31].

The two-film theory [32] is often used for calculating the rate of absorption of gases in liquids and the constant of proportionality for this rate law is written as:

$$\frac{1}{k_{OG}} = \frac{1}{k_G} + \frac{K}{k_L} \tag{1-1}$$

Here, k_{OG} is the overall mass transfer coefficient, k_G and k_L are the mass transfer coefficient associated with the gaseous and liquid side, respectively. The equilibrium relationship at the interface, K, i.e. the solubility of the solute in phase L, is given by the ratio of the mole fraction of the solute in the gas phase, y, to the mole fraction of the solute in the liquid phase x. In the case of ideal vapour liquid systems, Henry's constant, H, divided by the pressure, p, is often used for K.

This model is based on Fick's first law assuming equimolar counter-current diffusion and the mass transfer coefficients have the form:

$$k_G = {D^* p}/{RT\delta_G} \tag{1-2}$$

$$k_L = {D}/{v\delta_L} \tag{1-3}$$

In the above equations p, R and T have their standard meaning, v is molar volume of the liquid and δ_G and δ_L represent the width of these stagnant layers at the interface. The asterisk on D represents the diffusion coefficient of the solute in the gas phase. This value is typically several orders of magnitude higher than that of the liquid phase. The rate at which adsorption occurs is directly related to the rate at which CO_2 moves from the interface into the bulk of the brine liquid, which is governed by diffusion.

The resulting diffusion induced convective flow, resulting from the increased CO_2 saturated reservoir fluid density, ensures a large concentration gradient between the supercritical plume and reservoir fluids [33]. Once the injection of CO_2 has been completed "secondary" transport processes are likely to become dominant. After this, diffusion is likely to be the sole driving force in the movement of the CO_2 plume and dissolved CO_2 solution.

The ultimate fate of the trapped CO_2 is often considered to be reaction with salts to form carbonates [34]. Depending on the specific conditions present in the reservoir the speed at which this reaction takes place may be determined by the chemical reaction or by the rate at which the reactants diffuse to the substrate mineral.

Enhanced oil recovery (EOR) is also a promising partner for CCUS. As readily accessible conventional sources become scarcer, new technologies have emerged to increase the amount of hydrocarbons produced from a given formation [35, 36]. The addition of an agent such as CO_2 or natural gas, which is miscible with the hydrocarbons fluids (e.g. heavy oil) reduces the viscosity of these fluids and in turn increases production capability [36]. The rate at which the viscosity changes is once again determined by the rate at which CO_2 dissolves into the reservoir contents. High displacement efficiencies are possible when there is sufficient time for diffusion to swell the oil sufficiently [37]. The implementation of EOR is becoming more common, and, as shown in Figure 1-2, the use of gas injection based processes is gaining popularity.

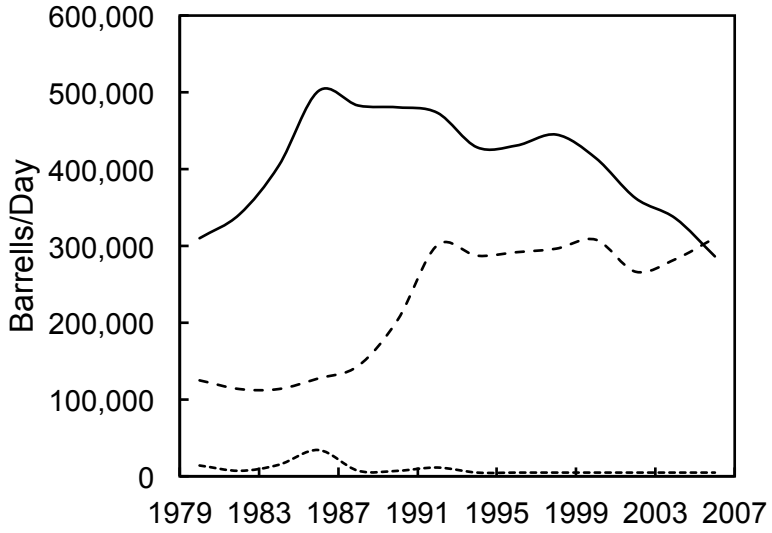

Figure 1-2. Historical production of oil from various enhanced recovery processes; ·····, chemical; - - - - gas and ——, thermal based EOR processes [35].

Introduction to Diffusion and Diffusion Coefficients

The Diffusion Process

Due it's inherent kinetic energy, a molecule in a volume, *V*, will continuously be in motion in a random manner. That is with respect to a fixed point within the volume, the location of the molecule will change over time. Statistically, a molecule will be equally probable to move in any direction, however, if a fraction of the molecules in a system move to an area of low concentration, a proportionally lower amount will transfer back to a volume of higher concentration. As the duration of this process increases the molecules will become increasingly homogeneously spread out through *V* (see Figure 1-3). This can be observed by the movement of a solute in solution from a volume of high concentration to low concentration, although this "random walk" rationale behind this observation is subtle.

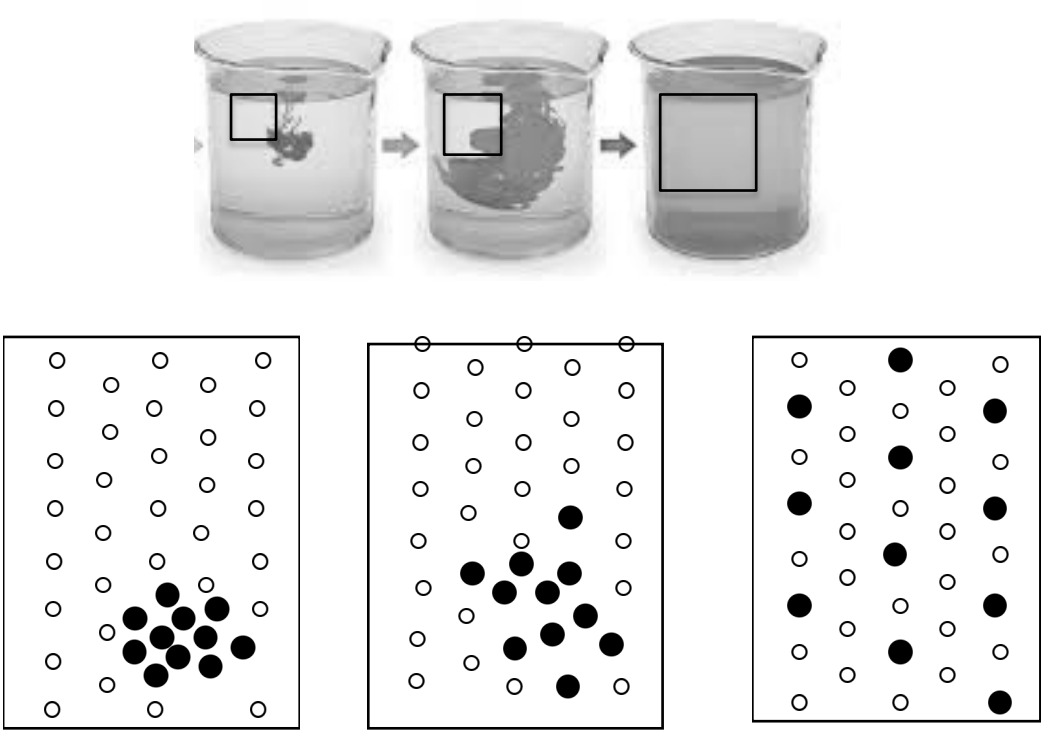

Figure 1-3. Diffusion of a few drops of black ink placed at the bottom of a tall beaker of water. The process progresses in time from left to right.

On a macroscopic scale, this observation that the flux of a component is proportional to its concentration gradient, defines the common description of diffusion. The constant of proportionality is called the diffusion coefficient, or diffusivity, the most commonly used of these being the phenomenological Fickian diffusion coefficient, *D*. The other widely used form of diffusion coefficient, primarily used in computational

predictions of diffusivity, is the Maxwell-Stefan, M-S, diffusion coefficient, D^{MS}. As opposed to the Fickian description of diffusion in which the concentration gradient is the driving force, chemical potential is the driving force in the M-S description. In the M-S approach the chemical potential gradient of component *i* is balanced by a friction force [38].

$$-\frac{1}{RT}\nabla\mu_i = \sum_{j=1, j\neq i}^{n} \frac{x_j\left(u_i - u_j\right)}{D_{ij}^{MS}} \tag{1-4}$$

Here R and T are the gas constant and absolute temperature, μ_i is the chemical potential of component *i* the numerator inside the summation denote the average velocities of component *i* and *j* times the mole fraction of *j* present. The M-S diffusion coefficient then describes the magnitude of the friction between *i* and *j*. For binary systems the Fickian diffusion coefficient is the product of the M-S diffusion coefficient and the activity coefficient, while for multicomponent systems the matrix of diffusion coefficients, discusses later in this chapter, can usually be interconverted by use of thermodynamic relations based on the components' fugacity coefficients [39]. Some other differences between these two formalisms will be mentioned throughout this section.

Unlike M-S diffusion coefficients, which are independent of any frame of reference, great care must be taken to select the correct frame of reference in diffusion studies when Fickian diffusion coefficients are used. Some common frames of reference include those moving with the local centre of mass, the local centre of volume and the local velocity of the solvent (or of any single component) [40-42]. Choosing the frame of reference in which the macroscopic flux is negligible is recommended [43]. In a binary system a single diffusion coefficient can fully describe the convection-free mass transfer in the system.

Binary Diffusion Coefficients

In the case of a single solute species diffusing in a single solvent species, Fick's first phenomenological law of diffusion asserts:

$$\begin{aligned} \mathbf{j}_A &= -D_{AB}\nabla c_A \\ \mathbf{j}_A + \mathbf{j}_B &= 0 \end{aligned} \tag{1-5}$$

Here, $\mathbf{j}_A$ is the molar flux vector of solute A having concentration c_A. The constant of proportionality, D_{AB}, is the diffusion coefficient.

Fick's second phenomenological law, which relates the concentration of the solute to the time passed, *t*, is:

$$\frac{dc_A}{dt} = -D_{AB}\nabla^2 c_A \qquad (1\text{-}6)$$

Except for the case of simple problems, the solution of this partial differential equation may require involved mathematical treatment [44].

Over the range of temperatures and pressures usually encountered, values in the order of 10^{-5} $m^2 \cdot s^{-1}$ and 10^{-9} $m^2 \cdot s^{-1}$ are typical for diffusion in gases and liquids, respectively [43].

The Effect of Solute Concentration on Diffusion

While Maxwell-Stefan diffusion coefficients are independent of concentration, Figure 1-4 to Figure 1-6 show the limitation of treating the Fickian diffusion coefficient, which is implicitly a function of temperature, pressure and composition, as independent of temperature and concentration. Two liquid-liquid systems and a gas-liquid system have been taken as examples.

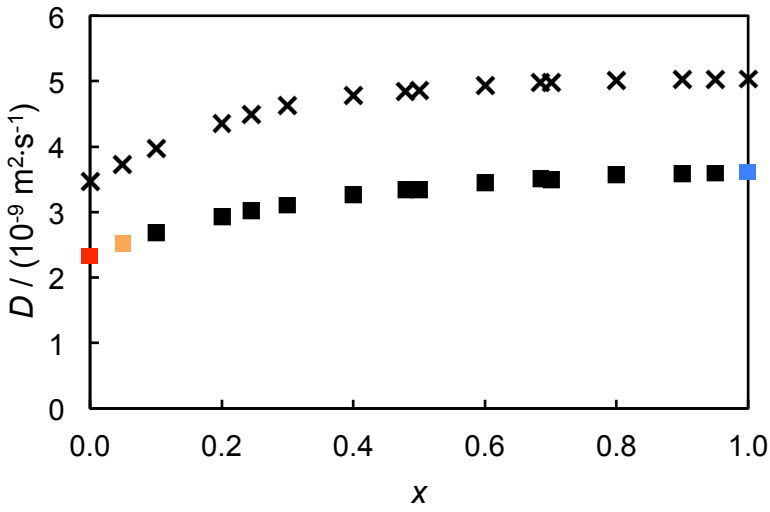

Figure 1-4. Diffusion coefficients of acetone in chloroform plotted against the mole fraction of acetone present [45].
The mutual diffusion coefficients are shown at; ■, T = 313.15 K and ×, T = 358.15 K.
Highlighted are the; ■, infinite dilution diffusion coefficient of acetone in chloroform; ■, the upper limit of the tracer diffusion coefficient of acetone in chloroform and ■, the self diffusion coefficient of acetone in chloroform (all measured at T = 313.15 K).

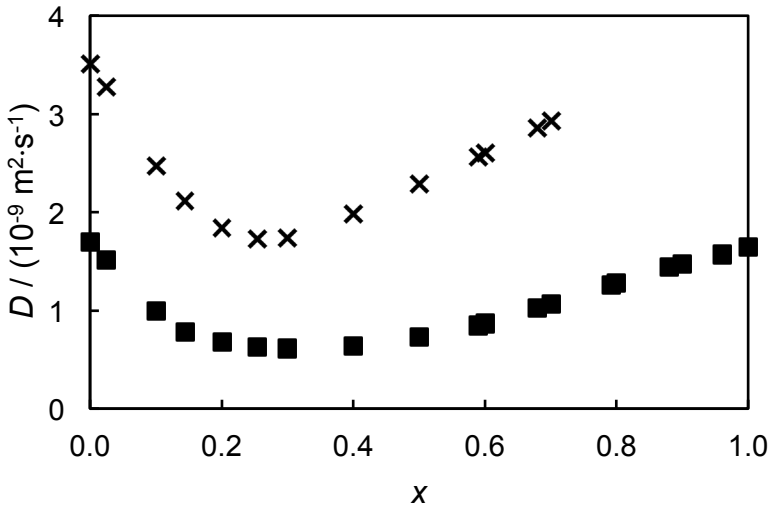

Figure 1-5. The diffusion coefficients of ethanol in water: ■, T =298.15 K, and ×, T = 328.15 K, are plotted against the mole fraction of chloroform present [45].

In Figure 1-5, the value of D decreases to a minimum when the mole fraction of ethanol present is approximately 25%. It is also noted that at T = 313.15 K, the diffusivity of infinitely dilute ethanol in water is only 3.6% higher than the diffusivity of infinitely dilute water in ethanol.

In contrast to the (ethanol + water) system, the (acetone + chloroform) system (Figure 1-4) has no saddle point. It quickly reaches a relatively constant value at about 40% mole acetone. Also unlike the (ethanol + water) system the diffusion coefficient increases by 55% from infinitely dilute acetone to infinitely dilute chloroform at T = 298.15 K.

The behaviour of the (CO_2 + heptane) gas-liquid system (Figure 1-6) is qualitatively similar to the (ethanol + water) system. As in the liquid-liquid system, a minimum D is observed and in the case of the (CO_2 + heptane) mixture this value is observed at close to a CO_2 mole fraction of approximately 0.8. The diffusion coefficient is reduced by as much as 33%.

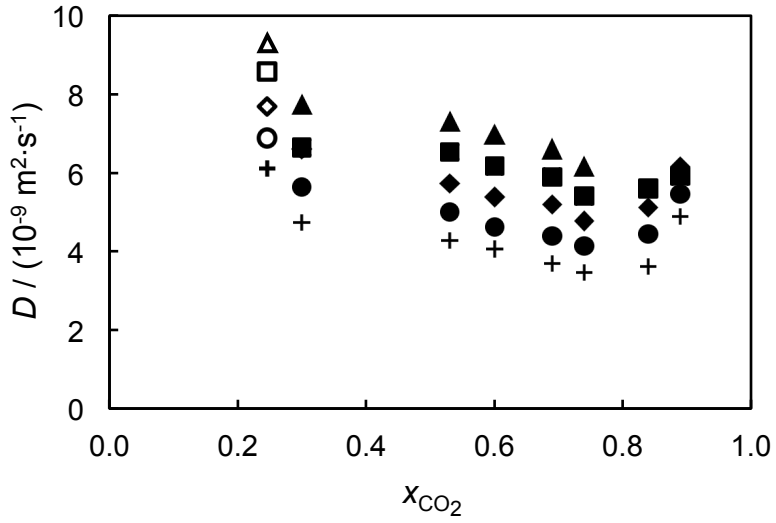

Figure 1-6. Diffusivity of CO_2 in heptane plotted as a function of the mole fraction of CO_2 present.
The results obtained were at: +, T = 283.15 K; ○, T = 293.15 K; ◇, T = 303.15 K; □, T = 313.15 K; △, T = 323.15 K.
Hollow symbols are based on [46] and the filled symbols [47].

In many scientific and engineering applications, it is common to make the assumption that the solute diffusing in a system is present only in low quantities. The expression *diffusion at infinite dilution* is used interchangeably with *tracer diffusion* and *limiting diffusion*. There are several benefits to and reasons behind this simplification. The diffusion coefficient required is often the diffusivity at infinite dilution, it is the most widely reported value, and the treatment of the model in question is simplified as there is no need to have a functional dependency of the diffusivity on the concentration of the solute.

In fact, many engineering applications where diffusivity is important are based on systems where the solute is only sparingly soluble. An example would be the removal of a contaminant from a stream where this species is present only in low amounts. In the case of CO_2 in water, the solute may be only slightly soluble in the solvent, e.g. at T = 293 K and p = 67 MPa CO_2 is only soluble in water at 3.7% on a molar basis. The solubility of CO_2 in brines is even lower due to the salting out effect [48].

Based on this, the diffusion coefficients of CO_2 at infinite dilution produced in this work were taken to be sufficient to describe the (CO_2 + H_2O) and (CO_2 + brine) systems at any temperature between (298 and 423) K. Tracer diffusion coefficients of CO_2 in hydrocarbons were also deemed sufficient for the scope of this work.

The Effect of Temperature on Diffusivity

Following the same line that has been previously discussed, the temperature effect can be observed in Figure 1-5 and Figure 1-6. Diffusivity increases with temperature. Figure 1-7 shows the available literature data available for the (CO_2 + H_2O) system. This system is of specific interest in the scope of this current work. Data above temperatures of 340 K are scarcer and more scattered. Only one source has investigated the effect of pressure on this parameter [49]. All sources treated the diffusion coefficient as the infinitely dilute diffusion coefficient.

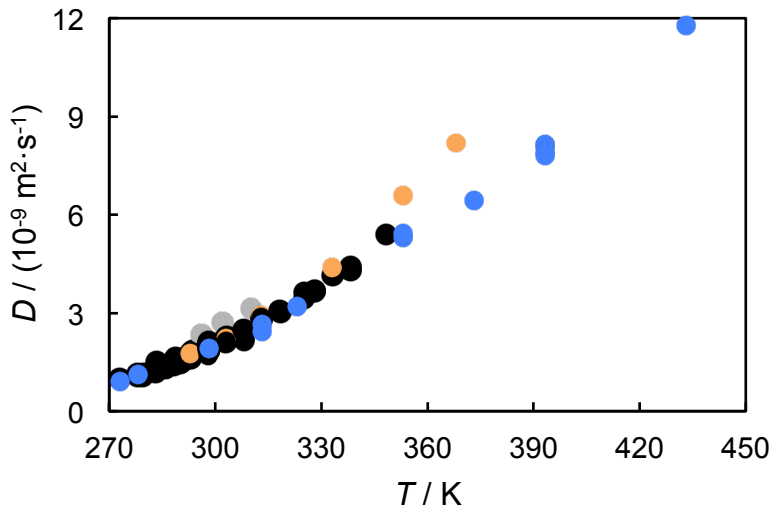

Figure 1-7. Reported values for the diffusion coefficient of CO_2 in water plotted again temperature.
The data presented is tabulated in Appendix 1A: ●, [49]; ●, [50]; ●, [51]; ●, [52-59]. The results of [49] and [50] diverge above 340 K to a difference of 30% at 373 K.

The qualitative increasing trend of diffusion against temperature of this mixture is consistent with diffusion in fluids in general. This is an intuitive finding in light of the previous explanation of diffusion being the result of random molecular translational motion. At higher temperatures there is more thermal energy available for molecular translation.

The Effect of Pressure on Diffusivity

Transport properties of fluids tend to be a far weaker function of pressure than of composition or temperature. If it is assumed diffusivity of a solute molecule is decreased by the solvent providing a resistance to motion, e.g. due to its viscosity, as pressure increases, and the resulting increase in viscosity, the observed diffusivity

should decrease. While the extent of this reduction may not be as pronounced as the effect of temperature, pressure may play a significant role at higher pressures. This may be especially true at the conditions pertinent to subsurface formations. Indeed, much of the literature available regarding the effect of pressure on the diffusion coefficients of gases in liquids has been carried out with respect to EOR processes. Figure 1-8 to Figure 1-11 show some examples of work performed to investigate the dependence of *D* on pressure, in various liquid systems.

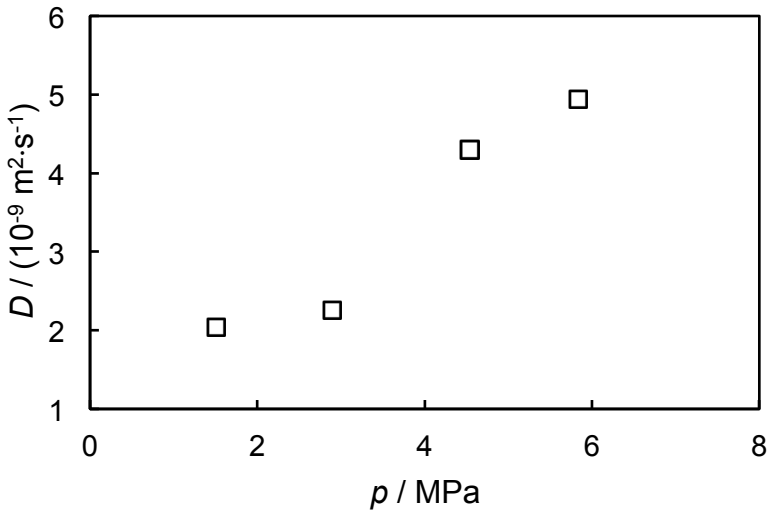

Figure 1-8. Diffusion coefficient of CO_2 in decane at T = 311 K plotted against pressure measured in a Berea-sandstone core [60].

Figure 1-8 indicates that pressure has a considerable impact on the observed diffusion coefficient of CO_2 in a hydrocarbon system. It appears that as pressure increases the diffusivity also increases, in this case by a magnitude of 2.5 times between p = (1 and 6) MPa. However, experimental shortcomings may need to be taken into consideration. The values were dependent on the orientation of the core for example, indicating gravity driven convection may have been a source of experimental error. Other works have also reported the diffusion coefficient of CO_2 and CH_4 in a liquid, Athabasca bitumen, increasing as pressure increases [61]. In these works, no reference was made to the effect of increasing pressure by means of adding the amount of solute, CO_2, present.

In contrast to the previous finding, another publication, in which the Taylor dispersion technique [62] (discussed further in Chapter 2 & 3) was used, reported a decrease in the diffusion coefficient of a solute in a hydrocarbon solvent at a given temperature as pressure increases [63] (see Figure 1-9 and Figure 1-10).

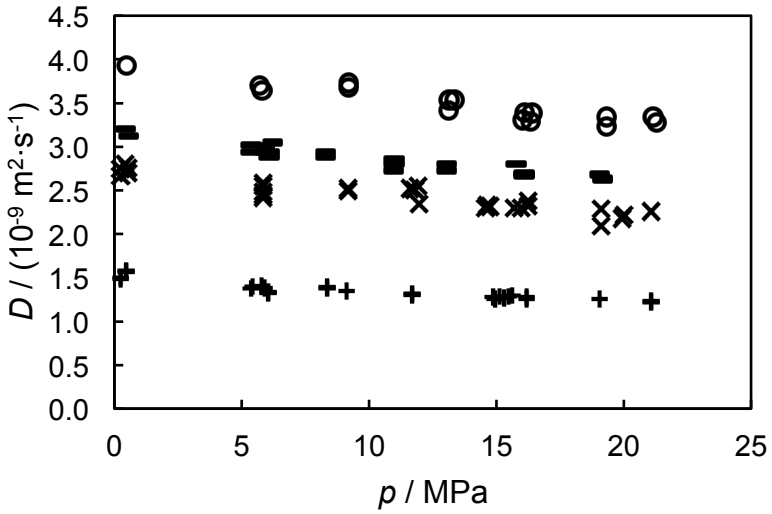

Figure 1-9. Diffusion coefficient of four different solutes in 94.6% hexane / 5.4% ethyl acetate over a range of pressures at T = 298.15 K [63].
The solutes investigated were: **O**, anisole; **-**, benzyl acetate; **×**, hexamethyl benzene and **+**, dodecyl phthalate.

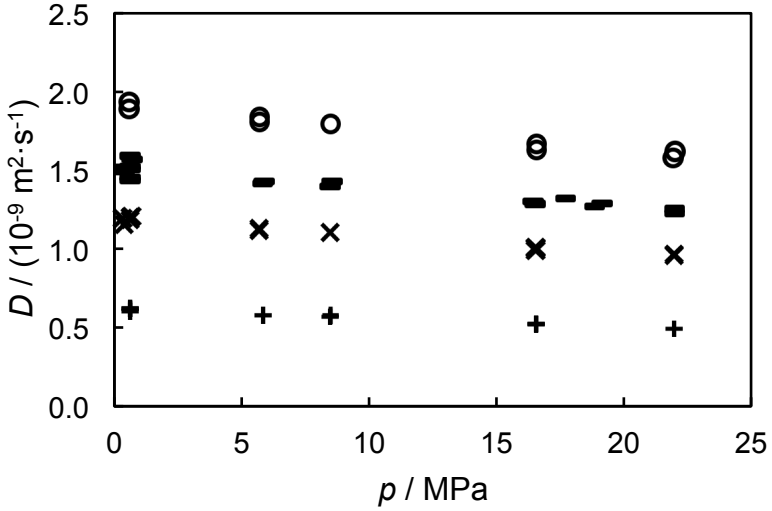

Figure 1-10. Diffusion coefficient of four different solutes in 94.7% decane / 5.3% ethyl acetate solution over a range of pressures at T = 298.15 K [63].
The solutes investigated were: **O**, anisole; **-**, benzyl acetate; **×**, hexamethyl benzene and **+**, dodecyl phthalate.

A 1% decrease in diffusivity for every 1 MPa increase in pressure between (0.25 and 22) MPa was noted, irrespective of the solute in both solvents.

Figure 1-11 shows a similar discrepancy with regards the effect of pressure on D, in this instance based on the diffusivity of CO_2 in aqueous systems.

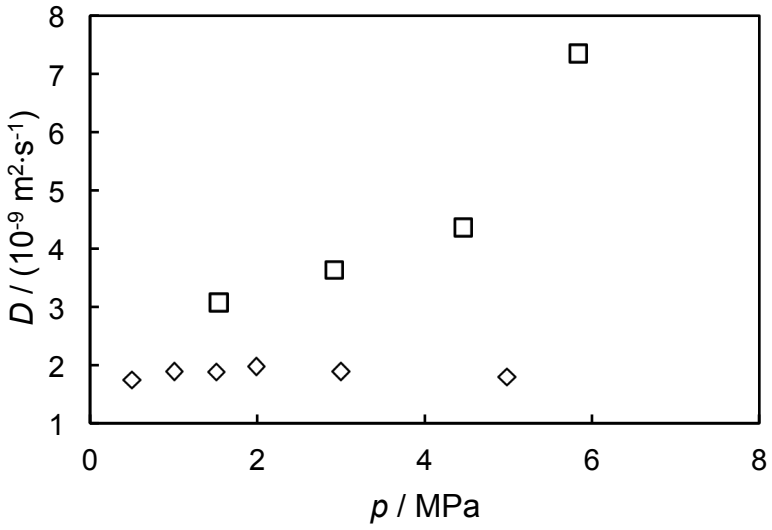

Figure 1-11. Diffusion coefficients D of CO_2 in an aqueous solvent plotted against pressure, p.
Results shown are of CO_2 in water at ◇, T = 299 K [64] and in a 0.25 mol·kg^{-1} NaCl solution at □, T = 311 K, [60]. The latter was performed in a Berea-sandstone core.

The finding that the diffusion coefficient of CO_2 in water at T = 299 K is essentially independent of pressure [64] can be easily rationalised. Water is an almost incompressible fluid due to the strong hydrogen bonds present. Pressure therefore has only a slight impact on its molar volume and viscosity. The change in the resistance of water to molecular movement of a solute then due to pressure is almost insignificant.

Multi-component Diffusion

In order to predict the behaviour of multicomponent systems, e.g. a crude oil, it is first required to be able to predict accurately the behaviour of simple binary systems at the high temperatures and high-pressure conditions of interest. However the complexity of multicomponent systems is exponentially larger than that of binary systems. Diffusional coupling, i.e. the flux of a component depending not only on its own concentration but also the concentration of other components in the system, can cause fluxes not observed in binary systems [65].

More complicated behaviour as the number of components increases beyond two. The treatment of *n*-component involves a matrix of $(n - 1)^2$ Fickian diffusion coefficients. Eq. (1-7) and Eq. (1-8) model the diffusion of a *N*-component system, i.e. *n* different solutes diffusing in a solvent [66].

$$\begin{bmatrix} -j_1 \\ -j_2 \\ \cdot \\ \cdot \\ \cdot \\ -j_{(N-1)} \end{bmatrix} = \begin{bmatrix} D_{11} & D_{12} & \cdot\ \cdot\ \cdot & D_{1(N-1)} \\ D_{21} & D_{22} & \cdot\ \cdot\ \cdot & D_{2(N-1)} \\ \cdot & \cdot & \cdot\ \cdot\ \cdot & \cdot \\ \cdot & \cdot & \cdot\ \cdot\ \cdot & \cdot \\ \cdot & \cdot & \cdot\ \cdot\ \cdot & \cdot \\ D_{(N-1)1} & D_{(N-1)2} & \cdot\ \cdot\ \cdot & D_{(N-1)(N-1)} \end{bmatrix} \begin{bmatrix} \nabla c_1 \\ \nabla c_2 \\ \cdot \\ \cdot \\ \cdot \\ \nabla c_{(N-1)} \end{bmatrix} \tag{1-7}$$

$$j_1 V_{m,1} + j_2 V_{m,2} + \ldots + j_{(N-1)} V_{m,(N-1)} + j_N V_{m,N} = 0 \tag{1-8}$$

D_{ij} is the Fickian diffusion coefficient of component *i* due to the concentration gradient of component *j*. Where *i* = *j* this values corresponds to the diffusion coefficient of the solute in the solvent due to the solutes own concentration – the *self-diffusion coefficient*. The resulting (*n* - 1) × (*n* - 1) matrix is not typically symmetrical for Fickian coefficients, however it is symmetric for Maxwell-Stefan diffusion coefficients, i.e. $D^{MS}_{ij} = D^{MS}_{ji}$. The "cross-term" coefficients are often small relative to the main diffusion terms, however, as they indicate coupling of molar fluxes and can have significant influence on the total molar flux. These theories are complex and the physical results are often counter-intuitive, e.g. reverse diffusion has been observed. In such a scenario, a solute molecule will act against the concentration gradient due to diffusional coupling between components. For example, in a aqueous solution of KCl and a molecule that selectively binds to free ions, 18-crown-6-ether or 18C6, free K^+ ions have been observed to diffuse toward regions of higher 18C6 concentration, counter-current to the 18C6 flux [67].

There is a considerable lack of experimental results for not only the values of diffusion coefficients in multicomponent systems but also no systematic studies on the dependence of these parameters on composition, temperature, or pressure. Due to the coupling of the flux of individual components in the mixture it should not be assumed that the diffusivities will simply follow the same trend with respect to composition, pressure or temperature as those of binary diffusion coefficients.

Effective binary diffusion coefficient

For many systems of interest, especially in the field of chemical engineering, there may be dozens of individual components in a system resulting in an impractical number of diffusion coefficients. In the case of CO_2 in a saline solution there are at least three diffusing components: CO_2, H_2O and a salt. For the case of a saline aquifer, where there may be in excess of 7 unique components, this corresponds to 36 Fickian diffusion coefficients. This is not only impractical to experimentally measure but also computationally expensive to incorporate in a model or simulation.

It is often advantageous to attempt to simplify the system, for example omitting trace elements, or treating a multicomponent system as an effectively pure-component solvent.

It is argued that for the case of the diffusion of CO_2 in brines a binary diffusion coefficient can be used to describe the molecular transport of CO_2 and provided that one component is present in a sufficiently low concentration this treatment is acceptable [43]. It has been proposed to analyse such a saline system using the Onsager coefficients to justify the calculation of Maxwell-Stefan diffusion coefficients, D^{MS}_{ij}, of CO_2 in a NaCl solution [39]. Fickian diffusion coefficients can be calculated from Maxwell-Stefan coefficients as follows:

$$\begin{bmatrix} D_{11} & D_{12} \\ D_{21} & D_{22} \end{bmatrix} = \begin{bmatrix} f\left(D_{11}^{MS}\right) & f\left(D_{12}^{MS}\right) \\ f\left(D_{21}^{MS}\right) & f\left(D_{22}^{MS}\right) \end{bmatrix}^{-1} \begin{bmatrix} \delta_{11} + x_1\left[\frac{\partial \ln \phi_1}{\partial x_1}\right] & \delta_{12} + x_1\left[\frac{\partial \ln \phi_1}{\partial x_2}\right] \\ \delta_{12} + x_2\left[\frac{\partial \ln \phi_2}{\partial x_1}\right] & \delta_{22} + x_2\left[\frac{\partial \ln \phi_2}{\partial x_2}\right] \end{bmatrix} \quad (1\text{-}9)$$

δ_{ii} is the Kronecker symbol and x_i and φ_i are the mole fraction and fugacity coefficient of component i, respectively. The functional form of the Maxwell-Stefan coefficients can be found in Garcia-Ratés *et al* [39]. Hence, when CO_2 and the salt are only present in dilute quantities and the Maxwell-Stefan diffusion matrix is sparse then the Fickian matrix will also be sparse.

Hence, under the assumption that the concentration of CO_2, c_1, is infinitesimal, Eq. (1-5) can be rewritten as:

$$-\left[\mathbf{j}_1 + \mathbf{j}_2\right] = \left(D_{11} + D_{21}\right)\nabla c_1 + D_{22}\nabla c_2 \qquad (1\text{-}10)$$

In this instance D_{22} corresponds to the diffusion coefficient of the second solute (e.g. NaCl) in the solvent and (D_{11} + D_{21}) corresponds to the diffusion coefficient of CO_2, also in the solvent. In this work (D_{11} + D_{21}) will be denoted by D. The main assumptions in this treatment are that the concentration of solute 1 is so low that there is effectively no diffusion interactivity with solute 2 and there is no chemical interaction between the two species. Naturally, for systems where both the solutes are present in high concentration and/or the solutes strongly interact these assumptions break down. Nonetheless, in the current study where the typical mole fraction of dissolved CO_2 is in the order of 0.01 it is proposed the mass transport equations can be constructed from diffusion coefficients measured by monitoring the translational diffusion of CO_2 (D_{11} + D_{21}) in the respective brine.

References

[1] B. Bijeljic, M.J. Blunt, Pore-scale modeling and continuous time random walk analysis of dispersion in porous media, Wat. Resour. Res. 42 (2006) W01202.

[2] T.K. Perkins, O.C. Johnston, A Review of Diffusion and Dispersion in Porous Media, SPE J. 3 (1963) 70-84.

[3] M. Sahimi, Flow and Transport in Porous Media and Fractured Rock, Wiley, Berlin, 1995.

[4] S.P. Cadogan, G.C. Maitland, J.P.M. Trusler, Diffusion Coefficients of CO_2 and N_2 in Water at Temperatures between 298.15 K and 423.15 K at Pressures up to 45 MPa, J. Chem. Eng. Data 59 (2014) 519-525.

[5] R.K. Jha, S. Bryant, L.W. Lake, Effect of Diffusion on Dispersion, SPE J. 16 (2011) 65-77.

[6] K.K. Al-Tarawneh, O. Buzzi, K. Krabbenhøft, A.V. Lyamin, S.W. Sloan, An Indirect Approach for Correlation of Permeability and Diffusion Coefficients, Defect and Diffusion Forum, Trans Tech Publications, 2009, pp. 504-514.

[7] G.E. Grisak, J.F. Pickens, Solute Transport Through Fractured Media: 1. The Effect of Matrix Diffusion, Wat. Resour. Res. 16 (1980) 719-730.

[8] P. Harriott, A Review of Mass Transfer to Interfaces, Can. J. Chem. Eng. 40 (1962) 60-69.

[9] K. Pruess, Numerical Modeling Studies of the Dissolution-Diffusion-Convection Process During CO2 Storage in Saline Aquifers, Lawrence Berkeley National Laboratory (2008).

[10] International Energy Agency, 2011. Available from: http://www.iea.org/statistics/statisticssearch/ [Accessed 24Nov2015].

[11] H3DWallpapers, World Map Pics, 2015. Available from: http://www.h3dwallpapers.com/world-map-pics-1736/ [Accessed 24Nov2015].

[12] F. Birol, World Energy Outlook 2010, International Energy Agency, Paris, 2010.

[13] S. Pacala, R. Socolow, Stabilization Wedges: Solving the Climate Problem for the Next 50 Years with Current Technologies, Science 305 (2004) 968-972.

[14] M.E. Boot-Handford, J.C. Abanades, E.J. Anthony, M.J. Blunt, S. Brandani, N. Mac Dowell, J.R. Fernández, M.-C. Ferrari, R. Gross, J.P. Hallett, Carbon capture and storage update, Energy Environ. Sci. 7 (2014) 130-189.

[15] N. MacDowell, N. Florin, A. Buchard, J. Hallett, A. Galindo, G. Jackson, C.S. Adjiman, C.K. Williams, N. Shah, P. Fennell, An overview of CO_2 capture technologies, Energy Environ. Sci. 3 (2010) 1645-1669.

[16] H. Yang, Z. Xu, M. Fan, R. Gupta, R.B. Slimane, A.E. Bland, I. Wright, Progress in carbon dioxide separation and capture: A review, J. Environ. Sci. 20 (2008) 14-27.
[17] A. Samanta, A. Zhao, G.K. Shimizu, P. Sarkar, R. Gupta, Post-Combustion CO_2 Capture Using Solid Sorbents: A Review, Ind. Eng. Chem. Res. 51 (2011) 1438-1463.
[18] B. Metz, O. Davidson, H. De Coninck, M. Loos, L. Meyer, CARBON DIOXIDE CAPTURE AND STORAGE, IPCC Geneva, 2005.
[19] D. Aaron, C. Tsouris, Separation of CO_2 from Flue Gas: A Review, Sep. Sci. Technol. 40 (2005) 321-348.
[20] R.S. Haszeldine, Carbon Capture and Storage: How Green Can Black Be?, Science 325 (2009) 1647-1652.
[21] C.M. White, B.R. Strazisar, E.J. Granite, J.S. Hoffman, H.W. Pennline, Separation and Capture of CO_2 from Large Stationary Sources and Sequestration in Geological Formations—Coalbeds and Deep Saline Aquifers, J. Air Waste Manage. Assoc. 53 (2003) 645-715.
[22] M. Wang, A. Lawal, P. Stephenson, J. Sidders, C. Ramshaw, Post-combustion CO_2 capture with chemical absorption: A state-of-the-art review, Chem. Eng. Res. Des. 89 (2011) 1609-1624.
[23] T.F. Wall, Combustion processes for carbon capture, Proc. Combust. Inst. 31 (2007) 31-47.
[24] B. Li, Y. Duan, D. Luebke, B. Morreale, Advances in CO_2 capture technology: A patent review, Appl. Energy 102 (2013) 1439-1447.
[25] A.B. Rao, E.S. Rubin, A Technical, Economic, and Environmental Assessment of Amine-Based CO_2 Capture Technology for Power Plant Greenhouse Gas Control, Environ. Sci. Technol. 36 (2002) 4467-4475.
[26] D.M. D'Alessandro, B. Smit, J.R. Long, Carbon Dioxide Capture: Prospects for New Materials, Angew. Chem. Int. Ed. 49 (2010) 6058-6082.
[27] M. Hesse, H.A. Tchelepi, F.M. Orr, Scaling Analysis of the Migration of CO_2 in Saline Aquifers, SPE Annual Technical Conference and Exhibition, Society of Petroleum Engineers, 2006.
[28] S. Iglauer, Dissolution Trapping of Carbon Dioxide in Reservoir Formation Brine– A Carbon Storage Mechanism, 2011.
[29] E.C. Efika, R. Hoballah, X. Li, E.F. May, M. Nania, Y. Sanchez-Vicente, J.P.M. Trusler, Saturated Phase Densities of CO_2 + H_2O at Temperatures from (293 to 450) K and Pressures up to 64 MPa, J. Chem. Thermodyn. (2015).
[30] R. Allen, S. Sun, Carbon Dioxide Sequestration: Modeling the Diffusive and Convective Transport under a CO_2 Cap, SPE Saudi Arabia Section Technical Symposium and Exhibition, Society of Petroleum Engineers, 2012.

[31] J.L. Duda, J.S. Vrentas, Laminar Liquid Jet Diffusion Studies, AlChE J. 14 (1968) 286-294.
[32] W.G. Whitman, THE TWO-FLM THEORY OF GAS ABSORPTION, Int. J. Heat Mass Transfer 5 (1962) 429-433.
[33] T.A. Torp, J. Gale, DEMONSTRATING STORAGE OF CO_2 IN GEOLOGICAL RESERVOIRS: THE SLEIPNER AND SACS PROJECTS, Energy 29 (2004) 1361-1369.
[34] C. Peng, J.P. Crawshaw, G.C. Maitland, J.P.M. Trusler, D. Vega-Maza, The pH of CO_2-saturated water at temperatures between 308K and 423K at pressures up to 15MPa, J. Supercrit. Fluids 82 (2013) 129-137.
[35] S. Thomas, Enhanced Oil Recovery - An Overview, Oil Gas Sci. Technol. 63 (2008) 9-19.
[36] M.E. Aguilera, A. López de Ramos, EFFECT OF CO_2 DIFFUSION ON WETTABILITY FOR HYDROCARBON-WATER-CO_2 SYSTEMS IN CAPILLARIES, Int. Commun. Heat Mass 31 (2004) 1115-1122.
[37] A.T. Grogan, W.V. Pinczewski, The Role of Molecular Diffusion Processes in Tertiary CO_2 Flooding, J. Petrol. Technol. 39 (1987) 591-602.
[38] X. Liu, S.K. Schnell, J.-M. Simon, D. Bedeaux, S. Kjelstrup, A. Bardow, T.J.H. Vlugt, Fick Diffusion Coefficients of Liquid Mixtures Directly Obtained From Equilibrium Molecular Dynamics, J. Phys. Chem. 115 (2011) 12921-12929.
[39] M. Garcia-Ratés, J.-C. de Hemptinne, J.B. Avalos, C. Nieto-Draghi, Molecular Modeling of Diffusion Coefficient and Ionic Conductivity of CO_2 in Aqueous Ionic Solutions, J. Phys. Chem. 116 (2012) 2787-2800.
[40] J.B. Brady, REFERENCE FRAMES AND DIFFUSION COEFFICIENTS, Am. J. Sci. 275 (1975) 954 - 983.
[41] J.G. Kirkwood, R.L. Baldwin, P.J. Dunlop, L.J. Gosting, G. Kegeles, Flow Equations and Frames of Reference for Isothermal Diffusion in Liquids, J. Chem. Phys. 33 (1960) 1505-1513.
[42] R. Taylor, R. Krishna, MULTICOMPONENT MASS TRANSFER, John Wiley & Sons, 1993.
[43] E.L. Cussler, Diffusion: Mass Transfer in Fluid Systems, Cambridge University 2009.
[44] R.K.M. Thambynayagam, THE DIFFUSION HANDBOOK: APPLIED SOLUTIONS FOR ENGINEERS, McGraw Hill, 2011.
[45] M.T. Tyn, W.F. Calus, Temperature and Concentration Dependence of Mutual Diffusion Coefficients of Some Binary Liquid Systems, J. Chem. Eng. Data 20 (1975) 310-316.

[46] A.V. Khristoforov, R.A. Dautov, SOLVATION OF GASEOUS CARBON-DIOXIDE IN LIQUID NORMAL-HEPTANE AS THE PHASE-TRANSFORMATION OF THE 1ST TYPE, Zh. Fiz. Khim. 61 (1987) 2656-2659.
[47] H. Saad, E. Gulari, Diffusion of Carbon Dioxide in Heptane, J. Phys. Chem. 88 (1984) 136-139.
[48] D. Li, Z. Duan, The speciation equilibrium coupling with phase equilibrium in the H_2O–CO_2–NaCl system from 0 to 250 °C, from 0 to 1000 bar, and from 0 to 5 molality of NaCl, Chem. Geol. 244 (2007) 730-751.
[49] W. Lu, H. Guo, I. Chou, R. Burruss, L. Li, Determination of diffusion coefficients of carbon dioxide in water between 268 and 473K in a high-pressure capillary optical cell with in situ Raman spectroscopic measurements, Geochim. Cosmochim. Acta 115 (2013) 183-204.
[50] A. Tamimi, E.B. Rinker, O.C. Sandall, Diffusion Coefficients for Hydrogen Sulfide, Carbon Dioxide, and Nitrous Oxide in Water over the Temperature Range 293-368 K, J. Chem. Eng. Data 39 (1994) 330-332.
[51] K. Gertz, H. Loeschcke, Bestimmung des Diffusionskoeffizienten von CO_2 in Wasser, Z. Naturforsch. B 11 (1956) 61-64.
[52] W.J. Thomas, M.J. Adams, Measurement of the Diffusion Coefficients of Carbon Dioxide and Nitrous Oxide in Water and Aqueous Solutions of Glycerol, T. Faraday Soc. 61 (1965) 668 - 673.
[53] M.J.W. Frank, J.A.M. Kuipers, W.P.M. van Swaaij, Diffusion Coefficients and Viscosities of CO_2+ H_2O, CO_2+ CH_3OH, NH_3+ H_2O, and NH_3+ CH_3OH Liquid Mixtures, J. Chem. Eng. Data 41 (1996) 297-302.
[54] A.A. Unver, D.M. Himmelblau, Diffusion Coefficients of CO_2, C_2H_4, C_3H_6 and C_4H_8 in Water from 6° to 65° C, J. Chem. Eng. Data 9 (1964) 428-431.
[55] B.P. Mandal, M. Kundu, N.U. Padhiyar, S.S. Bandyopadhyay, Physical Solubility and Diffusivity of N_2O and CO_2 into Aqueous Solutions of (2-Amino-2-methyl-1-propanol+ Diethanolamine) and (N-Methyldiethanolamine+ Diethanolamine), J. Chem. Eng. Data 49 (2004) 264-270.
[56] S. Hirai, K. Okazaki, H. Yazawa, H. Ito, Y. Tabe, K. Hijikata, MEASUREMENT OF CO_2 DIFFUSION COEFFICIENT AND APPLICATION OF LIF IN PRESSURIZED WATER, Energy 22 (1997) 363 - 367.
[57] F.C. Tse, O.C. Sandall, DIFFUSION COEFFICIENTS FOR OXYGEN AND CARBON DIOXIDE IN WATER AT 25ºC BY UNSTEADY STATE DESORPTION FROM A QUIESCENT LIQUID, Chem. Eng. Commun. 3 (1979) 147-153.

[58] R.A.T.O. Nijsing, R.H. Hendriksz, H. Kramers, Absorption of CO_2 in jets and falling films of electrolyte solutions, with and without chemical reaction, Chem. Eng. Sci. 10 (1959) 88-104.
[59] R.T. Ferrell, D.M. Himmelblau, Diffusion Coefficients of Nitrogen and Oxygen in Water, J. Chem. Eng. Data 12 (1967) 111-115.
[60] T.A. Renner, Measurement and Correlation of Diffusion Coefficients for CO_2 and Rich-Gas Applications, SPE Reservoir Engineering 3 (1988) 517-523.
[61] M. Jamialahmadi, M. Emadi, H. Müller-Steinhagen, Diffusion coefficients of methane in liquid hydrocarbons at high pressure and temperature, J. Pet. Sci. Eng. 53 (2006) 47-60.
[62] G. Taylor, Dispersion of soluble matter in solvent flowing slowly through a tube, Proc. R. Soc. London. Series A. 219 (1953) 186-203.
[63] J.G. Atwood, J. Goldstein, Measurement of Diffusion Coefficients in Liquid at Atmospheric and Elevated Pressure by the Chromatographic Broadening Technique, J. Phys. Chem. 88 (1984) 1875 - 1885.
[64] A. Sell, H. Fadaei, M. Kim, D. Sinton, Measurement of CO_2 Diffusivity for Carbon Sequestration: A Microfluidic Approach for Reservoir-Specific Analysis, Environ. Sci. Technol. 47 (2012) 71-78.
[65] P.W.M. Rutten, Diffusion in Liquids, Applied Sciences, TU Delft, The Netherlands, 1992.
[66] A.R. Cooper, The Use and Limitations of the Concept of an Effective Binary Diffusion Coefficient for Multicomponent Diffusion, Mass Transport in Oxides 296 (1968) 79-84.
[67] D.G. Leaist, Ternary Diffusion Coefficients of 18-Crown-6 Ether–KCl–Water by Direct Least-Squares Analysis of Taylor Dispersion Measurements, J. Chem. Soc., Faraday Trans. 87 (1991) 597-601.

2. Measurement and Modeling of Diffusion Coefficients

A wide variety of techniques exist for determining diffusion coefficients [1]. The methods for determining diffusion coefficients of gases in liquids may be broadly classified into two groups: techniques in which the liquid is in motion (e.g. the laminar jet method) and techniques in which the liquid is stagnant (e.g. the diaphragm cell method) [2]. In both techniques, the concentration of the solute is observed over a period of time, the length of which depends on the technique used and the magnitude of the diffusivity. The design, operating procedure, advantages, and limitations of the most common of these methods will be discussed further in this section. The Taylor dispersion technique and pulsed field-gradient nuclear magnetic resonance were used in this work and will be described in greater detail.

Modelling diffusion can also typically be broken down into two main philosophies; both however rely to some extent on correlative corrections. The first is a hydrodynamic approach where a diffusing molecule is considered a particle moving through a continuous medium that applies a resistance to flow. The second approach is based on kinetic theory, where both the diffusing molecule and the solvent are treated as particles in which the collision between different particles acts to oppose diffusivity. The kinetic theory for simple liquids is not as well developed as that for ideal/dilute gases and it cannot give accurate analytical predictions of diffusivities without corrections [3].

Measurement of Diffusion Coefficients

Absorption in a Liquid Body

One of the most commonly used methods to measure diffusion coefficients of gases in Newtonian liquids [4] involves monitoring the rate of gas absorption of a solute in a solvent in steady-state flow [5-11]. The diffusion coefficient can then be determined from an appropriate mass transfer model. The rate of solute absorption can be monitored through the pressure drop in the gas phase, a soap bubble meter or analysis of the composition of the eluent. Figure 2-1 shows an example of an apparatus used in such techniques.

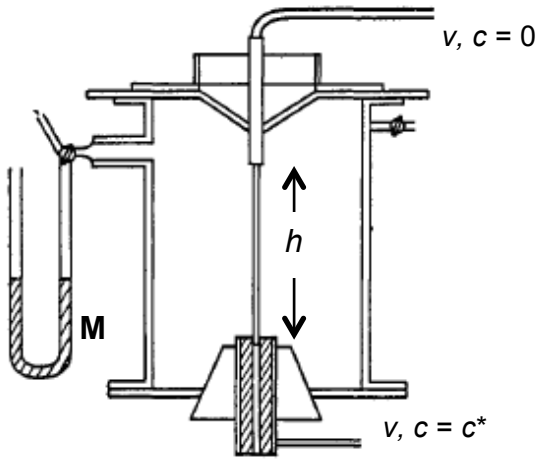

Figure 2-1. Diagram of a typical laminar jet apparatus [12].
The diffusion cell is pre-pressurised with the solute gas at the relevant temperature and pressure. A solute-free steady laminar flow of liquid enters the call with a defined superficial linear velocity, *v*. It is exposed to the gas under investigation through a height of liquid, *h*. The rate of absorption is measured, e.g. with a soap film meter, **M**.

Laminar flow, i.e. a laminar jet, is typically used as it can be treated mathematically with relative ease. The effect of interfacial resistance is usually assumed to be negligible [13]. The presence of surface-active agents may negate this assumption. Another key assumption is that no velocity gradients exist within the liquid. Due to the parabolic profile of laminar flow, different nozzles and configurations are used to minimise this parabolic nature. When suitable design considerations are employed experimental uncertainties of less than 1% are claimed [6]. This technique has been widely used to measure diffusion coefficients of CO_2 in water [5-7, 14-16] and in amine solvents [8, 10, 17].

In the case of a laminar jet, the diffusion coefficient, D, is typically related to the rate of solute absorption, ϕ, using a model based on the penetration theory of absorption [18, 19]:

$$\sqrt{D} = \left(4c^* \sqrt{v}\right)^{-1} \left(\phi / h\right) \tag{2-1}$$

c^* is the equilibrium concentration of the solute in the solvent, v and h are the liquid flow rate and the length of the jet, respectively.

One of the main limitations of this technique is the need to have solubility data for the system under investigation at least as accurate as the desired accuracy of D. This is demonstrated in Figure 2-2 where two of the most widely cited sources for the diffusion coefficient of CO_2 in water are reinterpreted using more recent solubility data [20]. As the liquid flow rate and length of the jet, v and h respectively, are given in these works along with the recorded transfer rate of solute, ϕ, and equilibrium solute solubility, c^*, these results could easily be reanalysed using more accurate values of c^*.

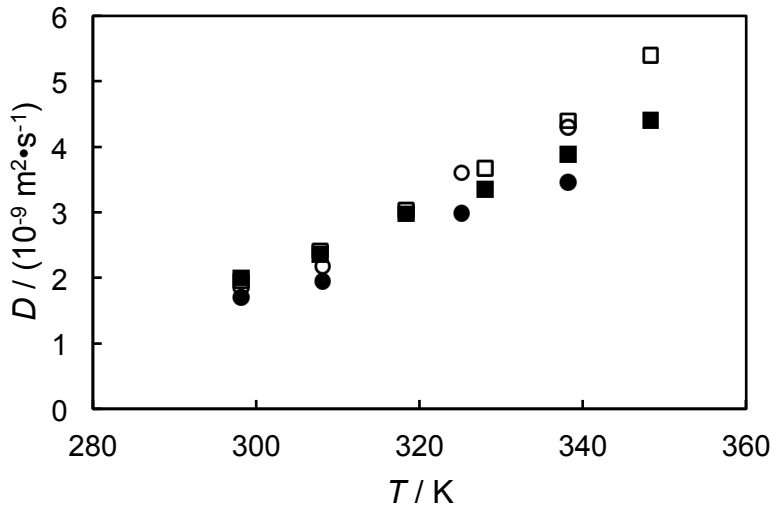

Figure 2-2: Original and reprocessed diffusion coefficients for CO_2 in water.
□ (original), ■ (reprocessed) [6] and ○ (original), ● (reprocessed) [5].

As can be seen in Figure 2-2, the values for D are altered by up to 20%. This change becomes more pronounced at higher temperatures, e.g. from (1.95 to 2.00) $m^2 \cdot s^{-1}$ at a temperature of 298 K to (5.40 to 4.40) $m^2 \cdot s^{-1}$ at T = 348 K [6]. The reprocessed value at T = 298 K agrees well with the value of 2.05 $m^2 \cdot s^{-1}$ reported elsewhere [7]. Despite this source of error, the relatively long run time, and the need for large quantities of fresh solvent, laminar jets have been one of the most popular methods for measuring the diffusion coefficients of gases in liquids.

Several variants of this technique exist, also based on absorption of the gas solute, in a liquid in laminar flow over a well-defined geometry, e.g. a wetted wall column absorber [21] or a wetted sphere apparatus [8, 17, 22]. In the latter technique, the gas is brought into contact with a liquid layer on a spherical body. A wetted-sphere apparatus may be preferable to the laminar jet method when the rate of solute absorption is sufficiently low, due to the longer gas-liquid contact times relevant to the latter [8].

A less common variant of the absorption technique is the analysis of the mass transfer of a gas into a quiescent liquid. A technique in which the isothermal pressure decay in a cell in which a solute gas rests on a hydrocarbon liquid is recorded to determine the diffusion coefficient has been reported [23-25].

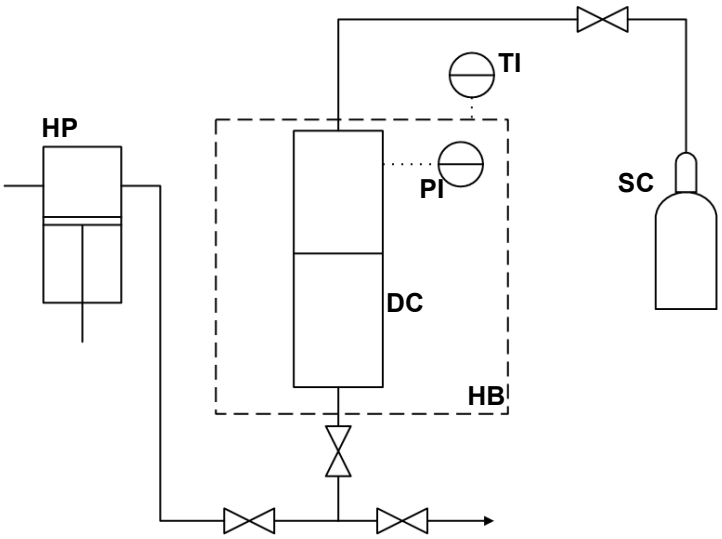

Figure 2-3. Diagram of a typical quiescent liquid diffusion apparatus [25].
The solute gas, supplied via **SC** is brought into typically charged first to the diffusion cell, **DC**, housed in a heating bath, **HB**. The liquid under investigation is then charged via **HP**. The pressure and temperature are then recorded via **PI** and **TI** and the time evolution of the pressure is then used to determine *D*.

The equipment is similar in design and operation to pressure-volume-temperature cells and solubility data is often reported alongside diffusivities in such reports. This has become a common method for the determination of CO_2 and other sparingly soluble gases in oils [26] along with several variants [24, 25, 27-29].

Typically the solute gas is brought into contact with the solvent and the system is allowed to equilibrate at the target pressure before the pressure drop is recorded. However, diffusivity is a function of concentration and these results may yield ambiguous results. This is especially true when the solute is very soluble in the solvent or the thermophysical properties of the solvent are a strong function of the

amount of the solute present, e.g. as in the case of the viscosity of the (CO_2 + squalane) system [30].

Another method that has been popular in measuring the diffusion coefficient of gases in liquids, especially hydrocarbons at high pressures and temperatures, also relies on the rate of adsorption of the solute. The hydrocarbon under study is charged to a cylindrical vessel before being saturated with the solute gas. The resulting reduction in hydrocarbon density is interpreted in terms of the rate of solute absorption, which in turn yields the diffusion coefficient. The resulting change in density, observed in terms of volume, can be recorded by means of a cathetometer, equipped with a sliding scope. Such experiments take two to six days per data point [31].

A method in which the swelling of a pendant drop of heavy oil due to the absorption of a solute gas is used to measure the diffusion coefficient [32, 33] has been reported. This so-called dynamic pendant drop volume analysis (DPDVA) method can operate at high temperatures and pressures. A high-pressure cell with a window is pressurised with the solute gas and heated to the desired temperature. A pendant drop of the solvent hydrocarbon is then introduced via a syringe pump. The change of volume of the drop is recorded by camera via the window. A numerical model, which predicts the rate of swelling based on the diffusivity and swelling factor, is then fitted to the experimental data. The equation describing the concentration of gas inside the droplet, c, is given in terms of a cylindrical coordinate system by:

$$\frac{\partial c}{\partial t} = D\left[\frac{1}{r}\frac{\partial}{\partial r}\left(r\frac{\partial c}{\partial r}\right) + \frac{\partial^2 c}{\partial z^2}\right]. \tag{2-2}$$

The initial condition for this PDE is $c = 0$. The boundary condition states that at the gas-liquid interface c is the saturation concentration, c_{sat}. In other words, as with the treatment of the laminar jet system, it is assumed there is no interfacial resistance. This system is the solved numerically using the semidiscrete Galerkin finite element method, based on the implementation of triangular meshing of the pendant drop.

The volume of the pendant is given by:

$$V_c(t) = V_0 + v_{gas} M_{gas} n(t). \tag{2-3}$$

Where, M_{gas} is the molecular mass of the gas and v_{gas} is the volume change per unit mass of gas dissolved in the gas-liquid mixture calculated from the liquid swelling factor, M_{gas} and c_{sat}. The number of moles dissolved in the pendant drop, $n(t)$, is calculated from:

$$n(t) = c_{sat} t_n^3 \iint_{(R,Z)\in\Omega} C\left(R, Z, \frac{Dt}{r_n^2}\right) \pi R \mathrm{d}R \mathrm{d}Z \,. \qquad (2\text{-}4)$$

Here, *C*, *R* and *Z* are dimensionless forms of *c*, *r* and *z*, respectively.

The above methods are however unsuitable for measuring infinite dilution diffusion coefficients at elevated pressures without a clear definition of the amount of CO_2 dissolved in the solvent. There is also a difficulty in discriminating between the concentration effects on the diffusion coefficient. The viscosity of hydrocarbons can be greatly reduced on the addition of CO_2 [30].

Diaphragm Cells

The simplest method to measure diffusion coefficients is the diaphragm-cell method. Figure 2-4 explains this method.

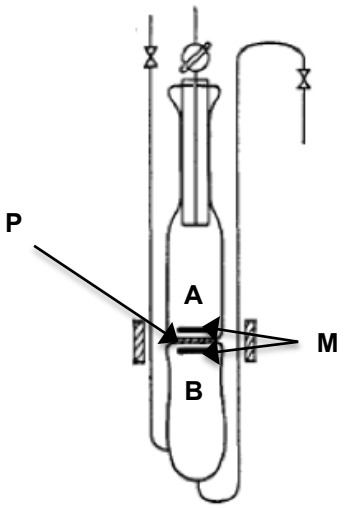

Figure 2-4. Diagram of a typical diaphragm cell apparatus [12].
Cells **A** and **B** are separated by a porous disc, **D**. A magnetic stirrer in each of these compartments, **M**, ensures that each is homogeneously mixed and that the only diffusion due to a concentration gradient is across **D**. Agitation is kept to a minimum to ensure the concentration gradient is the primary driving force for mass transfer.

Typically samples are routinely taken from each chamber and the concentration of the solute over time can be related to its diffusivity in the solvent [1]:

$$D = \left(1/\beta t\right) \ln\left[\Delta c_0 / \Delta c_t\right] \qquad (2\text{-}5)$$

The diffusivity, D, is related to the initial difference in the concentration of the solute in the two cells, Δc_0, the temporal concentration gradient Δc_t, an equipment specific parameter, β, and the amount of time elapsed, t.

An alternative method involves filling the top chamber with gas only and measuring the pressure decay over time the diffusion coefficient can also be extracted [34].
This is a secondary method and requires careful calibration with a system whose diffusion coefficient is accurately known to determine β. Due to various time variant factors, e.g. attrition of the diaphragm due to the mechanical stirring, calibrations must be frequently repeated. Another possible source of error is the loss of dissolved gas if an invasive sampling technique is used [12].
Relatively few authors have reported the use of this technique to measure sparingly soluble gases in liquids. The diffusion coefficients of CO_2 and propene in a selection of organic solvents and several sparingly soluble gases in water, respectively [34, 35] and CO_2 in a selection of binary solvents [36] are among the few systems have been reported using this technique.

Optical Techniques

Optical techniques for measuring diffusion coefficients can be sub-divided into interferometric and non-interferometric methods, Interferometric technique has been described as the most accurate method for determining diffusivities [37]. Of these techniques the Gouy and Rayleigh interferometric methods are considered the best. These methods typically relate the difference in the refractive index as a position along a diffusion cell to the diffusion coefficient; see for example Figure 2-5.

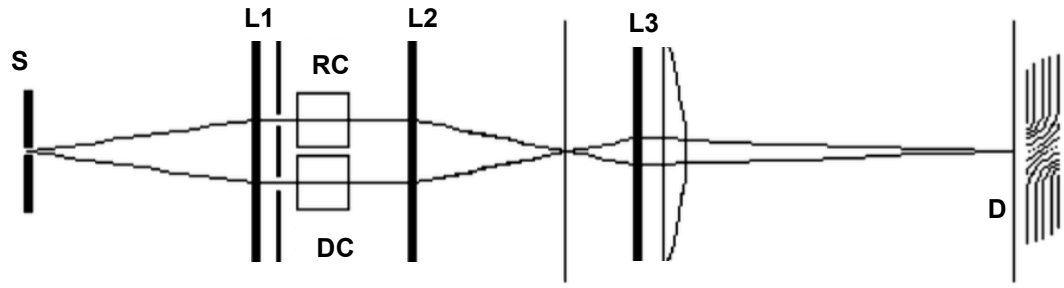

Figure 2-5. Diagram of a Rayleigh interferometer (bottom) [37].
A light source, **S**, is passed via a collimating lens, **L1**, through the diffusion cell, **DC**, and a reference cell, **RC**. This light is then refocused via **L2** and **L3** onto a detector.

A cell is carefully filled with a layer of the solvent and a layer of a solution of the solvent and diffusing solute. Fringe patterns related to the change in the refractive

index of the solution are produced by passing monochromatic light through a diffusion boundary within the diffusion cell. Rayleigh interferometers produce fringe patterns, which yield the refractive index at a corresponding cell level. The Gouy interferometer signal is the Fourier transform of the change in refractive index with respect to the distance symmetrically from the position of the maximum gradient [1].

This method can be extended to ternary systems [38-40]. Indeed it was measurements made using the Gouy interferometer than were used to validate Onsager's recipricol relationship for ternary diffusion [37, 41, 42]. A model for quaternary systems has also been developed [43], however as the number of components increase the complexity also increases.

The diffusion coefficients of CO_2 and O_2 in water using a method which is conceptually similar but uses in-situ Raman spectroscopy [44] and laser induced fluorescence [45], respectively. This technique involved monitoring CO_2 concentrations at fixed points at various times. The diffusion cell of the former as built was capable of measuring diffusion coefficients at high temperatures (< 473 K) and at pressures up to 45 MPa.

Finally, a method in which the diffusion of CO_2 is visually observed in a microfluidic channel has been used to measure CO_2 diffusivity in brine over a range of pressures (< 50 MPa) and molarities from (1 to 5) M NaCl [46]. A pH-sensitive fluorescent tracer was added to the solvent. As CO_2 is absorbed by and diffuses into the bulk solvent the resulting fluorescent intensity was used in conjunction with the solution of Fick's law for a semi-infinite channel to determine the diffusion coefficient. This method is very sensitive to the calibration technique followed and the choice of the indicator.

The working equation for these last three methods, based on free-diffusion, is:

$$c = \bar{c} + \frac{\Delta c}{2}\,\mathrm{erf}\left(y/\sqrt{D}\right) \tag{2-6}$$

c is the measured concentration and Δc is the concentration difference between the top and the bottom solutions. Where x is the distance from the interface at time t, y is given by:

$$y = x/\sqrt{4t} \tag{2-7}$$

The main limitations with optical techniques are the cost of the equipment and their delicateness. For example, while obtaining the baseline for the Gouy interferometer great care must be taken to ensure the incident light source is entirely stationary [1]. Effects such as diffusion induced convection and solvent swelling could prove to be

sources of experimental uncertainty when investigating systems where the solute is not sparingly present.

Before moving on to discuss Taylor dispersion in detail it is worth pointing out that many authors have deemed it necessary to incorporate methods of avoiding or suppressing reactions between the solute gas and solvent. For example, nitrogen dioxide, N_2O, is often used as a chemical analogue to CO_2, primarily in amine solvents [8, 11, 47-50]. In this method, N_2O is used instead of CO_2. It is then assumed the diffusion coefficient of CO_2 can be calculated as the product of the measured diffusion coefficient of N_2O in the amine and the ratio of the diffusion coefficient of CO_2 and N_2O in water, at the same temperature.

Separately, the diffusion coefficient of Cl_2 in water has been reported, using 0.35% of a 0.1 N HCl solution as the solvent in order to suppress the formation of HCl [51]. This "protonation" method has also been used to measure physical solubilities and diffusivities of CO_2 in amine solvents [17]. It may be difficult to properly quantify the effect of these approaches. In the case of the former, chemical interactions that influence diffusion are ignored, while in the case of the latter the system becomes a multicomponent mixture.

The Taylor Dispersion Technique: Design

The Taylor dispersion method (TDM) has become a popular method for determining diffusion coefficients of solutes in liquids since the mathematical formulation of the process was developed [52] (see Figure 2-6).

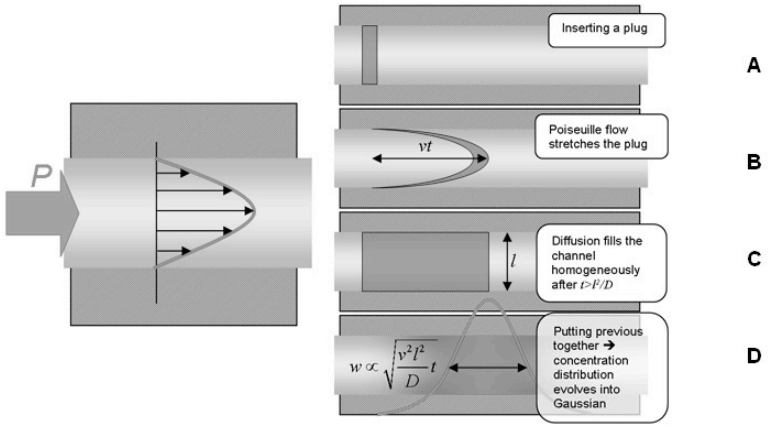

Figure 2-6: Physical diagram of Taylor dispersion.
A delta plug of solution containing an excess of solute is injected in **A**. In the absence of diffusion the solute will be dispersed longitudinally due to the parabolic velocity profile, **B**. In the absence of an external laminar velocity profile the solute will spread out homogeneously due to diffusion, **C**. What is observed, as shown in **D**, is the result of a combination of the two effects, i.e. a Gaussian concentration distribution.

The initial sharp, or delta pulse, will be spread out in the tube due to the convective and molecular diffusive forces acting upon it. In the absence of diffusion, solute particles close to the wall will essentially remain at the point of injection due to the no slip conditions present. Conversely, solute particles in the centre of the flow will progress through the tube fastest. Molecular diffusion will act to spread out these solute particles from high to low concentration. At the wall radial diffusion will have the effect to transport solute from the boundary layer into the faster flowing lamina further towards the centre of the tube. At the centre of the flow, particles will diffuse radially outwards into slower flowing lamina.

After a certain time after the injection is made the initial sharp pulse will adopt Gaussian shape. This Gaussian curve can then be interpreted to calculate the diffusion coefficient of interest [52, 53]. Taylor showed that axial diffusion can indeed be neglected if:

$$\frac{L}{v} \geq \frac{2R^2}{\left(3.8\right)^2 D_{AB}} . \tag{2-8}$$

Here, L is the length of the tube of internal radius R, v is the solvent mean superficial linear velocity and D_{AB} is the binary diffusion coefficient corresponding to the solute and solvent. The Taylor dispersion technique has previously been used to determine the diffusion coefficient of gases in aqueous [54] and organic solvents [55, 56]. This is a relatively quick method, due to the imposition of convection on diffusive transport [57], and accurate experiment. Only the NMR method allows measurements over similarly short time scales [1]. It also readily lends itself to the analysis of the diffusion of species in multicomponent systems [58-61]. It allows measurements to be performed under extreme conditions of temperature and pressure [62, 63] and has been previously used for gases diffusing in liquids [64]. Unlike many other techniques, the TDM also does not require knowledge of solubility data of the solute-solvent system [65]. As the concentration of the solute is not a critical parameter for the TDM it also makes it a very appealing choice when investigating gases that are only sparingly soluble in the solvent of interest.

The equipment used in the Taylor dispersion method (see Figure 2-7) is similar to that of High-Performance Liquid Chromatography (HPLC). The primary difference is as opposed to a HPLC where a matrix of components is separated due to their respective affinity for a solid bed of particles in the flow path, the TDA consists of an inert hollow capillary where a quantifiable dispersive behaviour occurs.

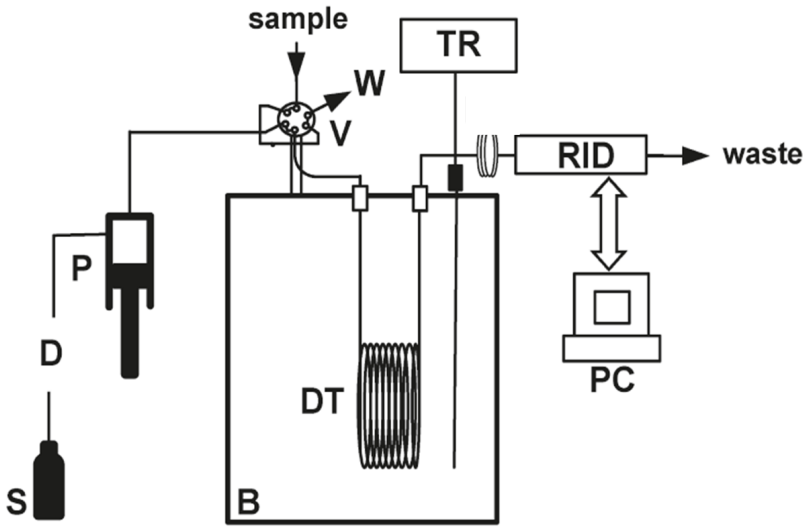

Figure 2-7: Basic diagram of the physical components of a Taylor dispersion apparatus [54].
A mobile phase **S**, e.g. water, is pumped, via **P**, through a vacuum degasser, **D**, a two-position valve **V**, a diffusion column, **DT**, housed in a thermostat, **B**, and subsequently a detector **RID**, e.g. a refractive index meter or conductivity meter. Sample of the solvent containing an excess of solute is fed to waste, **W**, and intermittently injected into the solvent at discrete times to ensure there is no overlapping of eluting solution.

Several constraints should be implemented to perform Taylor's technique as a consistent analytical technique for the determination of diffusion coefficients in liquid systems [66-69]. These constraints are largely concerned with the flow rate variable.

The Taylor Dispersion Technique: Flow Regime

The model proposed by Taylor assumed dispersion occurs in a straight tube, however, the tube is often coiled to increase its compactness [70]. In the case of laminar flow of a fluid through a cylindrical tube, the axis of which forms a small helical pitch, the primary flow field is accompanied by a secondary flow field which acts in a plane perpendicular to the tube [71, 72]. This secondary flow acts to increase mass transfer. To ensure secondary flow effects are negligible it is recommended that the product of the Dean number squared and the Schmidt number, De^2Sc, is kept less than twenty [68]. However, this is not a concrete value and for values of De^2Sc that are less than 100 may be no significant difference between a coiled column and a straight tube [68, 69, 72].

$$De = Re\sqrt{R/R_{coil}} \tag{2-9}$$

$$Sc = \eta/\rho D \tag{2-10}$$

Based on the De^2Sc number for sufficiently low solvent velocities the apparent diffusion coefficient will obtain a constant value that is the true diffusion value [64].
The Taylor Dispersion Method is based on laminar flow in a tube. The criterion that must be met for this regime is that the Reynolds number, $Re = \rho 2Rv/\eta$ must be in the range of 1.3 to 24 [63, 68]. If the flow regime is turbulent there will be additional mixing than that ascribed to diffusion. The mathematical treatment of such a scenario would not be satisfactory to produce reliable results. However, even for Reynold numbers far below the transition of flow from laminar to turbulent, increasing the value of *Re* can aggravate secondary flow in curved channels [68].
Further practical considerations will be discussed in further detail in the subsequent chapter.

The Taylor Dispersion Technique: Analysis

The concentration profile of an arbitrary solution is shown in Figure 2-8. Numerous methods exist for mathematical analysis of this obtained signal for the determination of the diffusion coefficient.

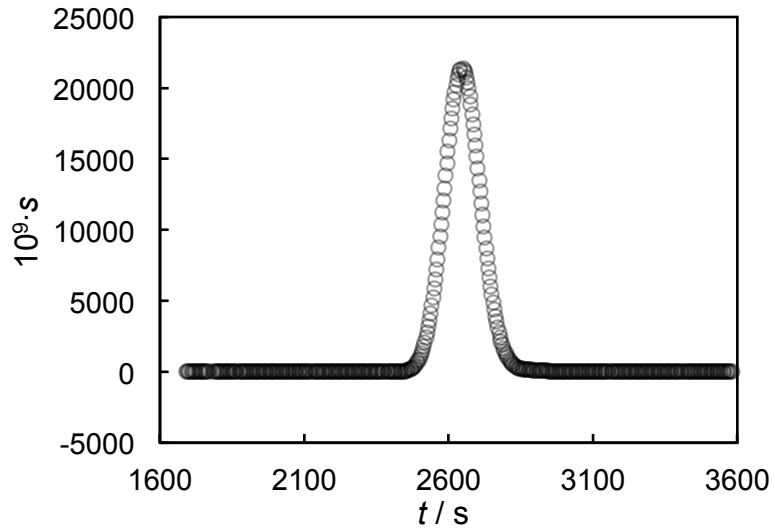

Figure 2-8: Observed dispersion profile, measured in terms of refractive index, *s*, plotted against time since injection.

These methods include the height-area method, discussed by Min et al. (2007), the peak width at half height [73-76] and moments calculations. The method used in the

current work is based on fitting the diffusion coefficient in order to minimise the difference between the experimental points and the analytical solution of Taylor's equation [63, 77]:

$$c(t) = \left\{ m \Big/ \left(\pi R^2 \sqrt{4\pi K t} \right) \right\} \exp\left[-(L - ut)^2 \Big/ 4Kt \right] \tag{2-11}$$

In Eq. (2-10) m is the mass of solute injected, K is the Taylor dispersion coefficient, L is the effective length of the diffusion column and v is the cross-section averaged axial velocity. The dispersion coefficient is related to the diffusion coefficient as follows [53]:

$$K = D + \frac{R^2 v^2}{48D} \tag{2-12}$$

In certain instances Eq. (2-12) does not strictly hold and modifications have been proposed [68, 69]. Once again, these cases will be discussed in further in the subsequent chapter.

Nuclear Magnetic Resonance: Design

Two main methods are known for measuring diffusion coefficients using nuclear magnetic resonance: analysis of relaxation data and pulsed-field gradient nuclear magnetic resonance (PFG-NMR). The latter is illustrated in Figure 2-9. The relaxation method is not as robust as PFG-NMR as it appears to be based on the incorporation of a Stokes-Einstein relation to calculate the diffusion coefficient, i.e. it is actually the solution viscosity that is being observed. Another issue with the relaxation method is that it is also sensitive to rotational diffusion.

In PFG-NMR, the attenuation of a spin-echo signal resulting from the dephasing of the nuclear spins due to the combination of the translation motion of the spins and the imposition of the spatially well-defined gradient pulses is used to measure motion [78]. This method can be used to measure values over a wide range of temperatures and pressures [79], for example up to 500 MPa by using a Be-Cu or Ti-alloy cell [1]. This technique has been used to measure the diffusion coefficients in carbonated beverages [80] and in a super-cooled sodium chloride solution [81].

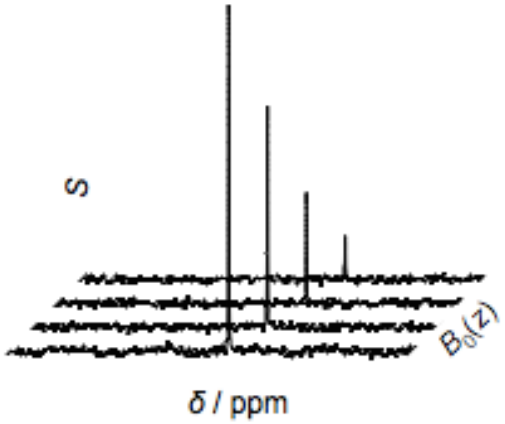

Figure 2-9: NMR signal attenuation, *S*, for a nucleus at various magnetic field gradient strengths, $B_0(z)$, at it's corresponding chemical shift, δ [82].

The Hahn-spin echo technique is a method initially employed to overcome magnetic field inhomogeneity in NMR experiments. Field inhomogeneity causes the precession frequency of the individual atoms in an ensemble to be slightly different from one another, i.e. some atoms precess faster, some slower. This can be easily rationalised from the Larmor equation:

$$\omega_0 = \gamma B_0 \tag{2-13}$$

γ is the gyromagnetic constant of a given isotope and ω_0 is its precession frequency for a given applied magnetic field, B_0.

However, by applying a sufficient torque, in the form of a radio frequency (r.f.) pulse, to rotate the atoms through 180°, effectively turn the spins upside down, the sign of the precession reverses and the spins refocus, or approach a maximum magnetic moment vector, as the spins realign. This torque is simply applied by increasing the torque used to move the atoms from being aligned with the magnetic field to being normal to it by a factor of 2. That is, an initial 90° or π/2 pulse is followed up by a subsequent 180° or π pulse. In the presence of a homogeneous magnetic field the spins fully refocus and a maximum signal is observed when they do. The length of time taken for the spins to realign or come back into phase is equal to the time between the first and second pulse.

However, if a gradient magnetic field is applied, e.g. in the z-axis or longitudinal to the constant magnetic field, the Larmor frequency will be a function of distance in the *z*-axis. That is the spins can be spatially labelled. It can be envisaged that the precession rate will be higher at the origin of the gradient, where B_0 is slightly higher, and lower further away from the magnetic source. In the absence of diffusion the effects of the two applied gradients cancel. However, if the sample experiences

translational diffusion the magnetic field experienced by a given spin is no longer constant in time, i.e. as the molecule moves in the applied gradient the Larmor frequency or precession rate varies. When the sign of the precession is switched the precession will still be affected by a novel magnetic environment.

The lack of ability for the spins to realign, i.e. the magnetic moment vector to refocus, due to attenuation by the combined effect of translational movement and a magnetic gradient causes dephasing, resulting in a diminished signal.

There are several reported advantages to applying the gradients as pulses; if the gradient were applied throughout a measurement there would be line width broadening and the r.f. pulse would have to be increased to cope with a gradient-broadened spectrum. Also, as the gradient is applied in pulses it is (normally) possible to separate the effects of diffusion from spin-spin relaxation. However, other authors have suggested using a constant field gradient produces better results and larger attenuation [83]. The steps involved in a PFG-NMR method are illustrated in Figure 2-10.

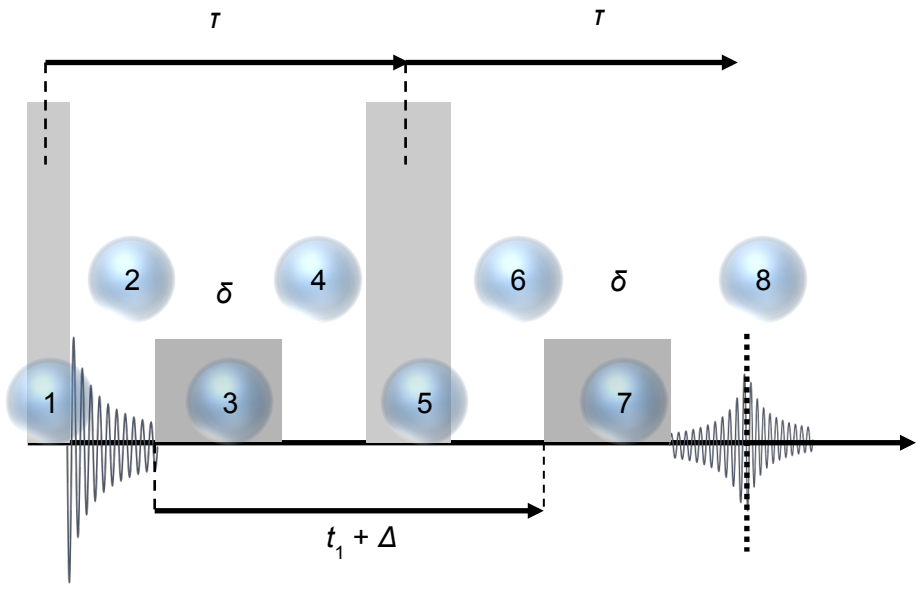

Figure 2-10: Time profile abstraction of a PFG NMR experiment.
At Step 1: A $\pi/2$ r.f. pulse is applied to act as a torque, moving the precession from the z-axis to the x-y axis. This makes the precession observable; Step 2: As the spins return from the excited phase to being aligned with the magnetic field, observed precession decreases.
Note: The amplitude of the signal 2 is greater than in 8, i.e. the signal from 8 is attenuated. Step 3: A magnetic gradient is applied for δ s. This causes the precession frequencies to be a function of distance along the z-axis; Step 5: At τ a π r.f. pulse is applied to act as a torque, rotating the precession 180°

about the x-y plane. This will cause the spins to realign and give a higher signal at time 2τ; Step 7: A magnetic field is applied for δ s. In the absence of diffusion this effectively cancels out the previous magnetic gradient pulse, 3, as while the sign of this gradient is the same, the signs of the precessions have reversed; and Step 8: The free induction decay, FID, is recorded (right side) after the spins refocus (left side).

The NMR method is capable of measuring self and intra-diffusion coefficients [84] and effective diffusion coefficients can be translated into intra-diffusion coefficients [61]. It should also be theoretically possible to measure inter-diffusion coefficients if individual species are labelled with different NMR active probes.

Nuclear Magnetic Resonance: Analysis

Mathematically the signal observed from a NMR experiment operated in the Hahn-spin echo technique is [85, 86]:

$$S(2\tau) = S(2\tau)_{g=0} \int_{-\infty}^{\infty} P(\varphi,2\tau) e^{i\varphi} d\varphi \tag{2-14}$$

$S(2\tau)$ is the normalised intensity (i.e. of attenuation) of the echo signal at $t = 2\tau$, $S(2\tau)_{g=0}$ is the signal in the absence of a field gradient and $P(\varphi,2\tau)$ is the relative phase distribution function. $P(\varphi,2\tau)$ is a normalised function, therefore $S(2\tau)$ is always less than the possible maximum when g is applied. φ is the phase shift, which at $t = 2\tau$; is given by:

$$\varphi_i(2\tau) = \left\{ \gamma B_0 \tau + \gamma g \int_{t_1}^{t_1+\delta} z_i(t) dt \right\} - \left\{ \gamma B_0 \tau + \gamma g \int_{t_1+\Delta}^{t_1+\Delta+\delta} z_i(t') dt' \right\} \tag{2-15}$$

This is simply the difference between the phase shift resulting from the first r.f. pulse and the second.

The exponential relaxation of this signal can then be related to the diffusion coefficient:

$$\ln\left[\frac{S(2\tau)}{S(0)}\right] = -\gamma^2 g^2 \delta^2 \left(\Delta - \delta/3\right) D \tag{2-16}$$

Hence, by performing an experiment where the intensity of an NMR signal is measured repeatedly to get an average displacement the diffusion coefficient of the probe can be calculated. The accuracy of this technique has been reported to be between (1 and 2)% [1].

There are also solutions available when there is net movement of the fluid and when this is coupled with 3-dimensional field gradients further informatin such as the structure of the system confining the probe species can be determined, as in the case of magnetic resonance imaging (MRI).

Modelling of Diffusion Coefficients

Hydrodynamic Approach and the Stokes-Einstein Equation

The Stokes-Einstein model is one of the earlier attempts at a predictive model not solely based on experimentally determined correlations. The underlying premise of the hydrodynamic theory of diffusion is that the system of interest can be considered from a macroscopic perspective. Conceptually, this model treats a large solute molecule moving slowly through a continuum with viscosity acting to reduce the magnitude of the solutes translational motion.

Einstein proposed the net velocity of a sphere moving through a continuous media was proportional to the force acting on it. This force was taken to be the negative of the chemical potential gradient [87], i.e.:

$$-\nabla\mu_1 = \left(n_{SE}\pi\eta a_0\right)\mathbf{v}_1 \tag{2-17}$$

For an ideal, dilute system the chemical potential of component *i* can be written as the sum of the standard chemical potential and the contributions of the individual components:

$$\mu_1 = \mu_1^0 + kT\ln\frac{c_1}{c_1+c_2} \doteq \mu_1^0 + kT\ln c_1 - kT\ln c_2 \tag{2-18}$$

Under the reasonable assumption that the concentration of the solute,c_1, is far lower than the concentration of the solvent, c_2, it holds that:

$$\nabla\mu_1 = \left(kT/c_1\right)\nabla c_1 \tag{2-19}$$

Therefore:

$$\mathbf{j}_1 = \mathbf{n}_1 = c_1\mathbf{v}_1 = -\frac{kT}{n_{SE}\pi\eta a_0}\nabla c_1 \tag{2-20}$$

In this treatment the flux is assumed to vary with the chemical potential gradient. However, this is known not to be the case for non-ideal mixtures near the critical point [87].

By analogy with Fick's first law of diffusion, Eq. (1-5), the diffusion coefficient can be extracted from Eq. (2-20) to produce the Stokes-Einstein equation to calculate the diffusion coefficient:

$$D = kT/\left(n_{SE}\pi\eta_B a_0\right) \tag{2-21}$$

Here k is the Boltzmann constant, T is the absolute temperature, η is the kinematic viscosity, a is the hydrodynamic radius of the solute in the solvent and n_{SE} is the dimensionless Stokes-Einstein number, which comes from the solution of Stokes model for a body falling through a continuous medium. Values for n_{SE} of 4 when the sizes of the solute and solvent are of a similar size, i.e. slip condition, and 6 when the solute molecules are relatively large compared to the solvent molecules are commonly reported, i.e. non-slip condition [3]. Models have been proposed for non-spherical solutes [88]. There are no widely accepted predictive methods for determining the value of a. The difficulty in producing such a model is also hampered by the fact the hydrodynamic radius is also dependent on the solvent species.

A generic modification of Eq. (2-21) is to group the diffusion coefficient, temperature, and viscosity together and assume that the remaining coefficients approximate to a constant, c.

$$D_{AB}\eta_B/T = c \tag{2-22}$$

For example, c has been reported to be 5.72×10^{-12} kg·m·s^{-2}·K^{-1} for the (CO_2 + H_2O) system [6, 89] where η has the units of mPa. This empirical correlation is based on experimental data [6] by dividing the product of the solvent viscosity and binary diffusion coefficient by the state temperature. The median value over seven temperatures was taken to be the constant of proportionality, c. However, a small but distinguishable trend can be seen in this work between the value calculated and the temperature at which the value was obtained.

Several correlations based on the hydrodynamic model have subsequently been proposed. One widely used model is that of Wilke and Chang [90]:

$$\frac{D_{AB}}{\mathrm{m^2\cdot s^{-1}}} = \frac{7.4\times10^{-8}\left[\phi\left(M_B/\left(\mathrm{g\cdot mol^{-1}}\right)\right)\right]^{1/2}\left(T/\mathrm{K}\right)}{\left(\eta_B/\left(\mathrm{mPa\cdot s}\right)\right)\left(V_A/\left(\mathrm{cm^3\cdot mol^{-1}}\right)\right)^{0.6}} \tag{2-23}$$

Here, M_B is the molar mass of the solvent, V_A is the molar volume of the solute at its normal boiling point and ϕ is the solvent association factor. The authors recommend using for ϕ a value of 2.6 when the solvent is water, 1.9 when methanol, 1.5 when ethanol, and 1 when modelling an un-associated solvent [88]. However, this method can only be used as a correlation in the determination of diffusion coefficient when CO_2 is a solute. CO_2 sublimes at atmospheric pressure and hence a parameter to replace V_A has to be fitted. This model cannot be used when water is the solute [88].

It is most suitable for dilute solutions and only non-electrolyte based solutions. Hence, this correlation, as it stands, is not adequate for determining diffusion coefficients in brine solutions.

A two-step empirical correlation for estimating diffusivities of gases in non-electrolytes has been reported. This method involves firstly predicting the value of D at T = 298 K and then using this value to calculate D at the specific temperature through an exponential relationship [91].

$$D_{12}^{298\mathrm{K}} = 6.02\times10^{-5} V_2^{0.36} \Big/ \left(\eta_2^{0.61} V_1^{0.64}\right) \tag{2-24}$$

Here V_i corresponds to the molar volumes of the solute (1) and solvent (2) at their normal boiling points.

$$D_{AB} = 4.996\times10^{3} D_{12}^{298\mathrm{K}} \exp\left\{-2539\ \mathrm{K}/T\right\} \tag{2-25}$$

The results obtained from this model are comparable with those obtained from the Wilke-Chang correlation based on a selection of organic and non-organic solutes and solvents. Further treatment of these models has been discussed in several works [88, 92].

Rough Hard Sphere Theory

Basis

In many theories of thermodynamic behaviour a molecule is treated as made up of simple geometrical shapes, usually spheres bonded together, i.e. tangentially joined as “rigid spheres”. In this current treatment of kinetic theory a molecule can be treated as a single spherical body. For an infinitely dilute single species gas, the diffusion coefficient is given by the low density Boltzmann self-diffusion coefficient, D^0:

$$D^0 = \frac{3}{8n\sigma^2}\sqrt{\frac{kT}{\pi m}} \tag{2-26}$$

Here, n is the number density of the particles with a molecular diameter σ and a molecular mass m, k is the Boltzmann constant and T is the absolute temperature.

This equation is slightly modified from the exact representation proposed by Enskog [88]; here the reduced collision integral, Ω_B,/$\pi\sigma^2$ and a correction factor f_D, usually 1, have been omitted for simplicity. In place of these parameters, which are based on the intermolecular force, the subsequent discussion will follow the available literature

in this topic, and adjust the diffusion coefficient predicted from Enskog's theory through a series of scaling factors.

For a binary system Eq. (2-26) can be corrected by incorporating an arithmetic mean of the core diameters at contact for σ_{12} and a geometric mean for the molecular masses, m_{12} [93].

For a gas system at a finite density Eq. (2-26) also needs to be corrected due to the increased collision frequency. That is, it is necessary to consider the likelihood that at the instance of a collision there is another solvent molecule within a distance r from the solute molecule. As the number of molecules within r from the solute increases the diffusivity will be reduced. This is accounted for through the radial distribution coefficient at contact, $g(\sigma)$ [94, 95].

$$D_E / D_0 = 1 / g_{12}\left(\sigma_{12}\right) \tag{2-27}$$

A selection of algebraic models have been proposed for the calculation of $g_{12}(\sigma_{12})$. This coefficient is often treated as a function of σ, n, and the mole fraction of component i present, x_i [93]:

$$\begin{gathered} g_{12}\left(\sigma\right) = \left[\sigma_1 g_{22}\left(\sigma\right) + \sigma_2 g_{11}\left(\sigma\right)\right] / \left(\sigma_1 + \sigma_2\right) \\ g_{ii}\left(\sigma\right) = \frac{1}{1-x} + \frac{3y_i}{2\left(1-x\right)^2} + \frac{y_i^2}{2\left(1-x\right)^3} \\ x = x_1 + x_2 \\ x_i = \pi n_i \frac{\sigma_i^3}{6} \\ y_i = \left(\sigma_i x_j + \sigma_j x_i\right) / \sigma_j \end{gathered} \tag{2-28}$$

This model corrects for the backscattering effect present at finite densities through relating the radial distribution functions to the compressibility factor by the virial theorem through a linear combination of the analytical solutions of the Percus-Yevick theory [96]. This expression readily simplifies for infinitely dilute binary diffusion [97].

Elevated Densities

The penultimate step in applying a kinetic treatment of the translational motion of an infinitely dilute gas to a dense liquid system is the incorporation of a correction for successive hard sphere collisions. The diffusion coefficient can be up to $1.3D_E$ at

densities from quarter to half the density of close packing [98]. At high densities the diffusion coefficient can be as low as $0.6D_E$ as a result of a backscattering effect [98]. Corrections for these deviations have been sought by incorporating a semi-empirical factor, *C*, in terms of the molar volume and the close packed molar volume [95, 98, 99], based on the diffusivities calculated from molecular dynamics.

$$D_{12} = D_{12}^{RHS} = D_{12}^{0} \frac{1}{g_{12}\left(\sigma_{12}\right)} C\left(\sigma_1, \sigma_2, m_1, m_2, V\right) A_{12} \tag{2-29}$$

$$D = \left[D^0 \Big/ g\left(\sigma\right) \right] \left(D_{HS} \Big/ D_E \right) \tag{2-30}$$

In Eq. (2-30), *D* is the corrected Enskog coefficient and (D_{HS}/D_E) is the ratio of molecular dynamics value to the classical Enskog coefficient.

$$\frac{V}{V_0} \cdot C\left(\sigma_1, m_1, V \Big/ V_0 \right) \cdot \frac{1}{g(\sigma_1)} = a\left[\frac{V}{V_0} - b \right] \tag{2-31}$$

V is the molar volume and V_0 is the hard sphere close-packed volume of the solvent. V_0 is typically calculated from viscosity data [100]. In the absence of information on V_0 the value can also be determined from the core diameter of the solvent.

$$V_0 = N_A \sigma_2^3 \Big/ \sqrt{2} \tag{2-32}$$

Eq. (2-29) was claimed to be valid over a range encompassing the high-density region down to less than one-half the close packing density. This is a similar result to that of other authors who reported an expression for corrected diffusion coefficients up to $1.4V_C$ based on correction incorporating V_0 [85, 99].

Similar corrections for correlated motions are also required when using rough hard sphere theory to calculate other transport properties, e.g. viscosity and thermal conductivity. However, molecular dynamic simulations to predict these values are typically more computationally expensive than those for diffusivity [101].

Inelastic Collisions

Unlike in the case of “rough hard sphere” collisions, there is no rotational or translational coupling for collisions between two smooth spheres i.e. collisions are elastic rather than inelastic. To treat inelastic collisions a coupling factor, *A*, less than or equal to unity, is often incorporated [97, 102]. Even for molecules as spherical as

carbon tetrachloride this coupling factor was found to have a large effect (factor of 2) [102]. A factor to incorporate the deviation from sphericity, R_D, correlated for alkanes based on self-diffusion coefficients has also been proposed [101, 103]. As A is usually a correlated parameter; the effect of coupling and sphericity are lumped together in much of the available literature.

It was also observed that for a given solvent, the slope of A_{12} plotted against temperature was parallel for the different solutes investigated. It was suggested that it is possible to predict tracer diffusion coefficients with knowledge of the solvent's self-diffusion coefficient in binary systems of n-alkanes over the entire temperature range. The value of A has been reported to be independent of temperature over large intervals, (304 to 435) K, and of a similar value for solutes ranging from n-pentane to n-tetradecane [97].

A similar approach is taken when calculating viscosity coefficints [87] however there does not seem to be any consistent trend between the values of the coupling parameters for the two properties [102, 104].

Simplification of the Model

At this point an expression for the diffusion coefficient of an arbitrary solute in a non-electrolyte solvent can be written as:

$$D_{12} = A_{12}\frac{3\sqrt{kT}}{8n\sigma_{12}^2}\sqrt{\left(\frac{m_1+m_2}{2\pi m_1 m_2}\right)}\frac{V_0}{V}\left[a\left(\frac{V}{V_0}-b\right)\right]. \qquad (2\text{-}33)$$

By grouping constants this reduces to [62]:

$$\frac{D_{12}}{\sqrt{T}} = \frac{K}{\sigma_{12}^2}\sqrt{\left(\frac{m_1+m_2}{2\pi m_1 m_2}\right)}\left[a\left(V-bV_0\right)\right] = \beta\left(V-bV_0\right). \qquad (2\text{-}34)$$

As $1/(nV)$ is equal to Avogadro's constant, N_A, K equals $A_{12}\cdot 3(k^{1/2})\cdot a/8N_A$. The β term on the right most is usually treated as temperature and pressure independent; bV_0 is also simplified and designated V_D. For diffusion at infinite dilution, the coefficient β is a function of the solute and solvent interactions, while V_D is a function only of the solvent and represents the molar volume at which diffusivity approaches zero.

The final result is a model in which the diffusion coefficient at a given temperature can be found in terms of the effective free volume of the system.

The volume at which diffusion ceases, V_D, was calculated to be 0.308 times the critical volume of the solvent when systems of $C_{(2n)}H_{2(2n)+2}$, where n = (4 to 8), in n-

heptane and *n*-dodecane were investigated [62]. However it was also found that this term was slightly dependent on the solute involved. These measurements covered a wide range of temperature, (298 to 573) K, and pressure, (0.101 to 3.45) MPa [62]. As the free volume for diffusion approaches zero, smaller solutes will still diffuse more easily that larger molecules and that this is the reason for this observation.

Several correlations based on experimental data have been proposed for β, for example:

$$\beta = aM_1^b \left(\frac{\sigma_1}{\sigma_2} \right)^c \tag{2-35}$$

From Eq. (2-35) and for dissolved gas solutes, a = 1.65 ± 1.11, b = -0.76 ± 0.002 and c = 3.02 ± 0.08 [62]. A second correlation put forwards claims $\beta = 32.88 M_1^{-0.61} V_D^{-1.04}$ [105]. Both these works reported the value of V_D to be correlated as 0.308 times the critical volume of the solvent, V_c.

In both these correlations β is a function of the solute and the solvent, whereas V_D is a parameter specific to the solvent. It is also worth noting that in the dilute region, i.e. $g \sim 1$, and both a and b ~1, then the correction from molecular dynamics is simply the free volume fraction of the solvent at a given state point, i.e. $(1 - V_0/V)$. This application of free volume based corrections to the Boltzman diffusion model based on computational calculations for self and mutual diffusion coefficients has also been derived by other authors [95, 106].

Clearly, one of the earliest limitations that arises in this model is the determination or prediction of σ. The available models to calculate this parameter are rudimentary at best. Often this value is obtained from fitting applicable models to viscosity coefficients. Any assumptions made in the models the data is fitted to will affect the calculated parameters. This is often accepted when calculating parameters from VLE data, for example, to be used in VLE models, as these assumptions effectively cancel out.

It is also assumed that the molecule can be treated as a spherical body. In the field of equilibrium thermodynamics there is a movement away from this assumption. Large non-spherical bodies are broken down into a collection of spherical components tangentially adjacent to one another.

Finally, this treatment emphasises harsh repulsive interactions while assuming any attractive interactions are relatively small. This indicates that due to strong hydrogen bonding molecules like water cannot be satisfactorily treated using this technique. However, it should be noted that other theories such as the statistical associating

fluid theory, SAFT, which were initially used to predict thermodynamic properties of non-polar fluids are being successfully advanced for aqueous systems [107]. This is accomplished by adding a contribution to the Helmholtz free energy summation for the water and ionic components.

Molecular Dynamics

Unlike diffusion coefficients obtained experimentally, which are necessarily Fickian diffusion coefficients, the diffusion coefficients calculated from molecular dynamics are Maxwell-Stefan diffusivities [108]. Several authors have presented results for the diffusivity of CO_2 in various systems calculated from molecular dynamics [108-111], however no literature was found for the diffusion of dilute CO_2 in the hydrocarbons studied in this work was found.

Molecular dynamic simulations calculate thermodynamic and transport properties based on intermolecular potentials. A working definition of molecular dynamics simulation is it is a technique by which atomic trajectories of a system of *N* particles are generated by numerical integration of Newton's equation of motion. The interatomic potential is required along with certain initial and boundary conditions [109].

Self-diffusivities can be calculated from both non-equilibrium and equilibrium molecular dynamic simulations. A typical method to calculate this quantity is:

$$D = \lim_{t \to \infty} \frac{\left\langle \left\langle R_{\text{c.m.}}(t) - R(0) \right\rangle^2 \right\rangle}{6t} \tag{2-36}$$

The contents inside the angle brackets on the right of Eq. (2-36) denote the ensemble average of displacement of the centre of mass of the solute molecule, $R_{\text{c.m.}}$, with respect to the initial position, $R(0)$, as a function of time, t.

Depending on the form of the attractive potential used, e.g. the Lennard-Jones 6-12 potential, different values for the intermolecular potential parameters must be used.

While molecular dynamic models are inherently only as good as the models used for the force fields, e.g. intermolecular force potential and size parameters, notably difficult to describe in the case of water, not only can accurate results be obtained for many systems but it can also be used as an important tool to investigate the behavior of other models. For instance, in the case of the rough hard sphere theory where qualitatively the comparison of results based on the Enskog model of diffusion with MD results have guided the development of arithmetic models for correlating and

predicting diffusion coefficients [98]. The use of molecular dynamics to predict diffusion coefficients will not be discussed further in this work as accessible work exists on this topic [109, 110].

Polarizability-Induced Dipole Moment Based Model

In the scope of this work, it is also worth pointing out that a model for the prediction of diffusion coefficients of H_2O in CO_2 or CO_2 in H_2O, both at infinite dilution, which explicitly includes the polar nature of H_2O and the polarizability of CO_2, has been reported [112]. Water molecules form aggregates due to the permanent dipole moment present in H_2O molecules. This permanent dipole induces a dipole moment in the CO_2 molecules. This is a semi-empirical method based in part on corresponding state theory and incorporates the temperature effect on the polarity of water and induced dipole moment of CO_2.

$$\frac{D_{AB}}{\mathrm{m^2 \cdot s^{-1}}} = \frac{k_1 \left(M_{AB}\mu_{AB}\right)^{k_2} T_\mathrm{r}^{k_3}}{p_\mathrm{r}^{k_4}\left[\left(\eta_B/\left(\mathrm{Pa \cdot s}\right)\right)\left(c_B/\left(\mathrm{mol \cdot m^3}\right)\right)\right]^{k_5}} \tag{2-37}$$

Subscript *A* and *B* refer to the solute and the solvent, respectively, while the subscript r denotes a reduced quantity. The parameter k_i was obtained from non-linear fitting of 180 experimental data points to the model proposed. For the CO_2 water system the values were determined to be; k_1, $10^{-7.23}$; k_2, 1.36×10^{-1}; k_3, 1.84×10^{0}; k_4, 2.42×10^{-3}; and k_5, 8.58×10^{-1}.

The effective mass, M_{AB}, is calculated from the molecular mass, *M*, of the solute, *A*, and solvent, *B*:

$$M_{AB} = \left(\frac{1}{M_A} + \frac{1}{M_B}\right)^{-1} \tag{2-38}$$

The dipole moments of CO_2 and H_2O were calculated as follows [112]:

$$\mu_{AB} = \mu_B / \mu_A \tag{2-39}$$

$$\left(\mu_{\mathrm{H_2O}}/\left(C \cdot m\right)\right) = -1.2142 \times 10^{-32}\left(T/\mathrm{K}\right) + 2.1236\left(\mu_0/\left(\mathrm{C \cdot m}\right)\right) \tag{2-40}$$

$$\mu_{CO_2} = \alpha_{CO_2} E_{field} \tag{2-41}$$

α_{CO2} and E_{field} were calculated from the attractive intramolecular potential and length of the respective molecules.

This model has been fitted to experimentally reported values for the diffusion coefficient of CO_2 in water at infinite dilution and the diffusion coefficient of water in CO_2 at infinite dilution. This approach also reportedly is appropriate for methane, ethane, propane and dihydrogen sulphide.

References

[1] W.A. Wakeham, A. Nagashima, J. Sengers, Measurement of the Transport Properties of Fluids, Blackwell Science, 1991.

[2] F.C. Tse, O.C. Sandall, DIFFUSION COEFFICIENTS FOR OXYGEN AND CARBON DIOXIDE IN WATER AT 25ºC BY UNSTEADY STATE DESORPTION FROM A QUIESCENT LIQUID, Chem. Eng. Commun. 3 (1979) 147-153.

[3] R.B. Bird, W.E. Stewart, E.N. Lightfoot, Transport Phenomena, 2002.

[4] K.K. Tan, R.B. Thorpe, Gas Diffusion into Viscous and Non-Newtonian Liquids, Chem. Eng. Sci. 47 (1992) 3565 - 3572.

[5] A.A. Unver, D.M. Himmelblau, Diffusion Coefficients of CO_2, C_2H_4, C_3H_6 and C_4H_8 in Water from 6° to 65° C, J. Chem. Eng. Data 9 (1964) 428-431.

[6] W.J. Thomas, M.J. Adams, Measurement of the Diffusion Coefficients of Carbon Dioxide and Nitrous Oxide in Water and Aqueous Solutions of Glycerol, T. Faraday Soc. 61 (1965) 668 - 673.

[7] J.K.A. Clarke, Kinetics of Absorption of Carbon Dioxide in Monoethanolamine Solutions at Short Contact Times, Ind. Eng. Chem. Fundam. 3 (1964) 239-245.

[8] H.A. Al-Ghawas, D.P. Hagewiesche, G. Ruiz-Ibanez, O.C. Sandall, Physicochemical Properties Important for Carbon Dioxide Absorption in Aqueous Methyldiethanolamine, J. Chem. Eng. Data 34 (1989) 385-391.

[9] J.M. Diaz, A. Vega, J. Coca, Diffusivities of CO_2 and N_2O in Aqueous Alcohol Solutions, J. Chem. Eng. Data 33 (1988) 10-12.

[10] M.-H. Li, M.-D. Lai, Solubility and Diffusivity of N_2O and CO_2 in (Monoethanolamine+ N-Methyldiethanolamine + Water) and in (Monoethanolamine+ 2-Amino-2-methyl-1-propanol+ Water), J. Chem. Eng. Data 40 (1995) 486-492.

[11] A.K. Saha, S.S. Bandyopadhyay, A.K. Biswas, Solubility and Diffusivity of N_2O and CO_2 in Aqueous Solutions of 2-Amino-2-methyl-1-propanol, J. Chem. Eng. Data 38 (1993) 78-82.

[12] D.M. Himmelblau, DIFFUSION OF DISSOLVED GASES IN LIQUIDS, Chem. Rev. 64 (1964) 527-550.

[13] J.L. Duda, J.S. Vrentas, Laminar Liquid Jet Diffusion Studies, AlChE J. 14 (1968) 286-294.

[14] A.F. Mazarei, O.C. Sandall, Diffusion Coefficients for Helium, Hydrogen, and Carbon Dioxide in Water at 25°C, AlChE J. 26 (1980) 154-157.

[15] R.A.T.O. Nijsing, R.H. Hendriksz, H. Kramers, Absorption of CO_2 in jets and falling films of electrolyte solutions, with and without chemical reaction, Chem. Eng. Sci. 10 (1959) 88-104.

[16] E.J. Cullen, J.F. Davidson, ABSORPTION OF GASES IN LIQUID JETS, T. Faraday Soc. 53 (1957) 113-120.
[17] M.K. Abu-Arabi, A.M. Al-Jarrah, M. El-Eideh, A. Tamimi, Physical Solubility and Diffusivity of CO_2 in Aqueous Diethanolamine Solutions, J. Chem. Eng. Data 46 (2001) 516-521.
[18] R. Higbie, The rate of absorption of a pure gas into still liquid during short periods of exposure, Trans. Am. Inst. Chem. Eng. (1935).
[19] S. Lynn, J. Straatemeier, H. Kramers, Absorption studies in the light of the penetration theory: I. Long wetted-wall columns, Chem. Eng. Sci. 4 (1955) 49-57.
[20] D. Li, Z. Duan, The speciation equilibrium coupling with phase equilibrium in the H_2O–CO_2–NaCl system from 0 to 250°C, from 0 to 1000 bar, and from 0 to 5 molality of NaCl, Chem. Geol. 244 (2007) 730-751.
[21] M.-H. Li, W.-C. Lee, Solubility and Diffusivity of N_2O and CO_2 in (Diethanolamine + N-Methyldiethanolamine + Water) and in (Diethanolamine + 2-Amino-2-methyl-1-propanol + Water), J. Chem. Eng. Data 41 (1996) 551 - 556.
[22] A. Tamimi, E.B. Rinker, O.C. Sandall, Diffusion Coefficients for Hydrogen Sulfide, Carbon Dioxide, and Nitrous Oxide in Water over the Temperature Range 293-368 K, J. Chem. Eng. Data 39 (1994) 330-332.
[23] S.R. Upreti, A.K. Mehrotra, Diffusivity of CO_2, CH_4, C_2H_6 and N_2 in Athabasca Bitumen, Can. J. Chem. Eng. 80 (2002) 116-125.
[24] L.-S. Wang, Z.-X. Lang, T.-M. Guo, MEASUREMENT AND CORRELATION OF THE DIFFUSION COEFFICIENTS OF CARBON DIOXIDE IN LIQUID HYDROCARBONS UNDER ELEVATED PRESSURES, Fluid Phase Equilib. 117 (1996) 364-372.
[25] A.K. Tharanivasan, C. Yang, Y. Gu, Measurements of Molecular Diffusion Coefficients of Carbon Dioxide, Methane, and Propane in Heavy Oil Under Reservoir Conditions, Energy Fuel. 20 (2006) 2509-2517.
[26] M.L. Rasmussen, F. Civan, Parameters of Gas Dissolution in Liquids Obtained by Isothermal Pressure Decay, AIChE J. 55 (2009) 9-23.
[27] H.H. Reamer, J.B. Opfell, B.H. Sage, Diffusion Coefficients in Hydrocarbon Systems Methane-Decane-Methane in Liquid Phase, Ind. Eng. Chem. 48 (1956) 275-282.
[28] L.-S. Wang, C.-Y. Sun, Diffusion of Carbon Dioxide in Tetradecane, J. Chem. Eng. Data 42 (1997) 1181-1186.
[29] P. Guo, Z. Wang, P. Shen, J. Du, Molecular Diffusion Coefficients of the Multicomponent Gas−Crude Oil Systems under High Temperature and Pressure, Ind. Eng. Chem. Res. 48 (2009) 9023-9027.

[30] F. Ciotta, G. Maitland, M. Smietana, J.P.M. Trusler, V. Vesovic, Viscosity and Density of Carbon Dioxide+ 2, 6, 10, 15, 19, 23-Hexamethyltetracosane (Squalane), J. Chem. Eng. Data 54 (2009) 2436-2443.
[31] M. Jamialahmadi, M. Emadi, H. Müller-Steinhagen, Diffusion coefficients of methane in liquid hydrocarbons at high pressure and temperature, J. Pet. Sci. Eng. 53 (2006) 47-60.
[32] C. Yang, Y. Gu, New Experimental Method for Measuring Gas Diffusivity in Heavy Oil by the Dynamic Pendant Drop Volume Analysis (DPDVA), Ind. Eng. Chem. Res. 44 (2005) 4474-4483.
[33] C. Yang, Y. Gu, Diffusion coefficients and oil swelling factors of carbon dioxide, methane, ethane, propane, and their mixtures in heavy oil, Fluid Phase Equilib. 243 (2006) 64-73.
[34] R.J. Littel, G.F. Versteeg, W.P. Van Swaaij, Diffusivity Measurements in Some Organic Solvents by a Gas-Liquid Diaphragm Cell, J. Chem. Eng. Data 37 (1992) 42-45.
[35] B. Jähne, G. Heinz, W. Dietrich, Measurement of the Diffusion Coefficients of Sparingly Soluble Gases in Water, J. Geophys. Res. Oceans 92 (1987) 10767-10776.
[36] M. Takahashi, Y. Kobayashi, H. Takeuchi, Diffusion Coefficients and Solubilities of Carbon Dioxide in Binary Mixed Solvents, J. Chem. Eng. Data 27 (1982) 328-331.
[37] D.G. Miller, The History of Interferometry for Measuring Diffusion Coefficients, J. Solution Chem. 43 (2014) 6-25.
[38] H. Fujita, L.J. Gosting, An Exact Solution of the Equations for Free Diffusion in Three-component Systems with Interacting Flows, and its Use in Evaluation of the Diffusion Coefficients, J. Am. Chem. Soc. 78 (1956) 1099-1106.
[39] H. Fujita, L.J. Gosting, A NEW PROCEDURE FOR CALCULATING THE FOUR DIFFUSION COEFFICIENTS OF THREE-COMPONENT SYSTEMS FROM GOUY DIFFUSIOMETER DATA1, J. Phys. Chem. 64 (1960) 1256-1263.
[40] D.G. Miller, A.W. Ting, J.A. Rard, L.B. Eppstein, Ternary diffusion coefficients of the brine systems NaCl (0.5 M)-Na_2SO_4 (0.5 M)-H_2O and NaCl (0.489 M)-$MgCl_2$ (0.051 M)-H_2O (seawater composition) at 25° C, Geochim. Cosmochim. Acta. 50 (1986) 2397-2403.
[41] D.G. Miller, The Validity of Onsager's Reciprocal Relations in Ternary Diffusion, J. Phys. Chem. 62 (1958) 767-767.
[42] D.G. Miller, TERNARY ISOTHERMAL DIFFUSION AND THE VALIDITY OF THE ONSAGER RECIPROCITY RELATIONS, J. Phys. Chem. 63 (1959) 570-578.

[43] D.G. Miller, A Method for Obtaining Multicomponent Diffusion Coefficients Directly from Rayleigh and Gouy Fringe Position Data, J. Phys. Chem. 92 (1988) 4222-4226.

[44] W. Lu, H. Guo, I. Chou, R. Burruss, L. Li, Determination of diffusion coefficients of carbon dioxide in water between 268 and 473K in a high-pressure capillary optical cell with in situ Raman spectroscopic measurements, Geochim. Cosmochim. Acta 115 (2013) 183-204.

[45] M. Jimenez, N. Dietrich, A. Cockx, Experimental Study of O_2 Diffusion Coefficient Measurement at a Planar Gas–Liquid Interface by Planar Laser-Induced Fluorescence with Inhibition, AIChE J. 59 (2013) 325-333.

[46] A. Sell, H. Fadaei, M. Kim, D. Sinton, Measurement of CO_2 Diffusivity for Carbon Sequestration: A Microfluidic Approach for Reservoir-Specific Analysis, Environ. Sci. Technol. 47 (2012) 71-78.

[47] B.P. Mandal, M. Kundu, N.U. Padhiyar, S.S. Bandyopadhyay, Physical Solubility and Diffusivity of N_2O and CO_2 into Aqueous Solutions of (2-Amino-2-methyl-1-propanol+ Diethanolamine) and (N-Methyldiethanolamine+ Diethanolamine), J. Chem. Eng. Data 49 (2004) 264-270.

[48] B.P. Mandal, M. Kundu, S.S. Bandyopadhyay, Physical Solubility and Diffusivity of N_2O and CO_2 into Aqueous Solutions of (2-Amino-2-methyl-1-propanol+ Monoethanolamine) and (N-Methyldiethanolamine+ Monoethanolamine), J. Chem. Eng. Data 50 (2005) 352-358.

[49] G.F. Versteeg, W. Van Swaalj, Solubility and Diffusivity of Acid Gases (CO_2, N_2O) in Aqueous Alkanolamine Solutions, J. Chem. Eng. Data 33 (1988) 29-34.

[50] J. Ying, D.A. Eimer, Measurements and Correlations of Diffusivities of Nitrous Oxide and Carbon Dioxide in Monoethanolamine+ Water by Laminar Liquid Jet, Ind. Eng. Chem. Res. 51 (2012) 16517-16524.

[51] A. Tang, O.C. Sandall, Diffusion Coefficient of Chlorine in Water at 25-60 ºC, J. Chem. Eng. Data 30 (1985) 189-191.

[52] G. Taylor, Dispersion of soluble matter in solvent flowing slowly through a tube, Proc. R. Soc. London. Series A. 219 (1953) 186-203.

[53] R. Aris, On the dispersion of a solute in a fluid flowing through a tube, Proc. R. Soc. London. Series A. 235 (1956) 67-77.

[54] S.P. Cadogan, G.C. Maitland, J.P.M. Trusler, Diffusion Coefficients of CO_2 and N_2 in Water at Temperatures between 298.15 K and 423.15 K at Pressures up to 45 MPa, J. Chem. Eng. Data 59 (2014) 519-525.

[55] E.D. Snijder, M.J.M. te Riele, G.F. Versteeg, W.P. van Swaaij, Diffusion Coefficients of CO, CO_2, N_2O, and N_2 in Ethanol and Toluene, J. Chem. Eng. Data 40 (1995) 37-39.
[56] M.A. Matthews, J.B. Rodden, A. Akgerman, High-Temperature Diffusion of Hydrogen, Carbon Monoxide, and Carbon Dioxide in Liquid n-Heptane, n-Dodecane, and n-Hexadecane, J. Chem. Eng. Data 32 (1987) 319-322.
[57] W. Baldauf, H. Knapp, MEASUREMENT OF DIFFUSIVITIES IN LIQUIDS BY THE DISPERSION METHOD, Chem. Eng. Sci. 38 (1983) 1031-1037.
[58] D.G. Leaist, Ternary Diffusion Coefficients of 18-Crown-6 Ether–KCl–Water by Direct Least-Squares Analysis of Taylor Dispersion Measurements, J. Chem. Soc., Faraday Trans. 87 (1991) 597-601.
[59] W.E. Price, Theory of the Taylor Dispersion Technique for Three-component-system Diffusion Measurements, J. Chem. Soc., Faraday Trans. 1. 84 (1988) 2431-2439.
[60] D.G. Leaist, P.A. Lyons, Electrolyte Diffusion in Multicomponent Solutions, J. Phys. Chem. 86 (1982) 564-571.
[61] Z. Deng, D.G. Leaist, Ternary mutual diffusion coefficients of $MgCl_2$+ $MgSO_4$+ H_2O and Na_2SO_4+ $MgSO_4$+ H_2O from Taylor dispersion profiles, Can. J. Chem. 69 (1991) 1548-1553.
[62] M.A. Matthews, A. Akgerman, Diffusion Coefficients for Binary Alkane Mixtures to 573 K and 3.5 MPa, AIChE J. 33 (1987) 881-885.
[63] C. Secuianu, G.C. Maitland, J.P.M. Trusler, W.A. Wakeham, Mutual Diffusion Coefficients of Aqueous KCl at High Pressures Measured by the Taylor Dispersion Method, J. Chem. Eng. Data 56 (2011) 4840-4848.
[64] M.J.W. Frank, J.A.M. Kuipers, W.P.M. van Swaaij, Diffusion Coefficients and Viscosities of CO_2+ H_2O, CO_2+ CH_3OH, NH_3+ H_2O, and NH_3+ CH_3OH Liquid Mixtures, J. Chem. Eng. Data 41 (1996) 297-302.
[65] K.C. Pratt, D.H. Slater, W.A. Wakeham, A rapid method for the determination of diffusion coefficients of gases in liquids, 28 Chem. Eng. Sci. (1973) 1901 - 1903.
[66] A.A. Alizadeh, W.A. Wakeham, Mutual Diffusion Coefficients for Binary Mixtures of Normal Alkanes, Int. J. Thermophys. 3 (1982) 307 - 323.
[67] A. Alizadeh, C.A. Nieto De Castro, W.A. Wakeham, The Theory of the Taylor Dispersion Technique for Liquid Diffusivity Measurements, Int. J. Thermophys. 1 (1980) 243-284.
[68] R.J. Nunge, T.S. Lin, W.N. Gill, Laminar dispersion in curved tubes and channels, J. Fluid Mech. 51 (1972) 3-5.

[69] M.E. Erdogan, P. Chatwin, The effects of curvature and buoyancy on the laminar dispersion of solute in a horizontal tube, J. Fluid Mech 29 (1967) 465-484.
[70] J.A. Moulijn, R. Spijker, J.F.M. Kolk, Axial dispersion of gases flowing through coiled columns, J. Chromatogr. 142 (1977) 155 - 166.
[71] A.N. Dravid, K.A. Smith, E.W. Merrill, P.L.T. Brian, Effect of Secondary Fluid Motion on Laminar Flow Heat Transfer in Helically Coiled Tubes, AIChE J. 17 (1971) 1114-1122.
[72] L.A.M. Janssen, AXIAL DISPERSION IN LAMINAR FLOW THROUGH COILED TUBES, Chem. Eng. Sci. 31 (1976) 215-218.
[73] E. Grushka, E.J. Kikta Jr, Extension of the Chromatographic Broadening Method of Measuring Diffusion Coefficients to Liquid Systems. I. Diffusion Coefficients of Some Alkylbenzenes in Chloroform, J. Phys. Chem. 78 (1974) 2297-2301.
[74] R. Callendar, D.G. Leaist, Diffusion coefficients for Binary, Ternary, and Polydisperse Solutions from Peak-Width Analysis of Taylor Dispersion Profiles, J. Solution Chem. 35 (2006) 353-379.
[75] M. Zou, Y. Han, L. Qi, Y. Chen, Fast and accurate measurement of diffusion coefficient by Taylor's dispersion analysis, Chin. Sci. Bull. 52 (2007) 3325-3332.
[76] T. Yonezawa, T. Tominaga, N. Toshima, Novel Characterization of the Structure of Surfactants on Nanoscopic Metal Clusters by a Physicochemical Method, Langmuir 11 (1995) 4601-4604.
[77] L.M.J.J. van der Ven-Lucassen, F.G. Kieviet, P.J.A.M. Kerkhof, Fast and Convenient Implementation of the Taylor Dispersion Method, J. Chem. Eng. Data 40 (1995) 407 - 411.
[78] W.S. Price, Pulsed-Field Gradient Nuclear Magnetic Resonance as a Tool for Studying Translational Diffusion: Part 1. Basic Theory, Concept. Magnetic Res. 9 (1997) 299-336.
[79] K.R. Harris, P.J. Newitt, Self Diffusion of Water at Low Temperatures and High Pressure, J. Chem. Eng. Data 42 (1997) 346 - 348.
[80] G. Liger-Belair, E. Prost, M. Parmentier, P. Jeandet, J.-M. Nuzillard, Diffusion Coefficient of CO_2 Molecules as Determined by ^{13}C NMR in Various Carbonated Beverages, J. Agric. Food Chem. 51 (2003) 7560-7563.
[81] P. Garbacz, W.S. Price, ^{1}H NMR Diffusion Studies of Water Self-Diffusion in Supercooled Aqueous Sodium Chloride Solutions, J. Phys. Chem. A (2014).
[82] S.P. Cadogan, J.P. Hallett, G.C. Maitland, J.P.M. Trusler, Diffusion Coefficients of Carbon Dioxide in Brines Measured Using ^{13}C Pulsed-Field Gradient Nuclear Magnetic Resonance, J. Chem. Eng. Data 60 (2014) 181-184.

[83] D. Le Bihan, Molecular Diffusion Nuclear Magnetic Resonance Imaging, Magn. Reson. Quart. 7 (1991) 1-30.
[84] P. Stilbs, FOURIER TRANSFORM PULSED-GRADIENT SPIN-ECHO STUDIES OF MOLECULAR DIFFUSION, Prog. Nucl. Magn. Reson. Spectrosc. 19 (1987) 1-45.
[85] H.Y. Carr, E.M. Purcell, Effects of Diffusion on Free Precession in Nuclear Magnetic Resonance Experiments, Phys. Rev. 94 (1954) 630-638.
[86] D.C. Douglass, D.W. McCall, Diffusion in paraffin hydrocarbons, J. Phys. Chem. 62 (1958) 1102-1107.
[87] E.L. Cussler, Diffusion: Mass Transfer in Fluid Systems, Cambridge University Press 2009.
[88] B.E. Poling, J.M. Prausnitz, J.P. O'Connell, R.C. Reid, The Properties of Gases and Liquids, 5 ed. McGraw-Hill, New York 2001.
[89] A.T. Grogan, W.V. Pinczewski, The Role of Molecular Diffusion Processes in Tertiary CO_2 Flooding, J. Petrol. Technol. 39 (1987) 591-602.
[90] C.R. Wilke, P. Chang, CORRELATION OF DIFFUSION COEFFICIENTS IN DILUTE SOLUTIONS, AIChE J. 1 (1955) 264-270.
[91] M. Díaz, A. Vega, J. Coca, CORRELATION FOR THE ESTIMATION OF GAS-LIQUID DIFFUSIVITY, Chem. Eng. Commun. 52 (1987) 271-281.
[92] H. Li, Ø. Wilhelmsen, Y. Lv, W. Wang, J. Yan, Viscosities, thermal conductivities and diffusion coefficients of CO_2 mixtures: Review of experimental data and theoretical models, Int. J. Greenhouse Gas Control 5 (2011) 1119-1139.
[93] J.H. Dymond, Limiting Diffusion in Binary Nonelectrolyte Mixtures, J. Phys. Chem. 85 (1981) 3291-3294.
[94] J.H. Dymond, B.J. Alder, Van der Waals Theory of Transport in Dense Fluids, J. Chem. Phys. 45 (1966) 2061-2068.
[95] J.H. Dymond, Corrected Enskog theory and the transport coefficients of liquids., J. Chem. Phys. 60 (1974) 969 - 973.
[96] B.J. Alder, W.E. Alley, J.H. Dymond, Studies in molecular dynamics. XIV. Mass and size dependence of the binary diffusion coefficient, J. Chem. Phys. 61 (1974) 1415-1420.
[97] C. Erkey, A. Akgerman, Translational-Rotational Coupling Parameters for Mutual Diffusion in N-Octane, AIChE J. 35 (1989) 443-448.
[98] B.J. Alder, D.M. Gass, T.E. Wainwright, Studies in Molecular Dynamics. VIII. The Transport Coefficients for a Hard-Sphere Fluid, J. Chem. Phys. 53 (1970) 3813-3826.
[99] J.H. Dymond, Self-diffusion Coefficients in Dense Fluids; the Corrected Enskog Theory, J. Chem. Soc., Faraday Trans. 2. 68 (1972) 1789-1794.

[100] M.J. Assael, J.P.M. Trusler, T.F. Tsolakis, Thermophysical Properties of Fluids, World Scientific 1996.
[101] M.J. Assael, J.H. Dymond, V. Tselekidou, Correlation of High-Pressure Thermal Conductivity, Viscosity, and Diffusion Coefficients for n-Alkanes, Int. J. Thermophys. 11 (1990) 863-873.
[102] D. Chandler, Rough hard sphere theory of the self-diffusion constant for molecular liquids, J. Chem. Phys. 62 (1975) 1358-1363.
[103] M.J. Assael, J.H. Dymond, P.M. Patterson, Correlation and Prediction of Dense Fluid Transport Coefficients. V. Aromatic Hydrocarbons, Int. J. Thermophys. 13 (1992) 895-905.
[104] J.H. Dymond, M.A. Awan, Correlation of High-Pressure Diffusion and Viscosity Coefficients for *n*-Alkanes, Int. J. Thermophys. 10 (1989) 941-951.
[105] M.A. Matthews, A. Akgerman, Hard-sphere theory for correlation of tracer diffusion of gases and liquids in alkanes, J. Chem. Phys. 87 (1987) 2285-2291.
[106] S.H. Chen, H.T. Davis, D.F. Evans, Tracer diffusion in polyatomic liquids. III, J. Chem. Phys. 77 (1982) 2540-2544.
[107] A. Galindo, A. Gil-Villegas, G. Jackson, A.N. Burgess, SAFT-VRE: Phase Behavior of Electrolyte Solutions with the Statistical Associating Fluid Theory for Potentials of Variable Range, J. Phys. Chem. 103 (1999) 10272-10281.
[108] X. Liu, S.K. Schnell, J.-M. Simon, D. Bedeaux, S. Kjelstrup, A. Bardow, T.J.H. Vlugt, Fick Diffusion Coefficients of Liquid Mixtures Directly Obtained From Equilibrium Molecular Dynamics, J. Phys. Chem. 115 (2011) 12921-12929.
[109] J. Li, BASIC MOLECULAR DYNAMICS, Handbook of Materials Modeling, Springer 2005, pp. 565-588.
[110] O.A. Moultos, I.N. Tsimpanogiannis, A.Z. Panagiotopoulos, I.G. Economou, Atomistic Molecular Dynamics Simulations of CO_2 Diffusivity in H_2O for a Wide Range of Temperatures and Pressures, J. Phys. Chem. (2014).
[111] D. Zabala, C. Nieto-Draghi, J.C. de Hemptinne, A.L. López de Ramos, Diffusion Coefficients in CO_2/*n*-Alkane Binary Liquid Mixtures by Molecular Simulation, J. Phys. Chem. 112 (2008) 16610-16618.
[112] J.W. Mutoru, A. Leahy-Dios, A. Firoozabadi, Modeling Infinite Dilution and Fickian Diffusion Coefficients of Carbon Dioxide in water, AIChE J. 57 (2011) 1617-1627.

3. Experimental Device and Operating Procedure

A Taylor Dispersion Apparatus (TDA) was used to measure of the diffusion coefficients of CO_2 in water and in hydrocarbons. To compensate for anomalous behaviour observed while investigating the (CO_2 + H_2O) system, a correction when analysing the dispersion coefficients was incorporated to allow experiments to be carried out at higher flow rates. There was no need to operate at elevated flow rates while investigating the (CO_2 + hydrocarbon) systems.

Due to these experimental issues arising in the (CO_2 + H_2O) system, using the TDA was deemed inappropriate for studying CO_2 diffusivity in brines. Measurements of diffusion coefficients of $^{13}CO_2$ in various brines were therefore performed using pulsed-field gradient nuclear magnetic resonance. The brine under study was slightly under-saturated with $^{13}CO_2$. Data analysis was performed using proprietary Bruker software.

Taylor Dispersion Apparatus

Apparatus

The Taylor dispersion apparatus (TDA) used in this study consisted of four modules: a solvent delivery system with a solution injection valve; a thermostatic oil bath housing the diffusion capillary; a differential refractive-index detector; and a solution preparation vessel. Figure 3-1 is a schematic diagram of this system.

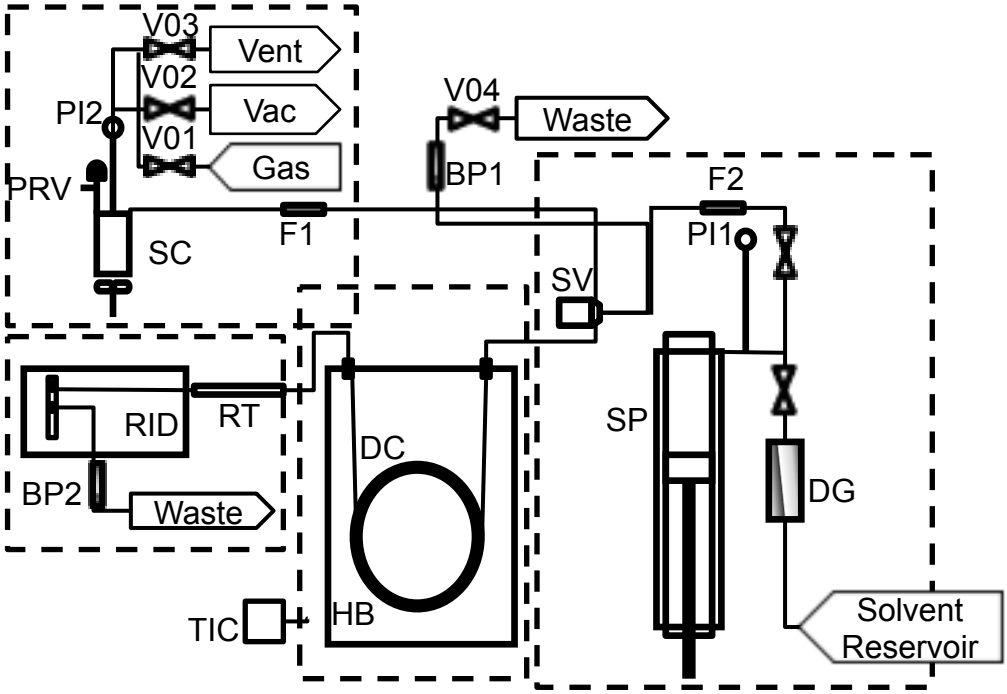

Figure 3-1. Schematic of the Taylor dispersion apparatus.
DG, vacuum degasser; SP, syringe pump; PI1 and PI2, pressure transducers; F1 and F2, filters; SV, sample valve; DC, diffusion column; HB, thermostatic oil bath; TIC, temperature controller; RT, restriction tube; RID, refractive index detector; BP1 and BP2, back pressure valves; SC, saturation chamber; PRV; proportional relief valve; V01, V02 and V03, gas and vacuum valves; V04; solution outlet valve.

A syringe pump (Teledyne ISCO, model 100DM) was used to provide a continuous flow of solvent through, in turn, a 6-port injection valve (VICI, Cheminert Model C72H – 1696D), a coiled diffusion column, housed in a thermostatic oil bath (Fluke, Model 6022), a PEEK-reinforced-silica restriction tube, a differential refractive index detector, RID, (Agilent 1200 series) and finally a back-pressure regulator. The purpose of the restriction tube was to permit high pressures in the diffusion column, up to the desired operating pressure, while allowing the refractive index detector to operate at a low pressure (typically 0.45 MPa). The latter was set by the back-pressure regulator. Several restrictor tubes were used in this work to allow

measurements to be performed at different pressures and flow rates. The syringe pump was operated in flow-control mode at various flow rates consistent with the desired operating pressure and the avoidance or limitation of secondary flow. The pressure was measured in the pump head, and the calculated pressure drop across the diffusion tube was found to be negligible. With the exception of the restriction tubes, all the tubing prior to the detector was made from Hastelloy C-276. The diffusion column had a length of 4.518 m, as measured with an ordinary tape measure, and an internal radius of 0.5398 mm, as determined gravimetrically [1]. This corresponds to a system working volume of 4.42 mL.

Measurements of diffusion coefficients of a solute in an aqueous solvent were limited to a maximum pressure of 50 MPa. This operating maximum was due to the ultra high molecular weight polyethylene (UHMWPE) seal used in the ISCO pump. However, the seal used in the hydrocarbon systems, graphite fiber reinforced PTFE, was capable of operating at higher pressures. Measurements in hydrocarbons were carried out at pressures up to 69 MPa.

During measurement of the (CO_2 + H_2O) system, the pump was maintained at T = 293 K by passing water from a chiller (Huber Minichiller) through a jacket around the syringe. The chiller also supplied a flow of water to a cold-finger inserted in the thermostatic bath to permit operation at temperatures below about T = 313 K at which natural heat loss was insufficient.

The temperature of the oil bath was measured with a secondary-standard platinum resistance thermometer (Fluke Hart Scientific, Model 5615) and readout unit (Fluke Hart Scientific, Model 1502A). The thermometer was calibrated on ITS-90 at the temperature of the triple point of water and by comparison in a constant temperature bath with a standard platinum resistance thermometer at nominal temperatures of (323, 373, 423 and 473) K. The standard uncertainty of the temperature measurements was 0.01 K. The solvent delivery pressure was measured at the outflow of the pump by means of the pressure transducer integrated into the pump. According to the manufacturer, the relative uncertainty of the pressure was 0.5% of the reading and we take this figure to be the expanded relative uncertainty with a coverage factor of 2.

The solution preparation vessel SC, fabricated from titanium, had an internal volume of 150 mL (for dimensions refer to Appendix 7) and was fitted with a PTFE-coated magnetic stirrer bar. This vessel was used, first, to degas a quantity of solvent and then to saturate it with gas at a pressure of up to 0.7 MPa.

A 5 µL sample-loop was used for the (CO_2 + H_2O) system and a 2 µL sample-loop was used for the CO_2-hydrocarbon investigation. Due to the higher solubility of CO_2

in the investigated hydrocarbons, this smaller sample loop allowed for a sufficiently low amount of solute to be placed on the diffusion column. The back-pressure regulator, BP2, served to prevent the solution degassing prior to injection into the diffusion column.

A data acquisition unit (Agilent LX1, Model 34970A) was fitted with a 20-channel general-purpose relay module to control the position of the solenoid valve on the outlet line of the sample line after the 6-port VICI valve. The solenoid valve was normally closed (NC) and operated via the completion of the electrical circuit, as controlled by the data acquisition unit. The actuation of this relay was controlled via the Agilent VEE control code in conjunction with the position of the 6-port VICI valve. The position of the VICI valve was controlled with a VICI two-position actuator control unit connected to the computer via a RS-232 cable. The assembled equipment is shown in Figure 3-2.

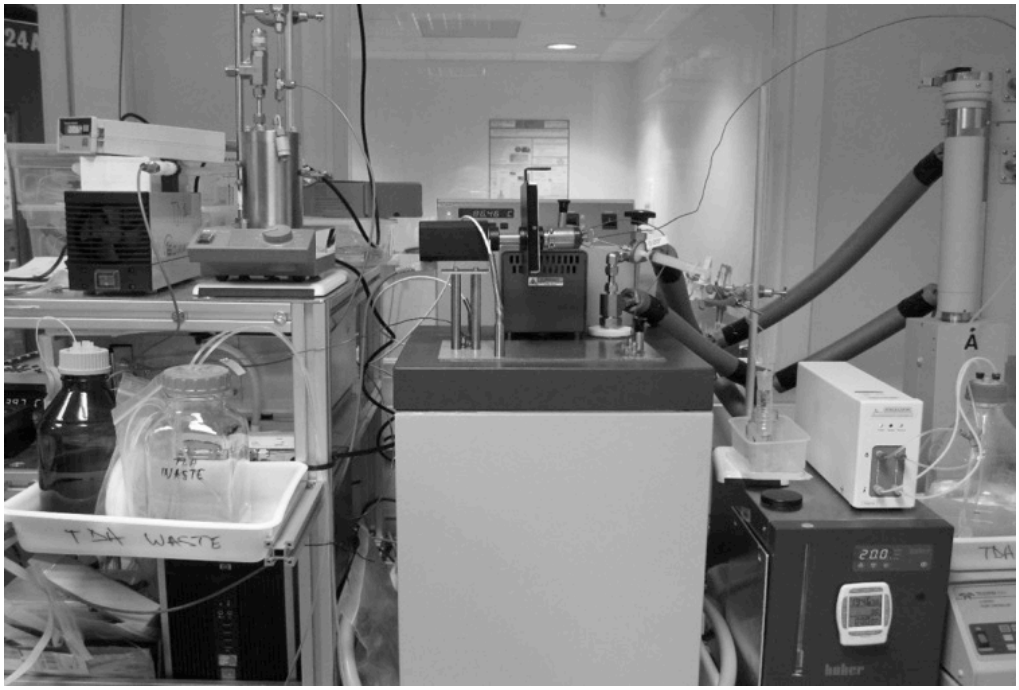

Figure 3-2. Picture of the Taylor Dispersion Apparatus.
The ISCO pump (right), oil bath, housing the diffusion column, (centre), saturation chamber (top right), and detector (left background) can be seen.

Due to the proximity of the freezing point of cyclohexane and hexadecane to ambient temperature at high pressures, ~ (30 and 50) MPa, respectively, trace heating was fitted to the tubes outside the heating bath prior to investigating these systems at high pressures.

A single path of resistance heating cable was fitted to the tubing from the pump to the sample valve, the sample loop, and sample valve to the lid of the bath. The resistance heating cable used had a resistance of 10 $\Omega \cdot m^{-1}$. Resistance heating was also fitted to the outlet tube between the lid of the oil bath and the union for the restriction tube. Finally, the restriction tube was also fitted with resistance heating, although the tube was only heated in selected measurements. The heater wire used for the latter two sections had a resistance of 25 $\Omega \cdot m^{-1}$. K Type thermocouples (TC Direct, 0.5 mm dia x 150 mm long) were placed next to the three respective runs of tubing inside the insulation.

A heated enclosure fabricated from aluminum was placed over the ISCO valve panel. 2.5 m of 10 $\Omega \cdot m^{-1}$ heating cable was evenly distributed around the outside of the enclosure, which was subsequently covered in insulation foam. An adhesive backed K type thermocouple (TC Direct, 0.3 mm thermocoule union attached to a 25 mm x 20 mm adhesive patch) was used to measure the temperature.

A multi-loop digital temperature controller (TC Direct, Model MA900) was used to control the temperature of the insulated tubes and the heated enclosure. This unit was a PID controller and each channel was controlled to an individual set point. The controller operated at 45 V a.c. and could supply at up to 10 A.

As part of the modifications required to investigate the systems containing hexadecane and cyclohexane it was also necessary to dedicate a separate circulating heated bath (Grant, Model LT D6G) to control the temperature of the pump heating jacket which operated independently of the cooling dip-tube associated with the oil bath.

Operating Procedure

Pure deionised water with an electrical resistivity of > 18.2 MΩ·cm at T = 298.15 K was used in this study. The solvent was degassed before entering the pump via an in-line degasser (Knauer, Model A5328). CO_2 and N_2, both of 99.995% purity, were supplied by BOC. All hydrocarbons were supplied by Sigma-Adrich and had a stated purity of > 99.9%.

Prior to beginning a campaign of measurements the system was flushed with fresh 2-propanol (Sigma Aldrich, anhydrous, > 99%). Both the VICI 6-port sample valve and the refractive index detector purge valve were switched intermittently during this process. A flow rate of 0.1 $mL \cdot min^{-1}$ was used and this process was carried out over typically 3 days.

Restriction tubes were pre-screened based on the desired pressure drop, Δp, within a suitable range of superficial flow rates, as per the Hagen-Pouiselle equation:

$$\Delta p = {8\eta L v}/{R^2} \qquad (3\text{-}1)$$

Solvent was firstly flushed through the system to atmosphere to clean the restriction tube and monitor the flow conditions of the solvent at the exit of the restriction tube. The solvent was flushed at a flow rate that was applicable to the subsequent experimental pressure. After the system had been flushed with the solvent of choice the restriction tube was connected to the RID.

After ensuring the pump cylinder was empty the solvent of choice was charged from a solvent reservoir. The volume of liquid in the reservoir was usually 200 mL so as to ensure that the bottle-bottom solvent filters were fully submerged while also minimising the inventory of solvent. This was as during the initial solvent flush process the contents of the solvent reservoir were disposed of to prevent contamination with 2-propanol from the sample lines and the reservoir itself. Once a stable baseline was observed flushing was ceased.

Solutions of the gas under study in the solvent were typically prepared at a pressure of 0.7 MPa. All solvents, with the exception of the mixed hydrocarbon, were degassed under vacuum for at least 30 minutes prior to saturation. As the concentration of heptane in the (heptane + hexadecane) mixed solvent was an input parameter in the calculation of the ternary diffusion coefficients such a vigorous degassing method was not suitable. It was found that vacuum degassing removed an unknown amount of heptane, as indicated by a Gaussian peak with positive polarity eluting through the refractive index detector, RID. In line with the scope of this element of the current work it was felt that the low levels of atmospheric gases present in the solvent would provide a negligible contribution to the diffusion coefficients determined. The (heptane + hexadecane) mixed solvent of was therefore not degassed under vacuum prior to saturation with CO_2 and the peaks produced were Gaussian distributions.

To perform a measurement at a given temperature, an Agilent VEE program was used to control the experiment. This program controlled the solvent flowrate and sample valve actuation and monitored the pressure, RID reading, and the sample valve position. Once thermal equilibrium in the thermostatic bath and steady-state flow were both established, as evidenced by a constant bath temperature and a constant pressure upstream of the column, a series of solution injections was made. Typically, 4 to 6 repeat measurements were made at each temperature and

pressure. Prior to an injection, the gas-saturated solution was passed under pressure, via a dip tube in the vessel, through the sample loop on the 6-port injection valve, and via the back-pressure regulator BP2 to waste.

The optimal operating conditions for a Taylor Dispersion apparatus have been discussed by several authors. The main criteria are that the flow should be laminar and that secondary flow induced by coiling of the capillary should be negligible. The second criterion is often associated in the literature with an upper limit on the product De^2Sc, where $De = Re(R/R_{coil})^{1/2}$ is the Dean number, $Sc = \eta/(\rho D)$ is the Schmidt number, $Re = (2Rv\rho/\eta)$ is the Reynolds number, R_{coil} is the coil radius, η is the solvent viscosity, and ρ is the solvent density. Using the same apparatus diffusion coefficients of the (KCl + H_2O) system had been studied at flow rates such that De^2Sc was less than about 20 and the measured signals $s(t)$ conformed closely to the working equation [1]. In the present work with gaseous solutes it proved necessary to re-appraise the optimal flow-rate and to consider corrections to the working equation, Eq. (3-4) below, for the effects of secondary flow [2,3].

Data Interpretation

The concentration difference between the flowing solution and the pure solvent was observed by means of changes in the refractive index. This differential refractive index signal $s(t)$ was analysed in terms of the relation:

$$s(t) = a + bt + \alpha c(t) \tag{3-2}$$

where a and b are baseline coefficients, t is time, c is molar solute concentration, and $\alpha = (\partial s/\partial c)_{T,p}$ is the sensitivity of the detector (assumed constant). As mentioned in Chapter 2, the concentration profile of a soluble matter in solvent flowing slowly through a tube is given by [4]:

$$c(t) = \left\{ n / \pi R^2 \sqrt{4\pi K t} \right\} \exp\left[-(L - vt)^2 / 4Kt \right] \tag{3-3}$$

Here, n is the amount of solute injected, R is the radius and L is the effective length of the column and v is the linear flow rate of solvent averaged over the cross-section of the tube and K, the dispersion coefficient, is normally related to the diffusion coefficient D by:

$$K = D + \left(R^2 v^2 / 48D \right). \tag{3-4}$$

The effective length is given by [1]:

$$L = L_c + (D/D_0)\sum_{i=1}^{3}(R_i/R_c)^4 L_i \qquad (3\text{-}5)$$

where D is the diffusion coefficient at the column temperature, D_0 is the diffusion coefficient at the ambient temperature and subscript i = 1, 2, 3, c denote the inlet, outlet, RID and column sections respectively. These dimensions are given in Appendix 6. This correction is small, with L typically being less than 1.5% greater than L_c.

The effect of the change of density of the solvent between the pump and the column was also accounted for from the ratio of molar volumes at the temperatures of the two devices, V_{Tp}/V_{Tc}.

The analysis consisted of adjusting: the time of injection, t_0, the baseline coefficients, a and b, the diffusion coefficient, D, and the product $n\alpha$, denoted by c, so as to best fit the experimental signal.

In this case of the (CO_2 + H_2O) system, the sensitivity coefficient α was estimated for CO_2 in water by flowing solution of known concentration directly through the RID, which was operated at T = 308.15 K. The concentration of CO_2 was determined from the model of Duan and Sun based on the temperature and pressure in the saturation chamber [5]. This gave α = -7.4 x 10^{-4} L·mol^{-1}; the negative sign indicates that the refractive index decreases with increasing concentration of solute. The sensitivity is not used in the analysis to determine D but was used to verify that the peak concentration of solute was below the solubility limit at the temperature and pressure prevailing in the detector.

To determine the diffusion coefficient matrix for the ternary system, two measurements must be performed, each with a different solution composition injected into the flowing solvent. One set of measurements involved the injection of the solvent with CO_2 and a slight excess of solvent 1. The complementary set of measurements involved the injection of the solvent with CO_2 without an excess of solvent 1 or solvent 2. It was assumed that one injection could be merely the addition of a dilute solution of CO_2. The rationale behind this decision was the diffusion remains ternary.

In order to analyse the ternary system investigated the following approach was taken [6]:

$$\tilde{s}(t) = (t_R/t)^{1/2} \left\{ \begin{array}{l} \dfrac{B_1}{B_1 + B_2} \exp\left(-12 D_1 \dfrac{(t - t_R)^2}{r^2 t} \right) \\ + \dfrac{B_2}{B_1 + B_2} \exp\left(-12 D_2 \dfrac{(t - t_R)^2}{r^2 t} \right) \end{array} \right\} \tag{3-6}$$

$$B_1 = \left[\left(D_{22} - R_2 D_{21}/R_1 \right) \alpha_1 + \left(D_{11} - R_1 D_{12}/R_2 \right) \left(1 - \alpha_1 \right) - D_1 \right] D_1^{1/2} \tag{3-7}$$

$$B_2 = -\left[\left(D_{11} - R_1 D_{12}/R_2 \right) \left(1 - \alpha_1 \right) + \left(D_{22} - R_2 D_{21}/R_1 \right) \alpha_1 - D_2 \right] D_2^{1/2} \tag{3-8}$$

Here, α_1 denotes the fraction of the initial refractive index, i.e. the product of the molar refractivity and the concentration perturbation, due to solute 1. R_i is given by the partial derivative of the refractive index of component i with respect to its concentration, c_i. The concentration dependence of the refractive index of the (heptane (solvent 1) + hexadecane (solvent 2)) system, needed in these calculations, was measured at varying mole fractions of heptane using a CETI manual refractometer at T = 302.65 K.

To determine the ternary diffusion coefficients the ternary diffusion coefficients and D_i are adjusted to minimise the difference between the model and the experimental data.

Discussion

During experiments involving the (CO_2 + H_2O) system qualitatively different behaviour to that predicted by the Taylor dispersion theory was observed. Figure 3-3 illustrates the expected Gaussian concentration distribution of solute at a fixed distance from the point of injection. The signal, $s(t)$, corresponding to an injection of N_2 into pure water flowing at 0.8 mL·min^{-1}, is plotted against the elapsed time since the injection. This corresponds to a measurement performed at p = 26.6 MPa and T = 423.15 K. Also shown is the deviation between the experimental points and the values predicted by the working equation.

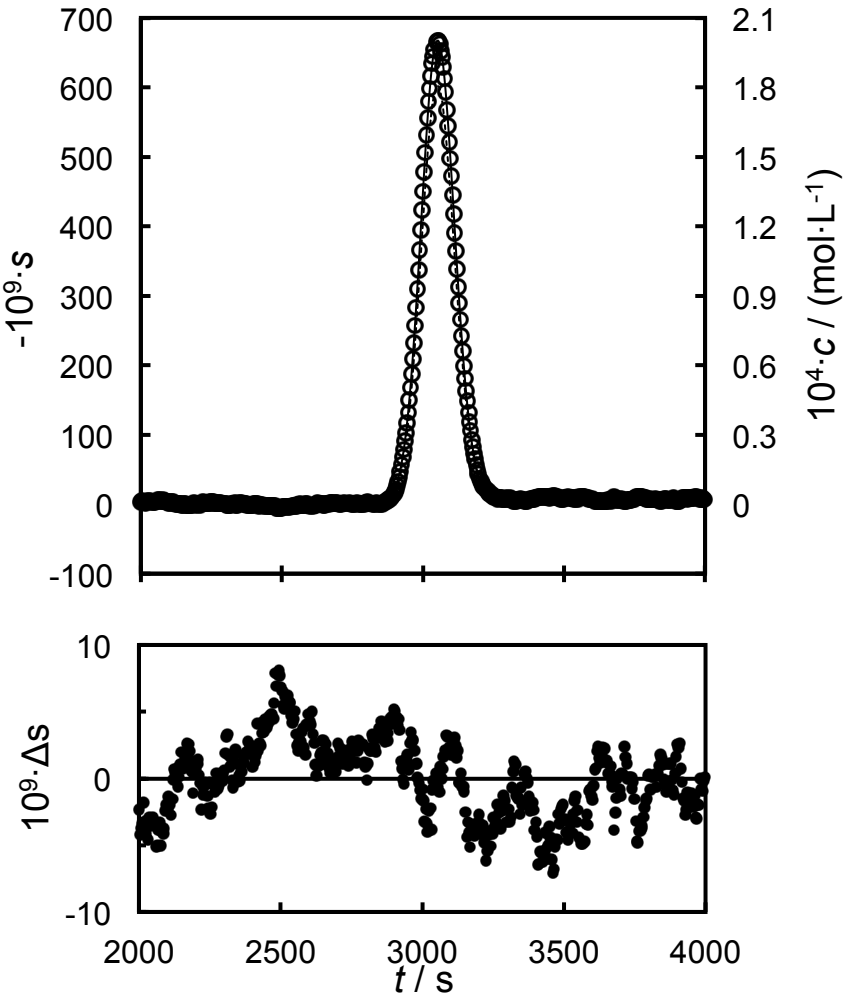

Figure 3-3. (top) Dispersion curve $s(t)$ for N_2 in water at T = 423 K, p = 26.6 MPa.
The flow rate used was 0.08 mL·min^{-1}: O, refractive index signal; ———, Aris model, Eq. (3-2) to Eq. (3-4) fitted to the experimental data.
(bottom) Deviation, Δs, between the experimental data and the fitted model.

The experimental data are seen to conform closely to the working equation with deviations not worse than about 1% of the peak signal. In this case, $De^2Sc \approx 5$.

The refractive index of the N_2 was converted to concentration from its molar refractivity. This calculation also validated the negative polarity of the peak produced.

In contrast to the situation with nitrogen, injections of CO_2(aq) resulted in an anomalous peak shape at comparable flow rates (roughly ≤ 0.12 mL·min^{-1}) and T ≥ 348.15 K. Figure 3-4 is an example of such behaviour and shows a pronounced pre-peak of reverse polarity.

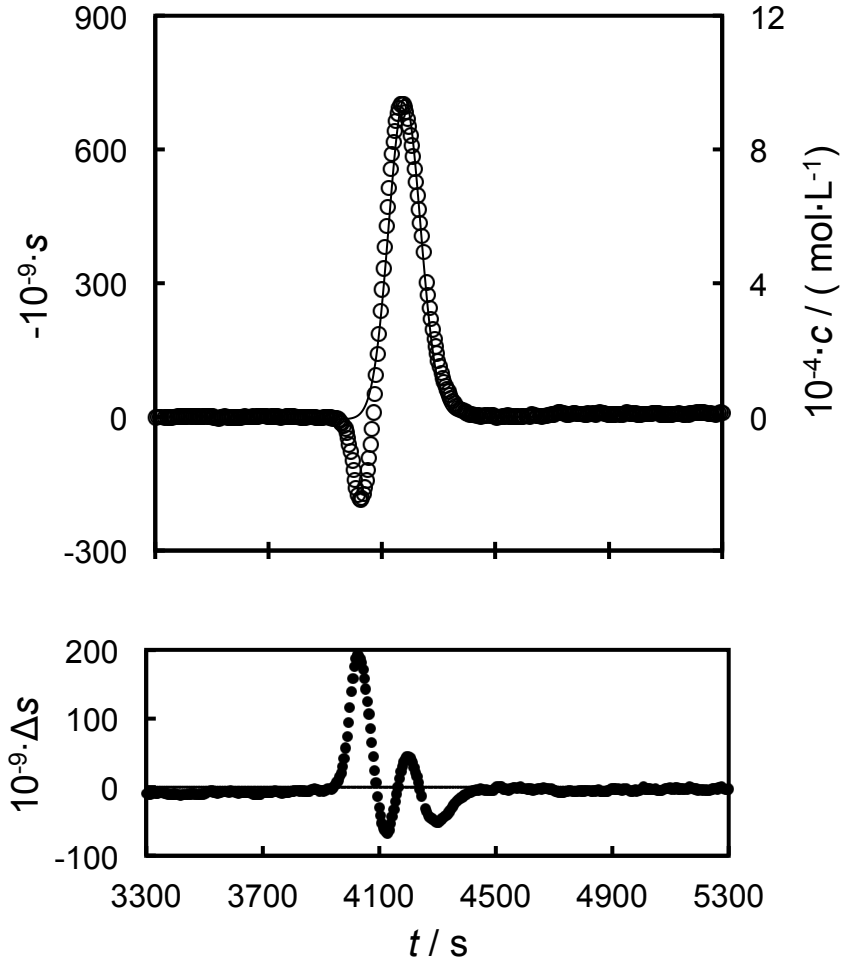

Figure 3-4. (top) Dispersion curve $s(t)$ for CO_2 in water at T = 423 K, p = 9.9 MPa.
The flow rate used was 0.03 mL·min^{-1}: O, refractive index signal; ———, Aris model, Eq. (3-2) to Eq. (3-4) fitted to the experimental data.
(bottom) Deviation, Δs, between the experimental data and the fitted model.

This behaviour became more pronounced at higher temperatures. This is likely due to the counter intuitive phenomena observed in Taylor dispersion. At higher temperatures, where the diffusion coefficient is higher, the width of the concentration distribution actually decreases. As the area under the distribution must be conserved, a peak with a larger signal intensity is produced.

Despite exhaustive investigations, the origin of this pre-peak, which has a transit time up to 60 seconds faster than the mean liquid residence time, has not been determined. It was observed that, with solvent flowing continuously, the height of the pre-peak (relative to the main peak) decreased in magnitude over a series of solute injections; however, it increased again after a period without injections. Most plausible mechanisms, such as adsorption and/or reaction of the mildly acidic solution at the capillary wall, are expected to give rise to either retention or tailing of

the main peak. The possibility that the CO_2 was coming out of solution in the detector was eliminated by comparing the measured concentration with the solubility limit and also by looking for bubbles in the solution flowing between the RID and the back-pressure regulator at the outlet (transparent tubing was installed for this purpose). The same behaviour was observed when a stainless-steel tube of similar dimensions replaced the Hastelloy diffusion tube. From this study, any effect due to surface interactions was ruled out. The use of a PEEK-Sil tube in place of the Hastelloy diffusion column was also attempted, however no meaningful concentration distributions were observed. The signal obtained had very low signal to noise ratios, were not of a Gaussian nature and exhibited a large degree of peak tailing, possibly due to absorption of CO_2 on the column. The use of a weakly acidic HCl solution (pH 5) as a mobile phase was also investigated but the signal to noise ratio became problematically low, possibly due to a salting out effect due to the HCl and the high contribution of HCl to the refractive index signal.

It was found that the pre-peaks were greatly diminished when the flow rate was increased. In order to supress the anomalous pre-peak whilst limiting the effects of secondary-flow effects, the measurements for CO_2 in water were made at flow rates of (0.305 to 0.325) mL·min^{-1}, corresponding to $80 < De^2Sc < 100$. Figure 3-5 shows and example of the RID signal measured for CO_2 in water at T = 423.15 K and a flow rate of 0.325 mL·min^{-1}, under which conditions no pre-peak is evident and the data conform to Eq. (3.2) to Eq. (3.4). The amount of solute eluting, obtained from the area under the peak, was found to agree to within about 15% of the calculated amount injected, based on the solubility model, the temperature and pressure in the solution preparation vessel and the nominal volume of the sample loop. We note that the value of D determined from the anomalous data shown in Figure 3-4 was 20% higher than the value obtained from the 'normal' dispersion curve shown in Figure 3-5.

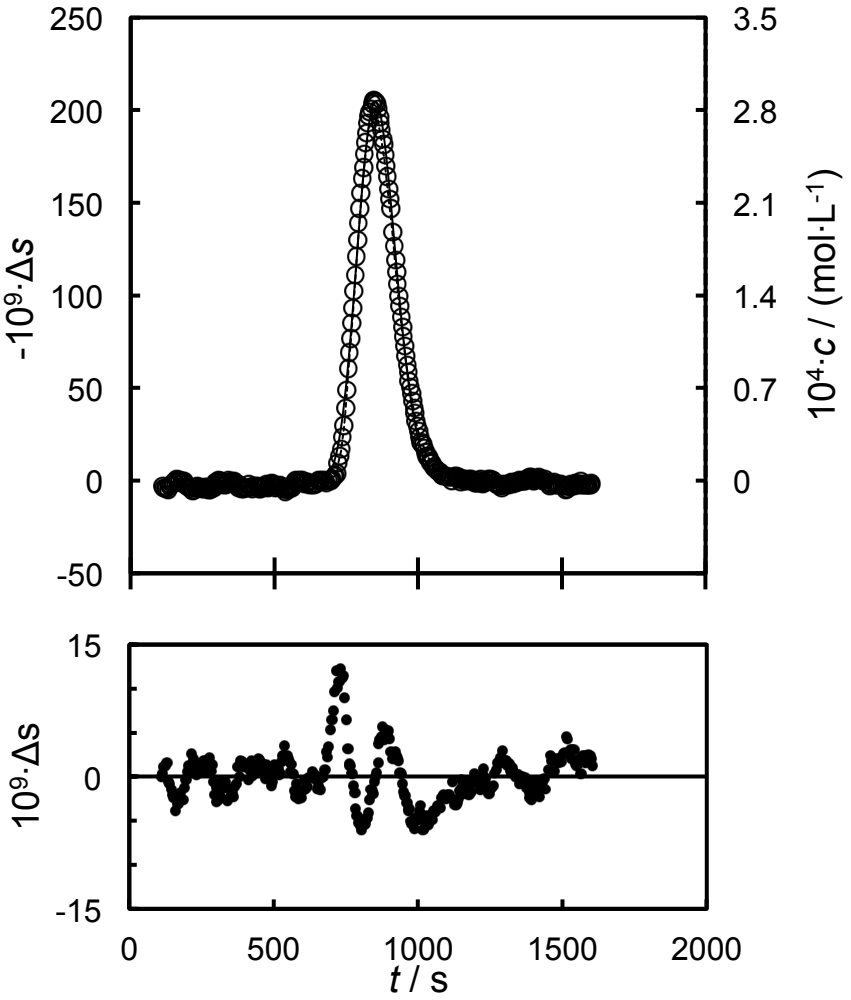

Figure 3-5. (top) Dispersion curve $s(t)$ for CO_2 in water at T = 423 K, p = 39 MPa.
The flow rate was 0.325 mL·min^{-1}: O, refractive index signal; ———, Aris model, Eq. (3-2) to Eq. (3-4) fitted to the experimental data.
(bottom) Deviation, Δs, between the experimental data and the fitted model.

At the flow rates necessary to achieve acceptable peak shapes, secondary flow effects are still small but not negligible. In order to account for this, Eq. (3-4) for the dispersion coefficient K was replaced by the more general expression [3]:

$$K = \left[D + \frac{R^2 v^2}{48D}\right] + (Pe^2 D)(De^2 Sc)^2 \left[\frac{1}{40 \times 576^2}\left\{\frac{-2569}{15840} + \frac{109}{43200\,Sc^2}\right\} + \frac{1}{72 \times 576\,Re^2}\left\{\frac{31}{60\,Sc} - \frac{25497}{13440\,Sc^2}\right\} + \frac{1}{Re^4 Sc^2}\left\{\frac{419}{11520} + \frac{1}{4}\left(\frac{1}{Pe^2} + \frac{1}{192}\right)\right\}\right] \quad (3\text{-}9)$$

The use of Eq. (3-9) in place of Eq. (3-4) to calculate D from K implies a relative correction of between -1.4% and -1.7% in the present work. We note that under

typical operating conditions for a Taylor Dispersion experiment, Sc ≫ 1, $10^0 \leq Re \leq 10^2$, and $K \gg D$, so that Eq. (3-9) reduces to the following simple expression in which the correction for secondary flow is directly proportional to $(De^2Sc)^2$:

$$K \approx \left(\frac{R^2v^2}{48D}\right)\left[1-\left(\frac{De^2Sc}{653}\right)^2\right]. \qquad (3\text{-}10)$$

Having determined the optimal operating conditions, measurements for CO_2 in water, as well as N_2 in water, were made over the temperature range (298 to 423) K at pressures up to 45 MPa. In these measurements, dispersion curves like those seen in Figure 3-5 were always observed and enable the diffusion coefficient to be extracted with an estimated standard relative uncertainty of 2.3%.

Dispersion profiles similar to those obtained for the (N_2 + H_2O) system (Figure 3-3) were observed during measurements of the diffusion coefficient of CO_2 in all hydrocarbons, i.e. no pre-peak or anomalous behaviour was observed. The flow rates used for measurements of the (CO_2 + hydrocarbon) systems were typically less than 0.15 mL·min^{-1}. Higher flow rates, where used, were used with the sole aim of reaching the desired operating pressure with the available restriction tubes.

Nuclear Magnetic Resonance

Experimental System

A Bruker 500 MHz AVANCE III HD spectrometer was used to perform the measurements reported. The spectrometer was equipped with a *z*-gradient tuneable probe and a BSMS GAB 10 amp gradient amplifier with a maximum gradient output of 53.5 $G \cdot cm^{-1}$.

As $^{12}CO_2$, carbon dioxide's most abundant isotope, is not NMR-active, $^{13}CO_2$ was used as an analogue. While the two compounds are chemically identical, the mass of $^{13}CO_2$ is 2.2% greater than that of $^{12}CO_2$. This difference is considered negligible and the results obtained are treated as effectively as those of $^{12}CO_2$.

The use of nuclear magnetic resonance to measure diffusion coefficients has been practised for the last 30 years, starting from the work of Hahn [7]. However, only one source has been found in the literature using this technique to measure the diffusion coefficient of CO_2 in an aqueous solvent [8]. The diffusion of CO_2 in various beverages was investigated but the multicomponent nature of these systems was not discussed. In this study $^{13}CO_2$ was formed in-situ via the reaction of sodium hydrogencarbonate-^{13}C, 99% atom ^{13}C, and dilute hydrochloric acid. There have however been several other studies of the diffusion of CO_2 in hydrocarbons [9,10] and ionic liquids [11]. CO_2 tends to have a higher solubility in these liquids.

The use of NMR to investigate saline solutions has also been previously reported [12]. No adverse effect to systems comprising electrolytes was reported. In this work protein configuration is elucidated at 3.5 M NaCl.

Operating Procedure

The aqueous solvent was saturated with $^{13}CO_2$ using the apparatus shown schematically in Figure 3-6.

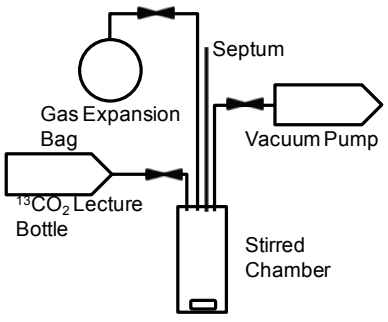

Figure 3-6. The $^{13}CO_2$ saturation system.

The system comprised of a 150 mL borosilicate-glass bottle containing a PTFE-coated magnetic stirrer bar, a cylinder of $^{13}CO_2$(g), a vacuum pump (VWR), and a gas expansion bag, which allowed samples to be extracted while mitigating any resulting pressure drop. $^{13}CO_2$ (^{13}C, 99%, < 1% ^{18}O) was supplied by CK Gases.

A solution of brine was prepared gravimetrically and filled in the stirred chamber; which was subsequently sealed and put under vacuum for 30 minutes to remove dissolved air. The sample was then saturated with measurement gas at ambient pressure.

To validate this experimental method the diffusion coefficient of $^{13}CO_2$ in D_2O was determined. The obtained value was scaled by the ratio of the viscosity of H_2O to D_2O. A CO_2 solution in H_2O was subsequently investigated. D_2O was used as an in-situ calibration lock similar to the method of Holz [13]. One end of a thin glass capillary was sealed using a naked flame. After the capillary cooled, it was filled with D_2O via a syringe. A naked flame was then used to seal the other end.

A long needled syringe was used to charge brine from the chamber to the NMR sample tube. A dry clean tube was filled with brine and emptied twice before the capillary was added to the tube. Fresh solvent was then added to the tube.

The salts used in this study were obtained from Sigma-Aldrich and had a stated purity of >99%.. The prototype brine was composed of 1.514 mol·kg^{-1} NaCl, 0.276 mol·kg^{-1} $CaCl_2$, 0.080 mol·kg^{-1} $MgCl_2$, 0.012 mol·kg^{-1} KCl, 0.011 mol·kg^{-1} Na_2SO_4, 0.004 mol·kg^{-1} $SrCl_2$, and 0.003 mol·kg^{-1} $NaHCO_3$, a total molality of 1.9 mol·kg^{-1}.

The recorded signals were analysed using the TopSpin 3.2 software. $^{13}CO_2$ was used as the tracer species. The data was processed with one order of zero-filling and using an exponential function with a line broadening of 2 Hz. Further processing was achieved using the Bruker Dynamics Centre software (Version 2.1.7). Error estimation was performed by a Monte Carlo method, also using the Bruker Dynamics Centre software. The pulsed field gradient technique [14] was used.

The attenuation of the observed signal is related to the translational diffusion coefficient as follows [15]:

$$f(x) = A\exp\left(-Dx^2\gamma^2\delta^2\left[\Delta - \delta/3\right]\right)\times 10^4 \qquad (3\text{-}11)$$

where γ is the gyromagnetic ratio for $^{13}CO_2$, 6726.8 rad·s^{-1}·Gauss^{-1}. The applied δ was 0.0052 s and Δ was 0.04990 s. A typical result is shown in Figure 3-7.

The spectra were collected at a frequency of 125.76 MHz (^{13}C) with a spectral width of 5.03 MHz (centred on 124.6 ppm) and 8192 data points. A relaxation delay of 200 s was employed along with a diffusion time, Δ, of 50 ms and a longitudinal eddy current delay (LED) of 5 ms. Bipolar gradients pulses, $\delta/2$, of 2.6 ms and homospoil

gradient pulses of 1.1 ms were used. The gradient strengths of the 2 homospoil pulses were -17.13% and -13.17%. 16 experiments were collected with the bipolar gradient strength, initially at 2% of the maximum gradient output (1st experiment), linearly increased to 95% (16th experiment). All gradient pulses were smoothed-square shaped (SMSQ10.100) and after each application a recovery delay of 200 µs was used.

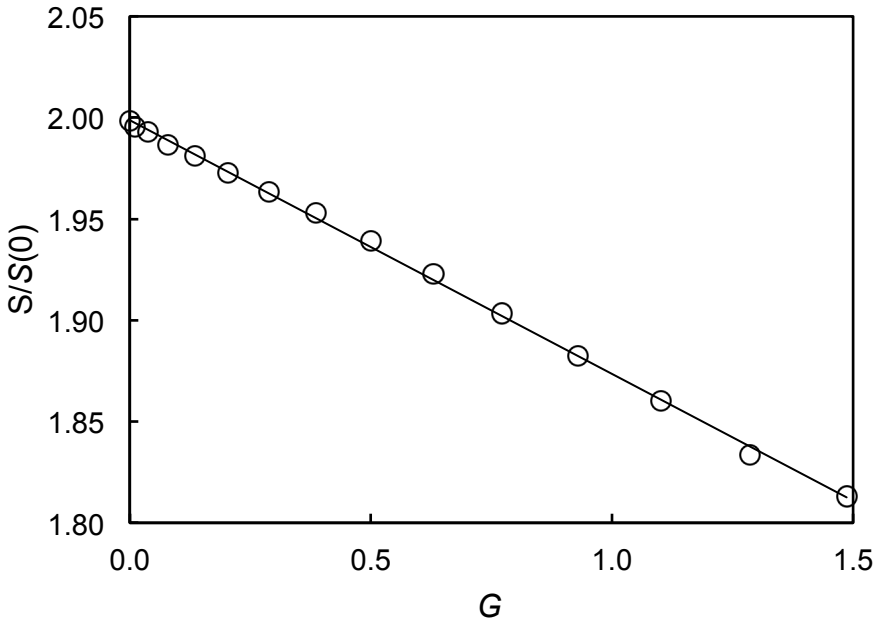

Figure 3-7. Signal intensity of $^{13}CO_2$ as a function of the magnetic field strength, *G*.
This behaviour can be described by the Stjeskal-Tanner equation [15,16].

Discussion

The gas saturation method detailed above has several advantages over other methods. It is cheap, effective and straightforward to implement. Unlike other methods [8], it also does not add extra components into the mixture under investigation. This work has shown that even with the salting out effect, PFG-NMR can resolve $^{13}CO_2$ in a brine of 5 M NaCl.

It was also noted that while PFG-NMR has been described as a rapid technique for determining diffusion coefficients, measurements took on average 14 hours for a single data point. The reason for this is due to the low intensity of the signal produced by the ^{13}C isotope several spin echoes had to be performed in order to get a satisfactory signal. An alternative method considered was the use of NMR tubes able to withstand elevated pressures. Such tubes would permit the brine to be

saturated with $^{13}CO_2$ at higher pressures, increasing the amount of dissolved gas and increasing the signal to noise ratio. In this work, it was deemed sufficient to pursue the reported procedure using glass capillaries.

References

[1] C. Secuianu, G.C. Maitland, J.P.M. Trusler, W.A. Wakeham, Mutual Diffusion Coefficients of Aqueous KCl at High Pressures Measured by the Taylor Dispersion Method, J. Chem. Eng. Data 56 (2011) 4840-4848.

[2] M.E. Erdogan, P. Chatwin, The effects of curvature and buoyancy on the laminar dispersion of solute in a horizontal tube, J. Fluid Mech 29 (1967) 465-484.

[3] R.J. Nunge, T.S. Lin, W.N. Gill, Laminar dispersion in curved tubes and channels, J. Fluid Mech. 51 (1972) 3-5.

[4] R. Aris, On the dispersion of a solute in a fluid flowing through a tube, Proc. R. Soc. London. Series A. 235 (1956) 67-77.

[5] Z. Duan, R. Sun, An improved model calculating CO_2 solubility in pure water and aqueous NaCl solutions from 273 to 533 K and from 0 to 2000 bar, Chem. Geol. 193 (2003) 257-271.

[6] D.G. Leaist, Ternary Diffusion of 18-Crown-6 Ether-KCl-Water by Direct Least-Squares Analysis of Taylor Dispersion Measurements, J. Chem. Soc., Faraday Trans. 87 (1991) 597-601.

[7] E.L. Hahn, Spin Echoes, Phys. Rev. 80 (1950) 580-594.

[8] G. Liger-Belair, E. Prost, M. Parmentier, P. Jeandet, J.-M. Nuzillard, Diffusion Coefficient of CO_2 Molecules as Determined by ^{13}C NMR in Various Carbonated Beverages, J. Agric. Food Chem. 51 (2003) 7560-7563.

[9] P. Etesse, W.G. Chapman, R. Kobayashi, Nuclear magnetic resonance measurements of spin-lattice relaxation and self-diffusion in supercritical CO2-n-hexadecane mixtures. Mol. Phys. 80 (1993) 1145-1164.

[10] J. Guzmán, L. Garrido, Determination of Carbon Dioxide Transport Coefficients in Liquids and Polymers by NMR Spectroscopy, J. Phys. Chem. B. 116 (2012) 6050-6058.

[11] E.D. Hazelbaker, S. Budhathoki, H. Wang, J.K. Shah, E.J. Maginn, S. Vasenkov, Relationship between Diffusion and Chemical Exchange in Mixtures of Carbon Dioxide and an Amine-Functionalized Ionic Liquid by High Field NMR and Kinetic Monte Carlo Simulations, J. Phys. Chem. Lett. 5 (2014) 1766-1770.

[12] B. Binbuga, A.F.B. Boroujerdi, J.K. Young, Structure in an extreme environment: NMR at high salt, Protein Sci. 16 (2007) 1783-1787.

[13] M. Holz, H. Weingartner, Calibration in Accurate Spin-Echo Self-Diffusion Measurements Using ^{1}H and Less-Common Nuclei, J. Magn. Reson. 92 (1991) 115-125.

[14] W.S. Price, Pulsed-Field Gradient Nuclear Magnetic Resonance as a Tool for Studying Translational Diffusion: Part 1. Basic Theory, Concept. Magnetic Res. 9 (1997) 299-336.

[15] E. Stejskal, J. Tanner, Spin Diffusion Measurements: Spin Echoes in the Presence of a Time-Dependent Field Gradient, J. Chem. Phys. 42 (1965) 288-292.

[16] J.E. Tanner, Use of the Stimulated Echo in NMR Diffusion Studies, J. Chem. Phys. 52 (1970) 2523-2526.

4. Diffusion Coefficients of CO_2 in Aqueous Systems

Fickian diffusion coefficients of CO_2 in water and several brine solutions at infinite dilution are reported. Pressure was found to have no observable effect on the values of the measured diffusion coefficients in these solvents. From the perspective of a hydrodynamic treatment, the hydrodynamic radius of CO_2 was found to be independent of pressure and brine composition. From this treatment, the diffusion coefficient at any temperature and pressure can be calculated from the corresponding viscosity of the solvent at that state point and a hydrodynamic radius, which is a function of temperature.

The work on the (CO_2 + H_2O) and (CO_2 + brine) systems have been reported in the literature [1, 2]. The results have been tabulated in Appendices 2 and 3, respectively.

Diffusion Coefficients of CO_2 in Water

Results

Despite the experimental difficulties regarding peak shape described in the previous chapter, the diffusion coefficients for CO_2 were measured at infinite dilution in water at 25 K intervals over the temperature range (298 to 423) K and at pressures of (14, 30, and 50) MPa using the Taylor dispersion method. The values for *D* are plotted as a function of temperature in Figure 4-1.

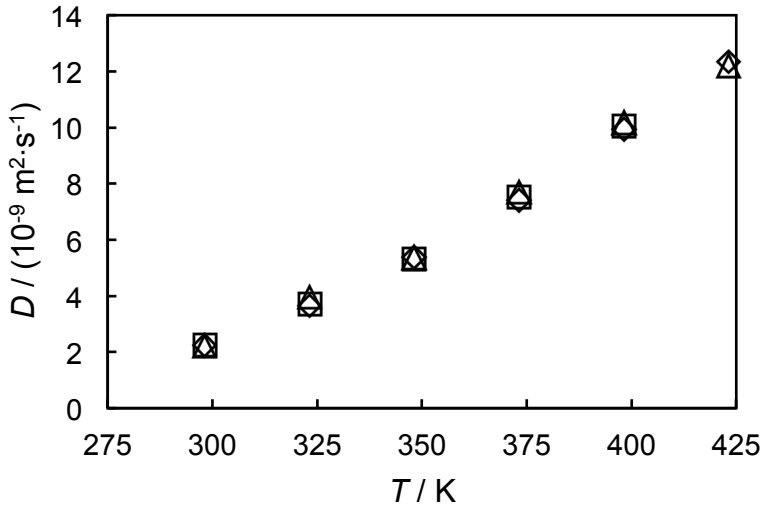

Figure 4-1.The diffusion coefficients, *D*, for CO_2 in water plotted against temperature, *T*.
Measurements were performed at: ◇, *p* = (14.0 to 14.9) MPa; □, *p* = (30.9 to 31.8) MPa; △, *p* = (47.7 to 49.3) MPa.

There is no apparent effect of pressure on the measured values of the diffusion coefficients, which is in agreement with other work [3, 4].

The standard relative uncertainty associated with these measurements was calculated from the following equation;

$$u_r^2(D) = u_r^2(K) + 4u_r^2(R) + 4u_r^2(v) + \left[(p/D)(\partial D/\partial p)u_r(p)\right]^2 + \left[D^{-1}(\partial D/\partial T)u(T)\right]^2 \quad (4\text{-}1)$$

where $u_r(X)$ denotes standard relative uncertainty and $u(X)$ standard uncertainty of variable *X*. $u_r(K)$ = 2.0%, estimated from the repeatability of the dispersion measurements, $u_r(R)$ = 0.20%, $u_r(v)$ = 0.50%, and $u_r(p)$ = 0.25%, while the standard uncertainty of temperature was 0.01 K. This led to $u_r(D)$ = 2.3% for both systems investigated. While the reproducibility in the present experiments was somewhat

lower than obtained using the same equipment measuring diffusion coefficients of the (KCl + H_2O) system [5], the results obtained were generally consistent within 3% at a given state point.

This figure is dominated by the repeatability of *K*, the uncertainties of *T* and *p* have negligible influence. The reproducibility of these measurements over a series of injections performed at a given state point is shown in Figure 4-2. Typically between 5 and 6 injections were made during an experimental run. There is no systematic trend in the reproducibility of the values obtained from various injection as a function of temperature.

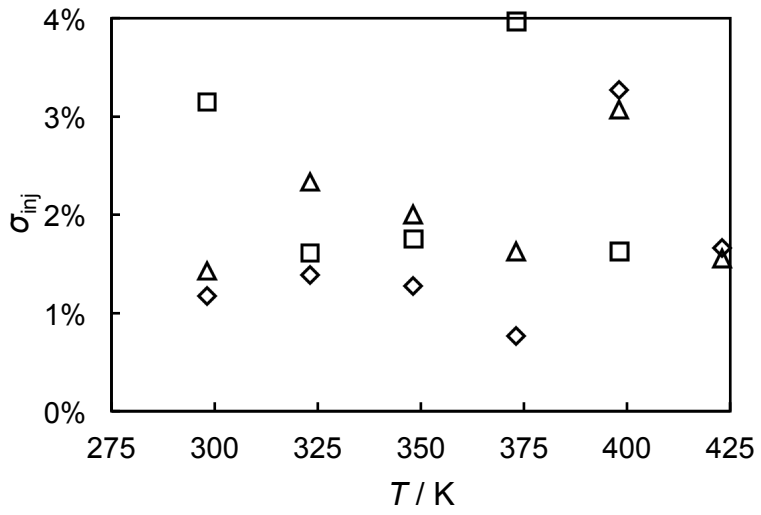

Figure 4-2. Standard deviation of the diffusion coefficient obtained from repeated injections at each state point.
Measurements were performed at: ◇, *p* = (14.0 to 14.9) MPa; □, *p* = (30.9 to 31.8) MPa; △, *p* = (47.7 to 49.3) MPa.

An interesting plot shows the parameter *c* against the calculated diffusion coefficient, including the data obtained for measurements in which the “pre-peak” was observed (Figure 4-3). The nature of *c* has been discussed in Chapter 3, and is the product of the number of excess moles of solute injected and the detector sensitivity to this solute. In this work this parameter is treated as a fitted variable. The value of the diffusion coefficient should be independent of *c*, however as can be seen in Figure 4-3, the value for *D* is not constant at a given temperature, especially at T > 373 K.

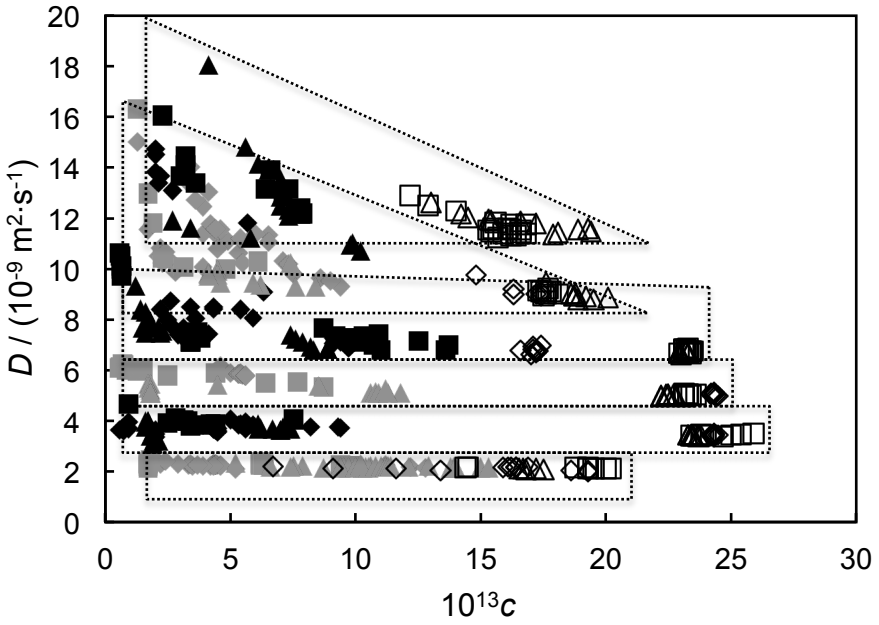

Figure 4-3. Fitted parameter c plotted against the determined diffusion coefficient *D*.
◆, *p* = (14.0 to 14.9) MPa; ■, *p* = (30.9 to 31.8) MPa; ▲, *p* = (47.7 to 49.3) MPa are experiments at *T* = (298.15, 348.15, and 398.25) K in ascending order. Experiments performed at *T* = (323.15, 373.15, and 423.15) K are denoted by: ◆, *p* = (14.0 to 14.9) MPa; ■, *p* = (30.9 to 31.8) MPa; ▲, *p* = (47.7 to 49.3) MPa.
Experiments in which CO_2(g) were injected are denoted by: ◇, *p* = (14.0 to 14.9) MPa; □, *p* = (30.9 to 31.8) MPa; △, *p* = (47.7 to 49.3) MPa. Isotherms have been grouped within the dashed lines.

At a given temperature the measured diffusion coefficient increases exponentially as *c* decreases to zero. This is most pronounced for the data towards the right of the graph which correspond to injections of CO_2(g) into the solvent. Naturally, these values do not correspond to the diffusivities of CO_2 in water as calculated from the Taylor-Aris approach as the dispersion of the solute will also be a function of the rate of gas dissolution.

As *c* is considered constant at the low concentrations involved in this work, the justification given for the observed behaviour in Figure 4-3 is that the signal to noise ratio becomes sufficiently low that values recorded are erroneous, especially prominent in cases in which the presence of a "pre-peak" was noted. The diffusion coefficient can be obtained reproducibly when the parameter *c* is greater than 10×10^{-13}. In light of the fact that the concentration perturbation should be as small as possible in this work the CO_2(aq) concentration was adjusted to try and maintain a value of between (10 and 15) $\times 10^{-13}$ for *c*.

Discussion

As expected, the value of the diffusion coefficient increases with increasing temperature. It is also found that the effect of pressure is negligible. Primarily due to hydrogen bonding water has a low compressibility and the molar volume and viscosity of water are only very weak functions of pressure. As these are likely to be the main contributors to the diffusivity from the solvent it is rational that *D* should not be affected by *p* when the solute is diffusing in H_2O.

Rutten has discussed use of a modified Stokes-Einstein equation to describe the temperature dependence of the diffusion coefficients of gases in liquids [6]. Temperature and solvent viscosity are the only independent variables in the following correlation:

$$D = k_B T \Big/ \left(n_{SE} \pi \eta a \right) \tag{4-2}$$

Here, k_B is Boltzmann's constant, T is temperature, n_{SE} is the Stokes-Einstein number, η is the solvent viscosity, and a is the hydrodynamic radius of the solute. For consistency with previous work, we take the Stokes-Einstein number to be 4. Typically, the hydrodynamic radius a is found to be a weak function of temperature and, in the present work, this term was correlated as follows:

$$a = a_{298\mathrm{K}} \left[1 + \alpha_a \left(T/\mathrm{K} - 298 \right) \right] \tag{4-3}$$

For the (CO_2 + H_2O) system, the hydrodynamic radius was given by [168 $\times$ (1+0.002(*T*/K-298))] pm. The inclusion of a temperature dependence of the hydrodynamic radius, as supported by [7], was an alternative to introduction of an exponent for the solvent viscosity in Eq. (4-2) as has been proposed by other authors [8-12]. The influence of temperature on the hydrodynamic radius has been discussed elsewhere [13, 14].

The deviation between this correlation and the reported values for *D* are shown in Figure 4-4 and Figure 4-5. The fitted parameters for the hydrodynamic radius are tabulated in Appendix 5.

A qualitative and quantitative difference is noted between the measured and previously reported data. This deviation is most pronounced at T = 298 K. A large degree of scatter exists in the available literature at T = 298 K, the diffusion coefficient ranging from (1.74 to 2.11) $m^2 \cdot s^{-1}$. The mode value for the 25 values reported at this temperature is 1.98 $m^2 \cdot s^{-1}$, which is 11% lower than the value reported in this work. A second technique was used to measure diffusivities in this work, i.e. NMR-PFG, which is discussed later in this chapter, and the diffusion

coefficient of CO_2 in water measured at T = 298 K and p = 0.1 MPa (2.13 $m^2 \cdot s^{-1}$) agreed well with the value predicted from the measurements using the TDA in this work (+ 4.7%).

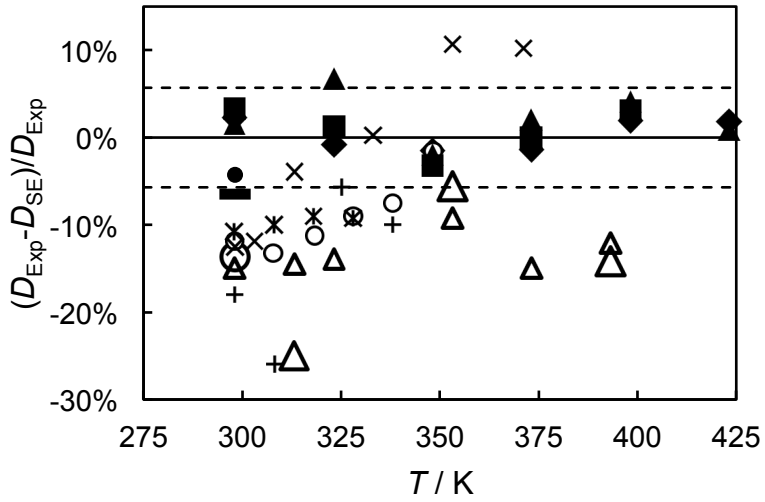

Figure 4-4. Deviation between reported values and presented correlation for the diffusion coefficient of CO_2 in H_2O.
Results obtained in this work are shown by: ◆, p = (14 to 14.9) MPa; ■, p = (30.9 to 31.8) MPa and ▲, p = (47.7 to 49.3) MPa. Literature values are indicated as follows: ✱, [15]; ○, [16]; -, [17]; x, [18]; +, [19]; O, [20] and •, [21] all at p = 0.1 MPa, and △ at p = 20 MPa and △ at p = 30 MPa [3]. The dashed lines represent twice the standard deviation from the correlation.

Figure 4-5 shows the deviation between several common methods and the method presented in this work for correlating the diffusion coefficient of CO_2 in water.

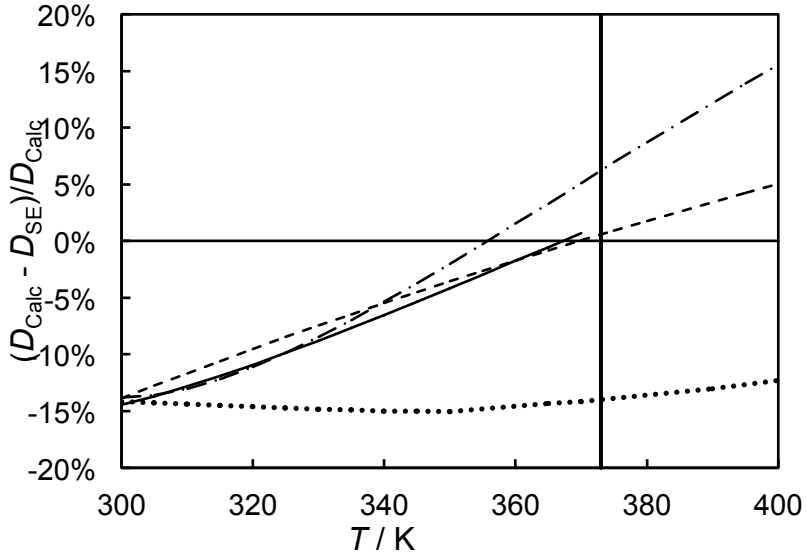

Figure 4-5. Comparison of the present correlation and selected available models.

The model corresponds to a pressure of 0.1 MPa up to a temperature of 373 K and a pressure of 1 MPa at temperatures between (373 and 400) K for models that are not solely functions of temperature: ⋯ [3], --- [22], -·-· [23], and - - - [16].

A clear qualitative difference can be seen between the correlation proposed based on the measurements performed in this work and several of the models previously reported [16, 22, 23]. This is due to the fact these models, including the more theoretically rigorous approaches, e.g. [22], are based on parameters that are obtained from correlating the ensemble of literature experimental data points available. One reported correlation, [3], while uniformly approximately 15% lower than the present correlation over the whole temperature range studied, represents a consistent difference with the current work.

The correlation used by Thomas and Adams [16] assumes the product of the diffusion coefficient divided by the viscosity is constant, as from hydrodynamic theory. The value of the proportionality factor was taken as the mode of a series of experimentally determined values. However, these values appear to be dependent on temperature.

It was also found that by fitting a parameter in the place of the molar volume at the normal boiling point of CO_2, that the Wilke-Chang correlation mimicked the correlation of Thomas and Adams [16] to within a few percent.

The correlation proposed from Versteeg and van Swaalj treats the diffusion coefficient as a function of temperature alone [23]. The correlation proposed from Lu *et al* [3] based on their experimental work differs from the correlation proposed here by approximately 15%. However, this deviation is surprisingly constant over the temperature range involved. Their correlation is only a function of temperature as in their measurements they also found pressure to have a negligible impact, reporting only a few percent difference over the investigated pressure range.

Moultos *et al* [24] have compared the measurements made in this work to values predicted from molecular dynamics and have found good agreement when using a SPC/E and TraPPE model for water and CO_2, respectively.

Eq. 4-3 was also fitted the results obtained for nitrogen diffusing in water over the same temperature and pressure range reported in this work, the results of which are shown in Figure 4-6. Once again, pressure was found to have a negligible impact on the diffusivity. The value of $a_{298\,K}$ was found to be 190 pm and α_a was found to be 0.0022 [1].

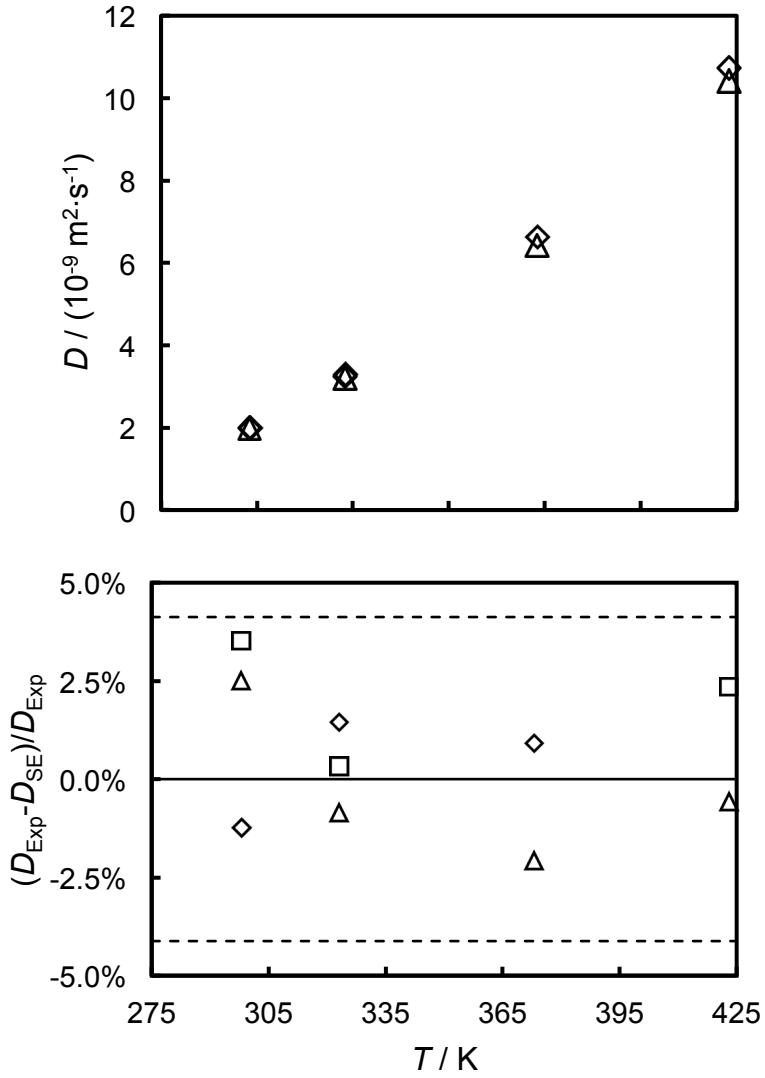

Figure 4-6. (top) Diffusion coefficients of N_2 in water plotted against temperature, *T*.
Measurements were performed at: ◇, *p* = (14.0 to 14.9) MPa; □, *p* = (30.9 to 31.8) MPa; △, *p* = (47.7 to 49.3) MPa. The data had an AAD was 2.0% and had a MAD of 3.3% over at least 3 repeated injections.
(bottom) Deviation between reported values and presented correlation for the diffusion coefficient of N_2 in H_2O also plotted against *T*. The dashed lines represent twice the standard deviation from the correlation.

Diffusion Coefficients of CO_2 in Brines

Results

As discussed in Chapter 1, one diffusion coefficient was considered sufficient to describe the translational motion of the CO_2 in brine, which was considered to be essentially a homogeneous solution. The measured diffusion coefficient, by PFG-NMR, is the carbon dioxide intradiffusion coefficient, D_1*, relating the flux of magnetically labelled CO_2, $\mathbf{j}^1$*, to the gradient in the concentration of magnetically labeled CO_2, (∇c_1*), i.e. $\mathbf{j}_1^* = -D_1^* \nabla c_1^*$, in solutions where the total CO_2 concentration (and the concentrations of water and salt) are constant. However, in the current limiting case of very low CO_2 concentrations, the mutual diffusion coefficient D_{11} is equal to the intradiffusion coefficient D_1*.

All measurements were performed at T = 298 K and p = 0.1 MPa. The effective binary diffusion coefficients for CO_2 in different brines are illustrated in Figure 4-7.

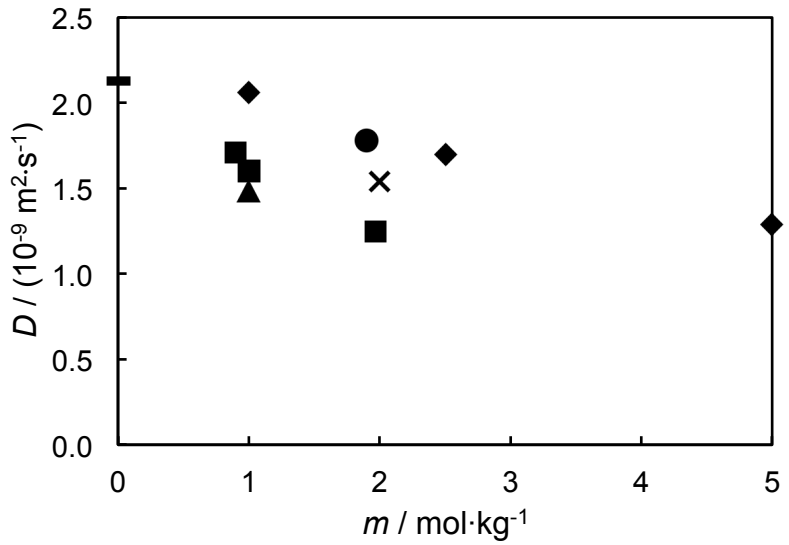

Figure 4-7. Diffusion coefficient of CO_2 plotted against brine molality.
The solutions investigated contained: -, no salt; ◆, NaCl; ■, $CaCl_2$; ▲, Na_2SO_4; ●, mixed brine [2].

Figure 4-7 indicates a decrease in the measured diffusion coefficient with increasing salt molality. This decrease appears to be essentially linear in the case of NaCl and $CaCl_2$ brines. The nature of this decrease is dependent on the salt species present.

The experimental uncertainty of these experiments (see Figure 4-8) is calculated by the lack of fit to the working equation and calculated by the proprietary TopSpin software.

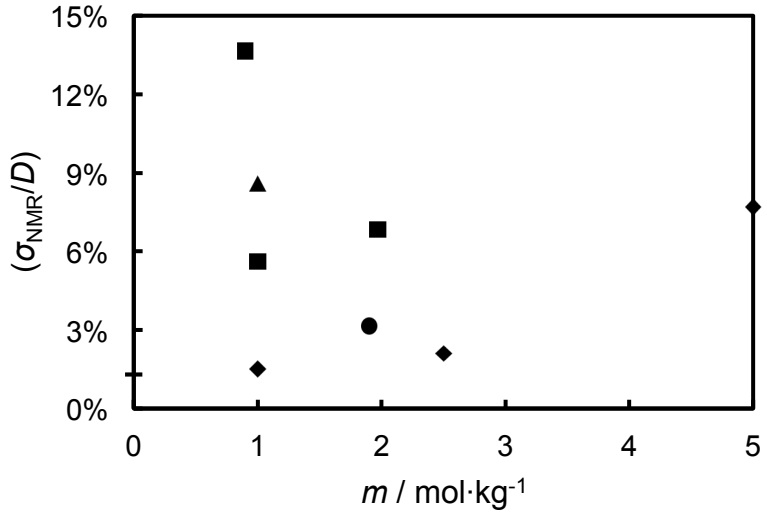

Figure 4-8. Uncertainty associated with the diffusion coefficient of CO_2 in a given brine plotted against brine molality *m*.
The brines investigated were: -, pure water; ◆, NaCl; ■, $CaCl_2$; ▲, Na_2SO_4; ●, mixed brine [2].

An attempt was made to extend the measurements to higher temperatures but it was found that the lower solubility of CO_2 at higher temperatures resulted in an unacceptable signal-to-noise ratio in the NMR measurements. This observation is made worse by the effect of temperature on the population distribution difference in NMR and to a lesser extent the increased signal attenuation caused by the larger diffusivity. Consequently, no useful results were obtained, except for a single point at T = 303.15 K in a 2.5 mol·kg^{-1} NaCl solution, which was found to be in good agreement with the value computed from Eq. (4-2) and Eq. (4-3). This is considered a limitation of the equipment used and it is likely that measurements could be performed at higher temperatures by using a larger magnetic field, a more sensitive detector, or pressurising the gas solution to increase the $^{13}CO_2$ concentration. Based on the work performed on the CO_2-water system, the effect of pressure was assumed to be negligible and therefore no experiments were performed above atmospheric pressure.

Discussion

The values of the diffusion coefficient for CO_2 in various salt solutions at T = 298 K and atmospheric pressure are plotted against the viscosity of the respective solution in Figure 4-9. The viscosities, with the exception of the prototype reservoir brine, were obtained from the relevant literature [25-28]. The viscosity of the 1.9 mol·kg^{-1}

mixed brine was measured at T = 298 K using an Ubbelohde capillary viscometer that had been calibrated with deionised water.

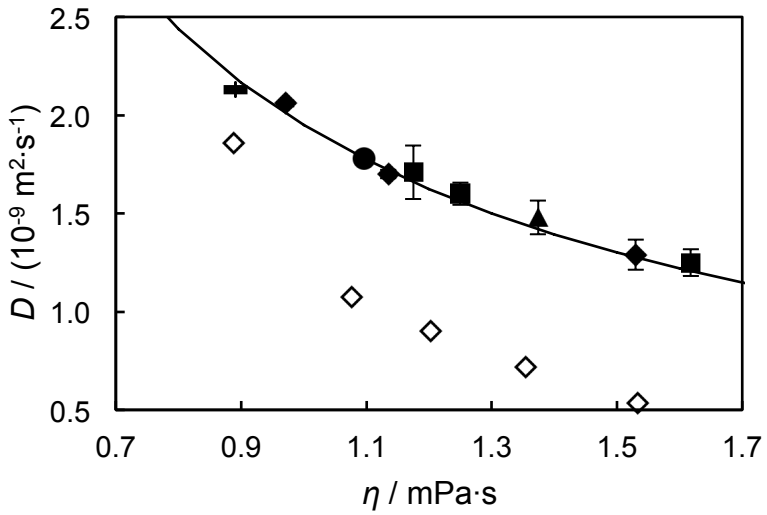

Figure 4-9. Diffusion coefficients, D, of CO_2 in the studied brines as a function of viscosity, η.
-, deionised water; ◆, NaCl; ■, $CaCl_2$; ▲, Na_2SO_4; ●, mixed brine. The solid line represents the Stokes-Einstein equation with a_{298} = 168 pm and n_{SE} = 4. Error bars shown the experimental uncertainty. Results are compared to previously reported values at T = 299 K and p = 5 MPa, ◇ [4].

Figure 4-9 shows a decrease in the diffusion coefficient with increasing solution viscosity. This trend lends itself to the theory that the diffusion coefficient of CO_2 can be treated as being a function of temperature and viscosity, without the need for determination of "*cross-diffusion*" parameters.

Quantitatively different behaviour from that reported elsewhere [4] is observed. It is highly unlikely that the cause of this difference is the difference between the two operating pressure. It should be noted that the operating procedure used in this source an aqueous fluorescent dye to identify the dispersion of the CO_2. The effect of this dye on the solution viscosity and the interfacial mass transfer was not reported but may impact on the results obtained.

The hypothesis to be tested in the present study was that the hydrodynamic radius of a CO_2 molecule in a brine is the same as that in pure water, so that the change in the tracer diffusion coefficient of CO_2 upon adding salt at constant temperature is simply a consequence of the change in the viscosity of the solvent. It is proposed that the effect of addition of salt has no appreciable effect on the hydrodynamic radius of the solute molecule. Figure 4-9 supports this hypothesis and illustrates a good agreement between the data obtained in this work and the values predicted *a priori*

from the modified Stokes-Einstein equation. Figure 4-10 shows the deviation between the measured values and the values predicted by this modified Stokes-Einstein correlation. All the data points obtained are within 5% of the predicted values.

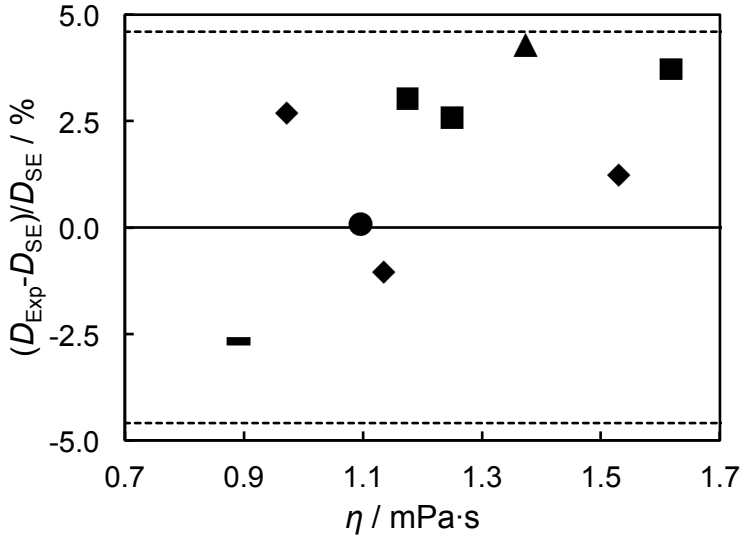

Figure 4-10. Deviation between the observed diffusion coefficients and those predicted from Eq. (4-2) and Eq. (4-3).
-, pure water; ◆, NaCl; ■, $CaCl_2$; ▲, Na_2SO_4; ●, mixed brine. The dashed line, ---, represents the expanded uncertainty. The dashed lines represent twice the standard deviation from the correlation, Eq. (4-2) and Eq. (4-3).

An alternative treatment of the data, also based on the Stokes-Einstein perspective on difffusion, is illustrated in Figure 4-11, below. The natural log of the diffusion coefficient was plotted against the natural log of the viscosity of the salt solution, Figure 4-11. The slope obtained from the collated data, approximately 0.93, agrees well with the typical value for many liquids [29].

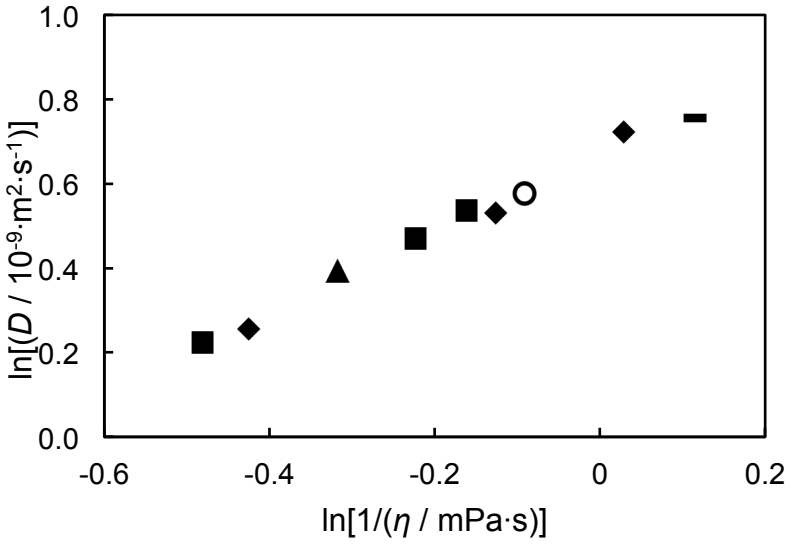

Figure 4-11. The natural log of the diffusivity plotted against the natural log of the brine viscosity.
-, pure water; ◆, NaCl; ■, $CaCl_2$; ▲, Na_2SO_4; ●, mixed brine.

Conclusions

The tracer diffusion coefficient of CO_2 in water, measured using the Taylor dispersion technique, between temperatures of (298 and 423) K is, within experimental uncertainty, independent of pressure. The diffusion coefficient can be predicted from the Stokes-Einstein equation, where the Stokes-Einstein number was taken to be 4 and the hydrodynamic radius is given by [168 $\times$ (1+0.002(T/K-298))] pm.

It is not possible to conclusively rationalise the lack of agreement between the results obtained in this work and the data obtained in the literature (refer to Appendix 1). It is pointed out that the bulk of the literature data was obtained prior to the 1970s using techniques that have not been as rigorously investigated as Taylor dispersion. The results obtained recently, using a technique based on Ramann IR [3] shows the same trend of diffusivity with temperature and pressure but the values are 15% lower than obtained in this work. As opposed to this technique, Taylor dispersion does not rely on using the solution of Fick's second law to determine the diffusion coefficient. The benefit of this is that often assumptions are used in the solution of Fick's laws, e.g. uni-directional diffusion, which may introduce errors or uncertainties in the calculated diffusion coefficients. For example, with respect to the aforementioned assumption and in light of the Taylor dispersion method, if the assumption of uni-directional diffusion is not strictly true, diffusion perpendicular to the main plane, i.e. smearing out of the solute, will not be accounted for and the measured diffusion coefficient will be correspondingly lower than the true value. It is also worth pointing out that the diffusion coefficient obtained at T = 298 K using the Taylor dispersion method was meaningfully similar, within 4.7%, to the value obtained using the NMR-PFG method. [2]

The diffusion of infinitely dilute CO_2 in a multi-component brine solution has been treated as tracer binary diffusion. Measurements were performed using pulsed field gradient-nuclear magnetic resonance and it was found the values obtained could be satisfactorily correlated using a modified Stokes-Einstein equation where the hydrodynamic radius was treated as a function of temperature and not a function of pressure or salinity. It is likely that the same pressure independence will exist for the CO_2-brine system as for the (CO_2 + water) system. The value of D for CO_2 in H_2O at T = 298 K as determined from nuclear magnetic resonance agreed well with the value obtained from Taylor dispersion.

References

[1] S.P. Cadogan, G.C. Maitland, J.P.M. Trusler, Diffusion Coefficients of CO_2 and N_2 in Water at Temperatures between 298.15 K and 423.15 K at Pressures up to 45 MPa, J. Chem. Eng. Data 59 (2014) 519-525.

[2] S.P. Cadogan, J.P. Hallett, G.C. Maitland, J.P.M. Trusler, Diffusion Coefficients of Carbon Dioxide in Brines Measured Using ^{13}C Pulsed-Field Gradient Nuclear Magnetic Resonance, J. Chem. Eng. Data 60 (2014) 181-184.

[3] W. Lu, H. Guo, I. Chou, R. Burruss, L. Li, Determination of diffusion coefficients of carbon dioxide in water between 268 and 473K in a high-pressure capillary optical cell with in situ Raman spectroscopic measurements, Geochim. Cosmochim. Acta 115 (2013) 183-204.

[4] A. Sell, H. Fadaei, M. Kim, D. Sinton, Measurement of CO_2 Diffusivity for Carbon Sequestration: A Microfluidic Approach for Reservoir-Specific Analysis, Environ. Sci. Technol. 47 (2012) 71-78.

[5] C. Secuianu, G.C. Maitland, J.P.M. Trusler, W.A. Wakeham, Mutual Diffusion Coefficients of Aqueous KCl at High Pressures Measured by the Taylor Dispersion Method, J. Chem. Eng. Data 56 (2011) 4840-4848.

[6] P.W.M. Rutten, Diffusion in Liquids, Applied Sciences, TU Delft, The Netherlands, 1992.

[7] R. Zwanzig, A.K. Harrison, Modifications of the Stokes–Einstein formula, J. Chem. Phys. 83 (1985) 5861-5862.

[8] H.A. Al-Ghawas, D.P. Hagewiesche, G. Ruiz-Ibanez, O.C. Sandall, Physicochemical Properties Important for Carbon Dioxide Absorption in Aqueous Methyldiethanolamine, J. Chem. Eng. Data 34 (1989) 385-391.

[9] P. Han, D.M. Bartels, Temperature dependence of oxygen diffusion in H_2O and D_2O, J. Phys. Chem. 100 (1996) 5597-5602.

[10] E.L. Cussler, Diffusion: Mass Transfer in Fluid Systems, Cambridge University 2009.

[11] G.L. Pollack, J.J. Enyeart, Atomic test of the Stokes-Einstein law. II. Diffusion of Xe through liquid hydrocarbons, Phys. Rev. A 31 (1985) 980.

[12] J. Guzmán, L. Garrido, Determination of Carbon Dioxide Transport Coefficients in Liquids and Polymers by NMR Spectroscopy, J. Phys. Chem. 116 (2012) 6050-6058.

[13] S.G. Schultz, A.K. Solomon, Determination of the Effective Hydrodynamic Radii of Small Molecules by Viscometry, J. Gen. Physiol. 44 (1961) 1189-1199.

[14] K. Krynicki, C.D. Green, D.W. Sawyer, Pressure and Temperature Dependence of Self-Diffusion in Water, Faraday Discuss. Chem. Soc. 66 (1978) 199-208.
[15] M.J.W. Frank, J.A.M. Kuipers, W.P.M. van Swaaij, Diffusion Coefficients and Viscosities of CO_2+ H_2O, CO_2+ CH_3OH, NH_3+ H_2O, and NH_3+ CH_3OH Liquid Mixtures, J. Chem. Eng. Data 41 (1996) 297-302.
[16] W.J. Thomas, M.J. Adams, Measurement of the Diffusion Coefficients of Carbon Dioxide and Nitrous Oxide in Water and Aqueous Solutions of Glycerol, Trans. Faraday Soc. 61 (1965) 668 - 673.
[17] J.K.A. Clarke, Kinetics of Absorption of Carbon Dioxide in Monoethanolamine Solutions at Short Contact Times, Ind. Eng. Chem. Fundam. 3 (1964) 239-245.
[18] A. Tamimi, E.B. Rinker, O.C. Sandall, Diffusion Coefficients for Hydrogen Sulfide, Carbon Dioxide, and Nitrous Oxide in Water over the Temperature Range 293-368 K, J. Chem. Eng. Data 39 (1994) 330-332.
[19] A.A. Unver, D.M. Himmelblau, Diffusion Coefficients of CO_2, C_2H_4, C_3H_6 and C_4H_8 in Water from 6° to 65° C, J. Chem. Eng. Data 9 (1964) 428-431.
[20] R.T. Ferrell, D.M. Himmelblau, Diffusion Coefficients of Nitrogen and Oxygen in Water, J. Chem. Eng. Data 12 (1967) 111-115.
[21] F.C. Tse, O.C. Sandall, DIFFUSION COEFFICIENTS FOR OXYGEN AND CARBON DIOXIDE IN WATER AT 25ºC BY UNSTEADY STATE DESORPTION FROM A QUIESCENT LIQUID, Chem. Eng. Commun. 3 (1979) 147-153.
[22] J.W. Mutoru, A. Leahy-Dios, A. Firoozabadi, Modeling Infinite Dilution and Fickian Diffusion Coefficients of Carbon Dioxide in Water, AlChE J. 57 (2011) 1617-1627.
[23] G.F. Versteeg, W. Van Swaalj, Solubility and Diffusivity of Acid Gases (CO_2, N_2O) in Aqueous Alkanolamine Solutions, J. Chem. Eng. Data 33 (1988) 29-34.
[24] O.A. Moultos, I.N. Tsimpanogiannis, A.Z. Panagiotopoulos, I.G. Economou, Atomistic Molecular Dynamics Simulations of CO_2 Diffusivity in H_2O for a Wide Range of Temperatures and Pressures, J. Phys. Chem. (2014).
[25] J.R. Cooper, R.B. Dooley, The International Association for the Properties of Water and Steam, 2008.
[26] J. Kestin, H.E. Khalifa, R.J. Correia, Tables of the dynamic and kinematic viscosity of aqueous NaCl solutions in the temperature range 20–150 C and the pressure range 0.1–35 MPa, J. Phys. Chem. Ref. Data 10 (1981) 71-88.
[27] F.A. Goncalves, J. Kestin, The Viscosity of $CaCl_2$ Solutions in the Range 20–50°C, Ber. Bunsen. Phys. Chem. 83 (1979) 24-27.
[28] T. Isono, Density, Viscosity, and Electrolytic Conductivity of Concentrated Aqueous Electrolyte Solutions at Several Temperatures. Alkaline-Earth Chlorides,

$LaCl_3$, Na_2SO_4, $NaNO_3$, NaBr, KNO_3, KBr, and $Cd(NO_3)_2$, J. Chem. Eng. Data 29 (1984) 45-52.

[29] K.R. Harris, The fractional Stokes–Einstein equation: Application to Lennard-Jones, molecular, and ionic liquids, J. Chem. Phys. 131 (2009) 054503 - 054508.

5. Diffusion Coefficients of CO_2 in Hydrocarbons

Measurements of diffusion coefficients of CO_2 at infinite dilution in various hydrocarbons are presented in this section. The solvents selected were n-heptane, n-hexadecane, 2,6,10,15,19,23-hexamethyltetracosane (squalane), cyclohexane and toluene. Flow rates were chosen to ensure the Reynolds number and De^2Sc number were both less than 20 for all systems studied. With the exception of the (CO_2 + heptane) system, these parameters were typically less than 10. Pressure was found to have a significant effect on the diffusion coefficient of these systems at a given temperature.

The diffusion coefficient of CO_2 in a mixed hydrocarbon containing equal moles of heptane and hexadecane was also investigated. The measurements were analysed based on a pseudo-binary treatment and a ternary solution of the Taylor dispersion model [1].

The results have been tabulated in Appendix 4.

Binary Diffusion of CO_2 in Liquid Hydrocarbons

Results

Diffusion coefficients at infinite dilution of CO_2 in heptane (C_7H_{16}), hexadecane ($C_{16}H_{34}$), squalane ($C_{30}H_{62}$), cyclohexane (C_6H_{12}), and toluene (C_7H_8) were measured over a range of temperatures (273 K < T < 423 K) and pressures (p < 69 MPa) using the Taylor dispersion apparatus (TDA). Figure 5-1 to Figure 5-5 show the measured diffusion coefficients plotted against temperature.

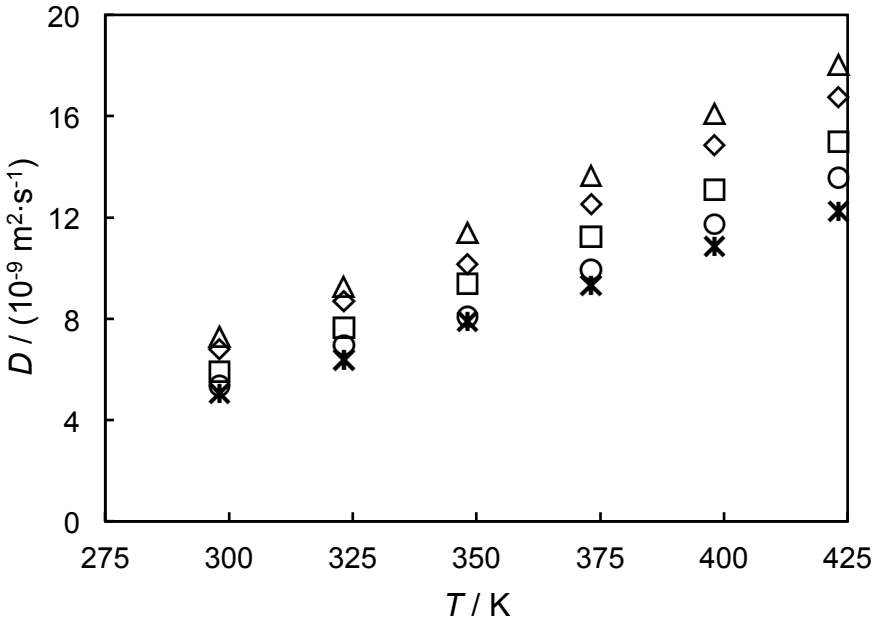

Figure 5-1. Infinite dilution diffusion coefficients of CO_2 in heptane plotted as a function of temperature.
Measurements were performed at: △, p = 1 MPa; ◇, p = 10 MPa; □, p = 30 MPa; ○, p = 50 MPa; ✱, p = 69 MPa.

Unlike the (CO_2 + H_2O) system, pressure has a pronounced effect on the diffusion coefficient of CO_2 in heptane, reducing D at a given temperature by as much as 33% between (1 and 69) MPa. This effect is consistent through the hydrocarbon systems investigated and reflects the greater compressibility of the hydrocarbon liquids compared with water.

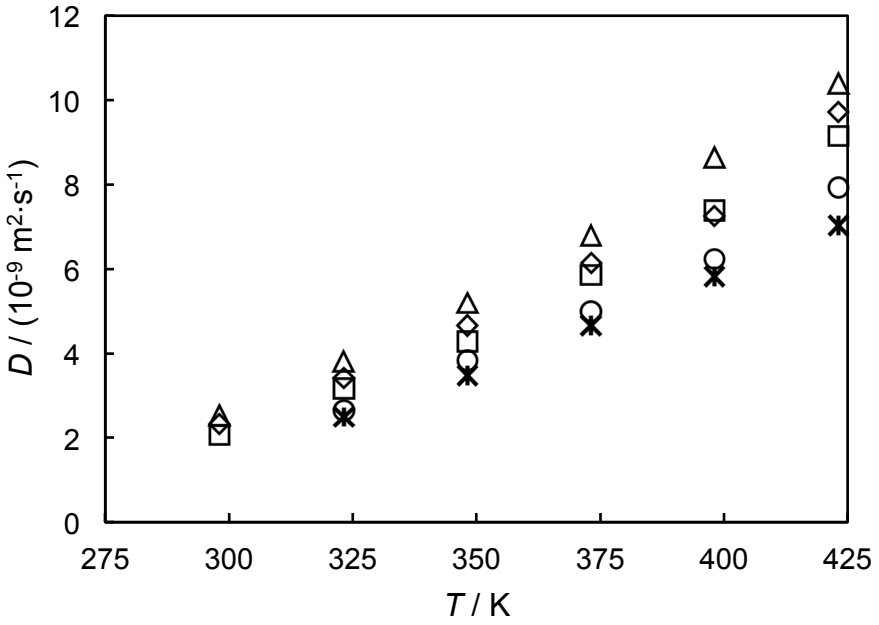

Figure 5-2. Infinite dilution diffusion coefficients of CO_2 in hexadecane plotted as a function of temperature.
Measurements were performed at: △, p = 1 MPa; ◇, p = 10 MPa; □, p = 30 MPa; ○, p = 50 MPa; ✱, p = 69 MPa.

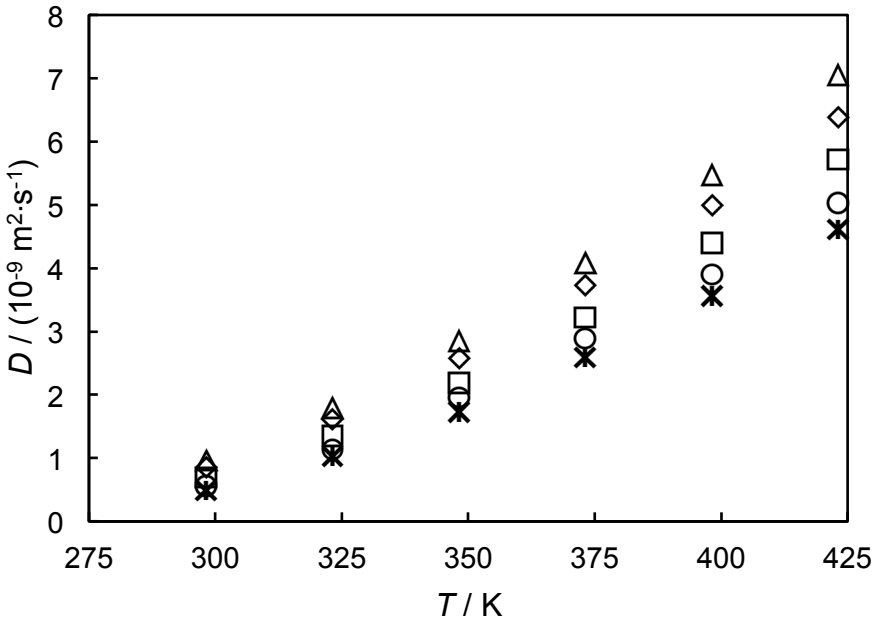

Figure 5-3. Infinite dilution diffusion coefficients of CO_2 in squalane plotted as a function of temperature.
Measurements were performed at: △, p = 1 MPa; ◇, p = 10 MPa; □, p = 30 MPa; ○, p = 50 MPa; ✱, p = 69 MPa.

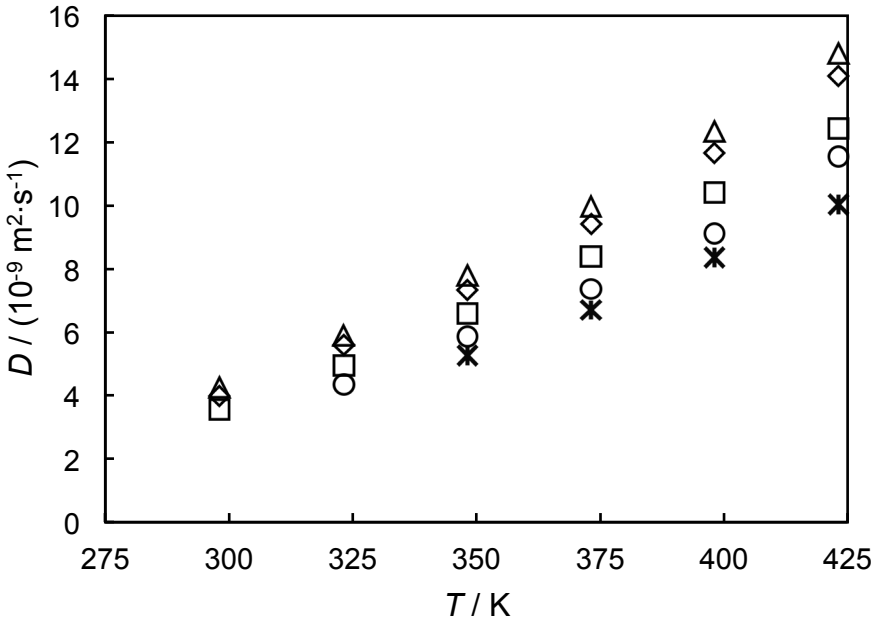

Figure 5-4. Infinite dilution diffusion coefficients of CO_2 in cyclohexane plotted against temperature.
Measurements were performed at: △, p = 1 MPa; ◇, p = 10 MPa; □, p = 30 MPa; ○, p = 50 MPa; ✱, p = 69 MPa.

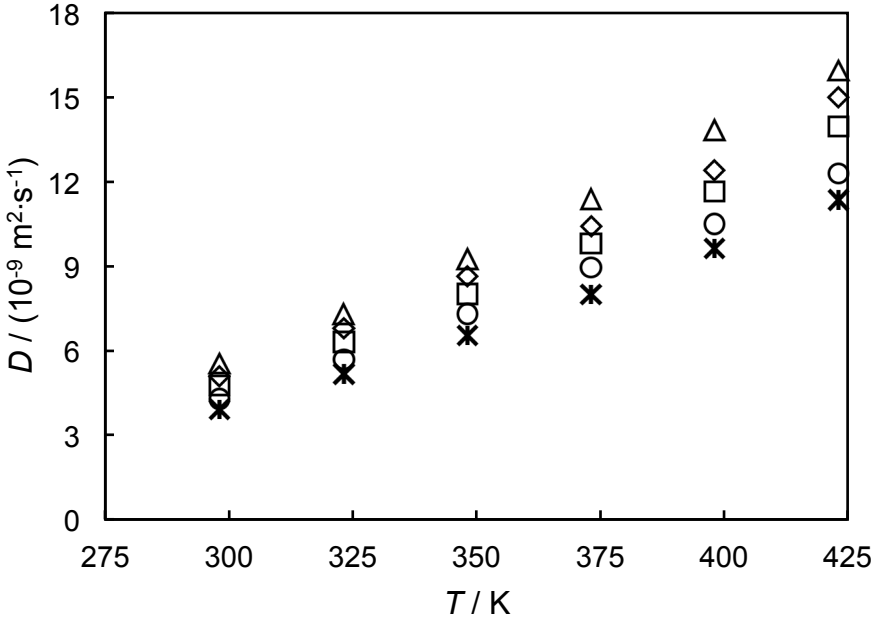

Figure 5-5. Infinite dilution diffusion coefficients of CO_2 in toluene plotted as a function of temperature.
Measurements were performed at: △, p = 1 MPa; ◇, p = 10 MPa; □, p = 30 MPa; ○, p = 50 MPa; ✱, p = 69 MPa.

The standard relative uncertainty associated with these measurements was calculated from the following equation:

$$u_r^2(D) = u_r^2(K) + 4u_r^2(R) + 4u_r^2(v) + \left[(p/D)(\partial D/\partial p)u_r(p)\right]^2 + \left[D^{-1}(\partial D/\partial T)u(T)\right]^2 \quad (5\text{-}1)$$

where $u_r(X)$ denotes standard relative uncertainty and $u(X)$ standard uncertainty of variable X. The standard uncertainties appearing on the right of Eq. (5-1), with the exception of $u_r(K)$, were as those used in the standard relative uncertainty for the (CO_2 + H_2O) system. This led to $u_r(D)$ = 1.5% for the systems investigated. The uncertainty was once again largely dominated by the uncertainty in the dispersion coefficient, K. The (CO_2 + $C_{16}H_{34}$) system exhibited the largest uncertainty with an average uncertainty of 2.0% and a maximum uncertainty of 9.3% (see Appendix 4B). The reason for this is the proximity of hexadecane to its freezing point at T = 323 K and p = 50 MPa. This resulted in a less stable pressure during the experiment, possibly due to fluctuations in the solvent viscosity.

Discussion

The magnitude of the diffusion coefficients for the (CO_2 + C_6H_{12}) and (CO_2 + C_7H_8) systems are similar to those of the (CO_2 + C_7H_{16}) system.The diffusivity is markedly smaller for the (CO_2 + $C_{16}H_{34}$) and (CO_2 + $C_{30}H_{64}$) systems. The diffusion coefficient for CO_2 in squalane at T = 423 K and p = 65 MPa is approximately 60% lower than the value obtained for the (CO_2 + C_7H_{16}) system. As the carbon number of a hydrocarbon increases the viscosity and molar volume of that molecule also tends to increase. The effect of this is to increase the resistance of the solvent to translational motion, reducing the diffusivity.

Figure 5-6 shows the diffusivity of CO_2 in heptane as a function of pressure. A similar trend with pressure was observed for all the (CO_2+hydrocarbon) systems studied.

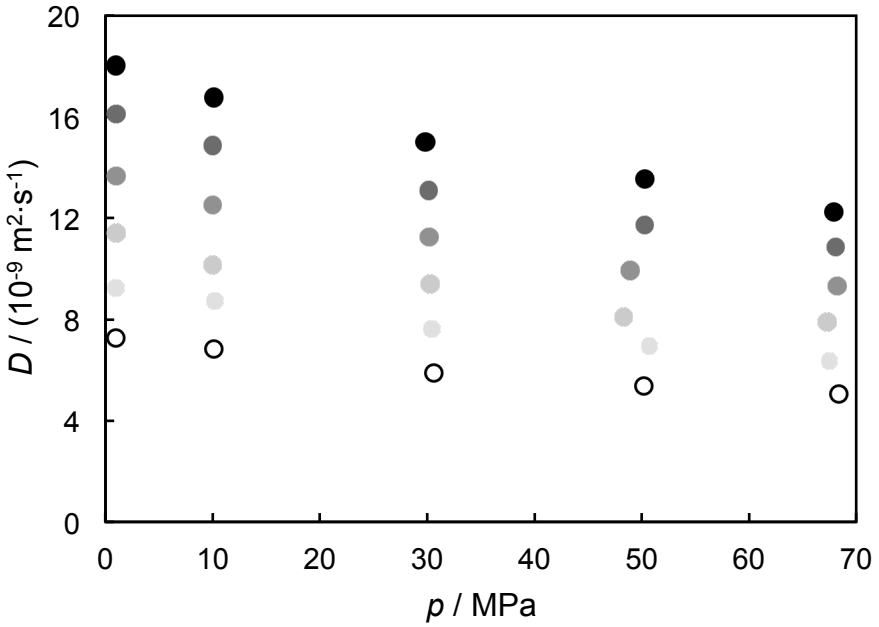

Figure 5-6. Diffusion coefficients of CO_2 in heptane plotted against pressure. Isotherms illustrated are at: ○, T = 298 K; ●, T = 323 K; ●, T = 348 K; ●, T = 373 K; ●, T = 398 K; and ●, T = 423 K.

The results presented here contradict the hypothesis that the diffusivity of a solute increases in a hydrocarbon with pressure [2-4]. This contradiction may be rationalised by the considering two separate phenomena. It has been shown that the solubility of a gas increases in a liquid as pressure increases. Because, in the literature sources [2-4], the diffusion coefficient of the solute is quantified from an absorption law, an increased difference between the equilibrium solubility and the solute concentration will result in a higher diffusion coefficient being observed. The second issue is due to the reduction in viscosity resulting from CO_2 addition. The effect of CO_2 addition on the viscosity of squalane, an often-used analogue for reservoir hydrocarbons, is very pronounced [5]. Both of these issues were not discussed in previous experimental literature [2-4].

Stokes-Einstein Model Based Correlation

Unlike the (CO_2 + H_2O) system, due to the effect of pressure, treating the hydrodynamic radius as solely a function of temperature was deemed insufficient. The hydrodynamic radius of the solute molecule is actually a function of both the intermolecular size of the solute molecule and the size of the cluster of solvating molecules. It is likely that while pressure has a negligible effect on the size of the solute molecule, it may have an influence on the distribution of the solvating

molecules around the solute. A modified Stokes-Einstein equation, in which the hydrodynamic radius of the solute was treated as a function of the solvent compressibility, treated through its density, was used to correlate the measured values.

Once again, the Stokes-Einstein equation is of the form:

$$D = \{k_B T / (n_{SE} \pi \eta a)\}. \quad (5\text{-}2)$$

Where, k_B is Boltzmann's constant, n_{SE} is the Stokes-Einstein number, taken to be 4, η is the solvent viscosity, and a is the hydrodynamic radius of the solute. All units are S.I.

Viscosities and densities were calculated using NIST RefProp based on previous literature; NIST14, Version 9.08 and [6] (heptane), 'RefProp', and [7] (toluene), and [8] and [9] (cyclohexane). These properties were calculated for hexadecane and squalane from recent literature [5, 10] as they were not available through NIST.

The hydrodynamic radius was correlated with the solvent denisty as follows:

$$a_i = \alpha_s \rho_m + c \quad (5\text{-}3)$$

The hydrodynamic radius corresponding to a measured diffusion coefficient was calculated for each data point from Eq. (5-2). These were then plotted against the solvent density respective state point (see Figure 5-7 and Figure 5-8).

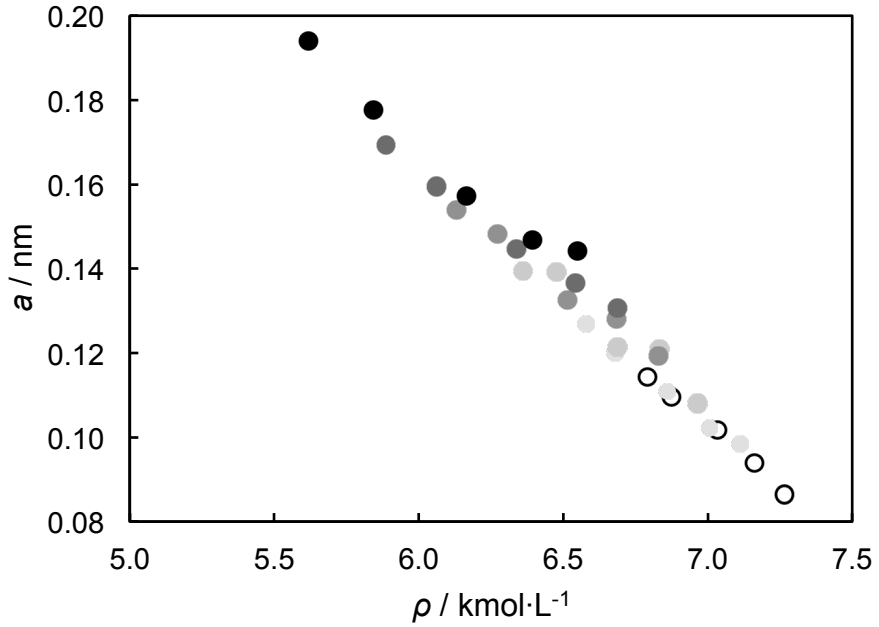

Figure 5-7. The fitted hydrodynamic radius of CO_2 in $C_{16}H_{34}$ plotted against solvent density.
Isotherms illustrated are at: ○, T = 298 K; ●, T = 323 K; ●, T = 348 K; ●, T = 373 K; ●, T = 398 K; and ●, T = 423 K.

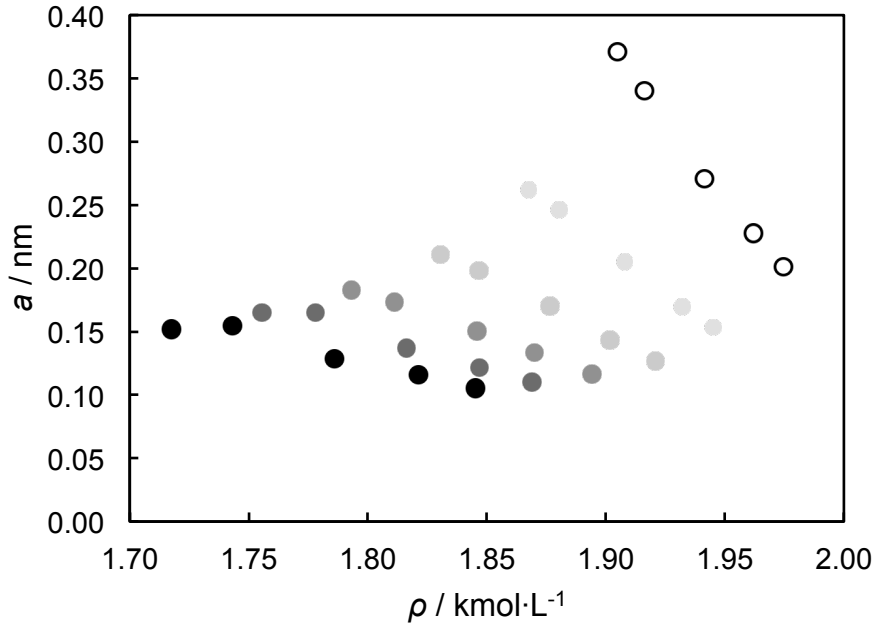

Figure 5-8. The fitted hydrodynamic radius of CO_2 in squalane plotted against solvent density.
The data is grouped by isotherms: ○, T = 298 K; ●, T = 323 K; ●, T = 248 K; ●, T = 373 K; ●, T = 398 K and ●, T = 423 K.

The hydrodynamic radius of CO_2 in heptane approximates very well as a linear function of density over the temperature and pressure range investigated. In the case of squalane the trend is not as clear, however it is noted that for a given isotherm there is a trend of decreasing hydrodynamic radius with increasing density. It is possible that as the length of an alkane increases the molecule becomes less rigid, i.e. the carbon-carbon bonds of the molecule become more capable of rotating. The hydrodynamic radius depends on the interactions between the solute and solvent. At higher temperatures the inter-molecular bonds in squalane have more energy to rotate and this is why its hydrodynamic radius becomes less sensitive to changes in density as T increases. As T increases, a decreases. It may be that at higher temperatures the methyl branches are rotating around the backbone at a high rate makes the molecule increasingly sterically hindered and increasingly insensitive to pressure. An interesting comparison to test the validity of this argument is to compare the change in a as a function of density for squalane ($C_{24}C_6$) and *n*-hexadecane (C_{16}), the second biggest solvent molecule investigated, bearing in mind hexadecane unlike squalane has no methyl branches associated with the main carbon backbone.

Finally, it should be mentioned that it is sometimes argued that the Stokes-Einstein equation is only suitable for systems in which the solute molecule is much larger than the solvent molecule [11]. It may be that the CO_2 solute molecule no longer experiences the squalane solvent as a continuous media, but rather as a discontinuous media in which collisions with both the molecule and the methyl branches act as a resistance to diffusivity.

The hydrodynamic radius was treated as a linear function of the solvent density for all hydrocarbons, except squalane. This relationship was then used to correlate the diffusion coefficient using the Stokes-Einstein equation. The quality of this correlation can be seen in Figure 5-9 to Figure 5-12. The fitted parameters for the hydrodynamic radius are tabulated in Appendix 5.

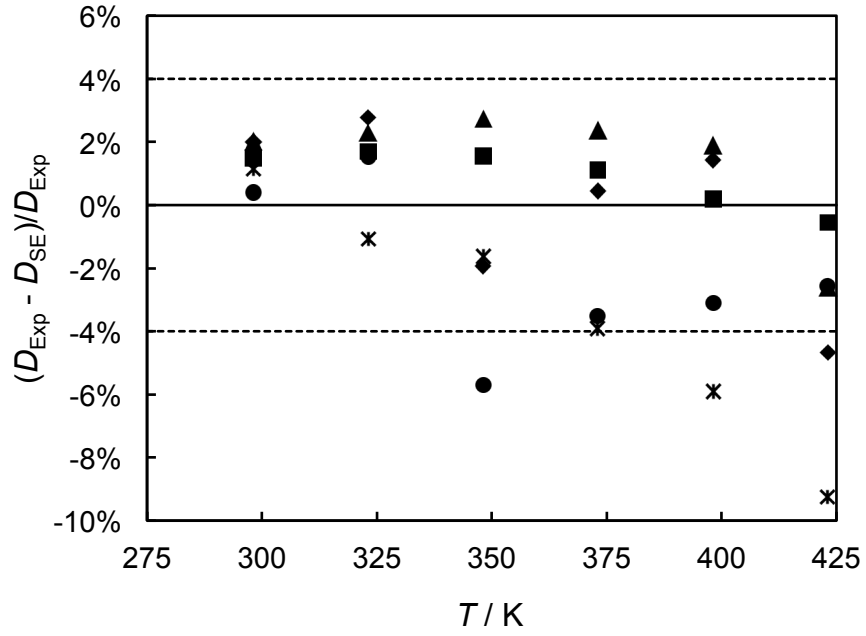

Figure 5-9. Deviation between measured and correlated diffusivities of CO_2 in heptane.
Measurements were performed at: ▲, p = 1 MPa; ◆, p = 10 MPa; ■, p = 30 MPa; ●, p = 50 MPa; ✱, p = 69 MPa. The dashed lines represent twice the standard deviation from the correlation.
α_S = -0.0625, c = 0.5416.

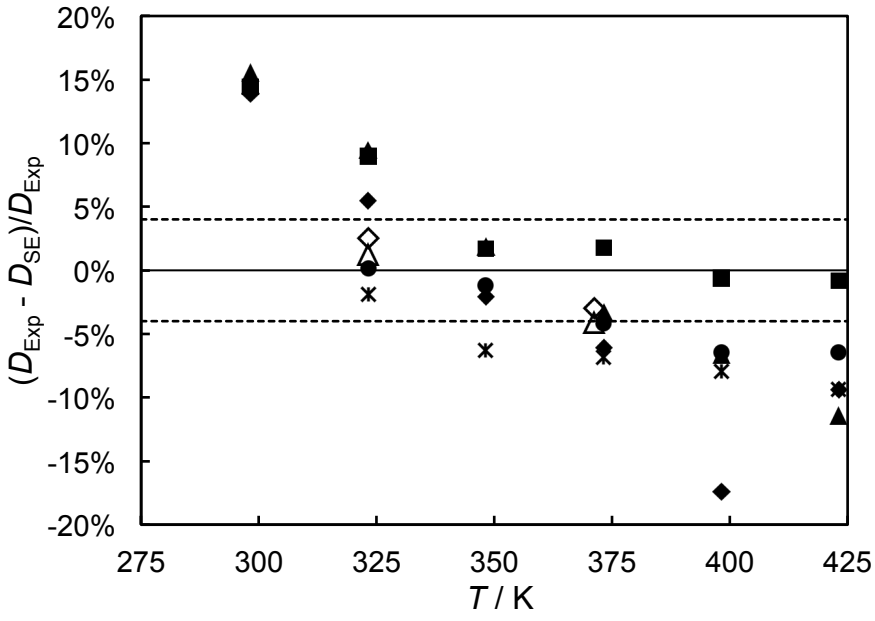

Figure 5-10. Deviation between measured and correlated diffusivities of CO_2 in hexadecane.
Measurements were performed at: ▲, p = 1 MPa; ◆, p = 10 MPa; ■, p = 30 MPa; ●, p = 50 MPa; ✱, p = 69 MPa. The dashed lines represent twice the standard deviation from the correlation.
α_S = -0.0764, c = 0.3073.

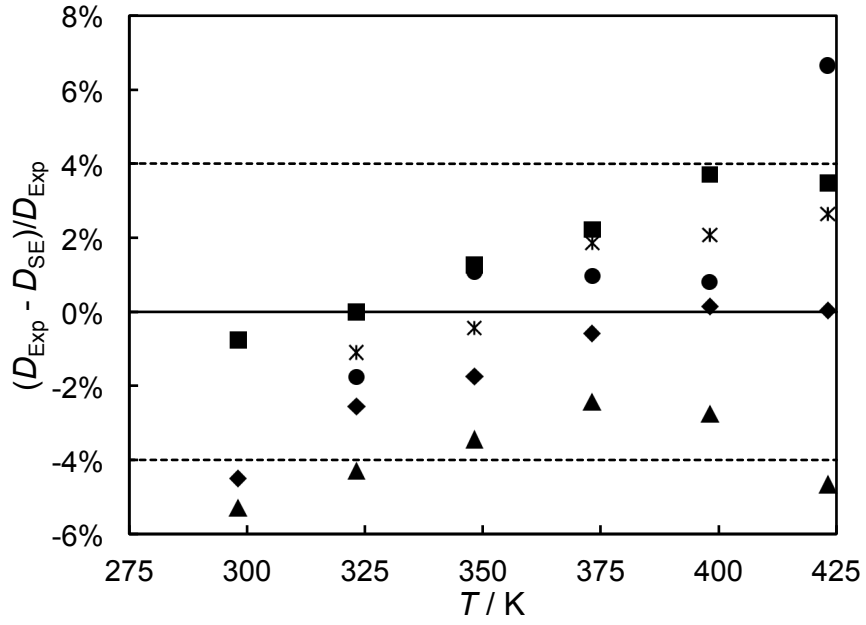

Figure 5-11. Deviation between measured diffusivities and the correlated diffusivities of CO_2 in cyclohexane.
Measurements were performed at: ▲, p = 1 MPa; ◆, p = 10 MPa; ■, p = 30 MPa; ●, p = 50 MPa; ✱, p = 69 MPa. The dashed lines represent twice the standard deviation from the correlation.
α_S = -0.0438, c = 0.4846.

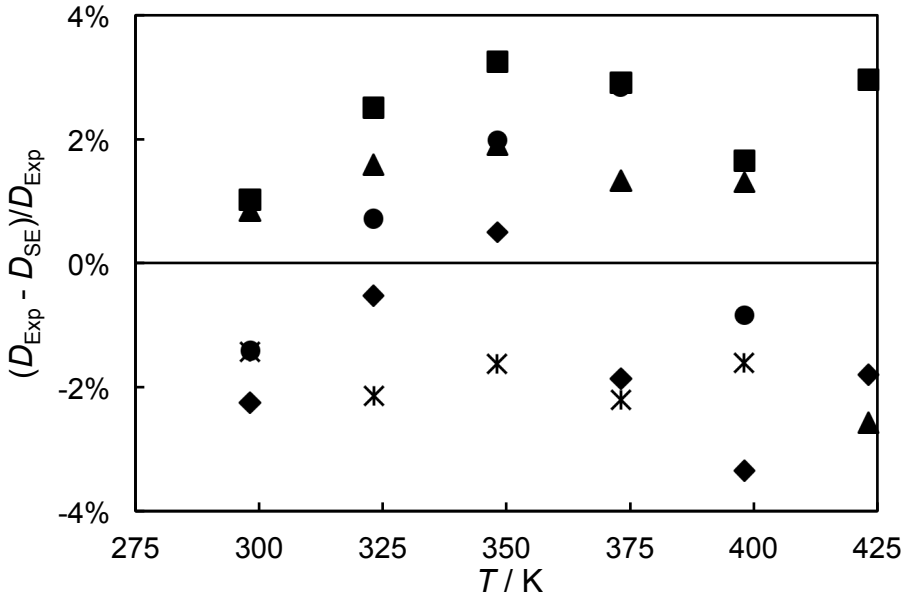

Figure 5-12. Deviation between the obtained data points and those correlated diffusivities of CO_2 in toluene.
Measurements were performed at: ▲, p = 1 MPa; ◆, p = 10 MPa; ■, p = 30 MPa; ●, p = 50 MPa; ✱, p = 69 MPa. The dashed lines represent twice the standard deviation from the correlation.
α_S = -0.0334, c = 0.4222.

As can be noted from Figure 5-8, treating the hydrodynamic radius of CO_2 in squalane as a linear function of the corresponding density of squalane was insufficient, yielding an average deviation of 24%. Instead α_S and c were treated as second-order order polynomials in *T*. The average deviation between the hydrodynamic radius fitted to the *D* from the Stokes-Einstein relationship and value calculated from the polynomial correlation was 7.1% with a maximum deviation of 15%. The greatest deviations were at *T* = 298 K.

$$\alpha_s = \sum_{i=0}^{2} A_i \left(T/K\right)^i \tag{5-4}$$

$$c = \sum_{i=0}^{2} C_i \left(T/K\right)^i \tag{5-5}$$

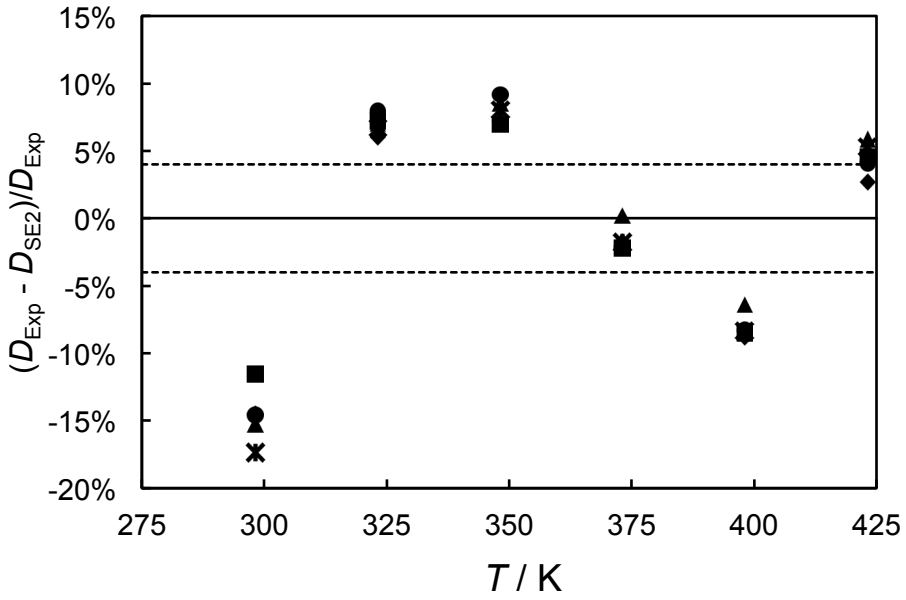

Figure 5-13. Deviation between measured and correlated diffusivities of CO_2 in squalane.
Measurements were performed at: ▲, *p* = 1 MPa; ◆, *p* = 10 MPa; ■, *p* = 30 MPa; ●, *p* = 50 MPa; ✱, *p* = 69 MPa. The dashed lines represent twice the standard deviation from the correlation.
A_0 = -20.32, A_1 = 0.0941, A_2 = -1.111 x 10^{-4}.
C_0 = 42.06, C_1 -0.1953, C_2 2.313 x 10^{-4}.

Another modification of the Stokes-Einstein hydrodynamic method for modelling diffusion coefficients involves a hydrodynamic radius that is essentially independent of temperature or pressure and includes an exponent term related to the solution viscosity [12-15]. This method was also used to correlate the diffusivities obtained.

By fitting the hydrodynamic radius, *a*, and the viscosity power, *ζ*, a good fit to the data for the (CO_2 + C_7H_{16}), (CO_2 + C_6H_{12}) and (CO_2 + C_7H_8) systems with an AAD of (1.71, 3.04 and 1.80)% and MAD of (4.87, 7.48 and 3.28)% obtained, respectively. However, as with the other approaches, this approach was not as successful for the remaining systems. The AAD and MAD corresponding to the (CO_2 + $C_{16}H_{34}$) and (CO_2 + $C_{30}H_{62}$) systems were (9.86 and 20.56)% and (28.00 and 82.33)% respectively. Fixing *ζ* to 2/3 [14] increased the deviations between the experimental points and the prediction by approximately 45%.

Rough Hard Sphere Theory Based Correlation

The Stokes-Einstein model clearly has some limitations in describing the diffusivities of CO_2 in a hydrocarbon solvent, so another correlation, based on the rough hard sphere kinetic theory, in terms of the molar volume at the experimental state point and the close packed molar volume, as defined in the hard-sphere theory of transport properties in pure liquids, at the experimental pressure, was fitted to the experimental data.

$$D/\sqrt{T} = \beta\left(V - bV_0\right) \tag{5-6}$$

The nomenclature is as per Chapter 2, V and V_0 denote the molar volume and close packed molar volume, β and b are fitted variables associated with lumped constants of the rough hard sphere theory and corrections for high density from empirical treatment of the model. Figure 5-14 illustrates suitability of this treatment.

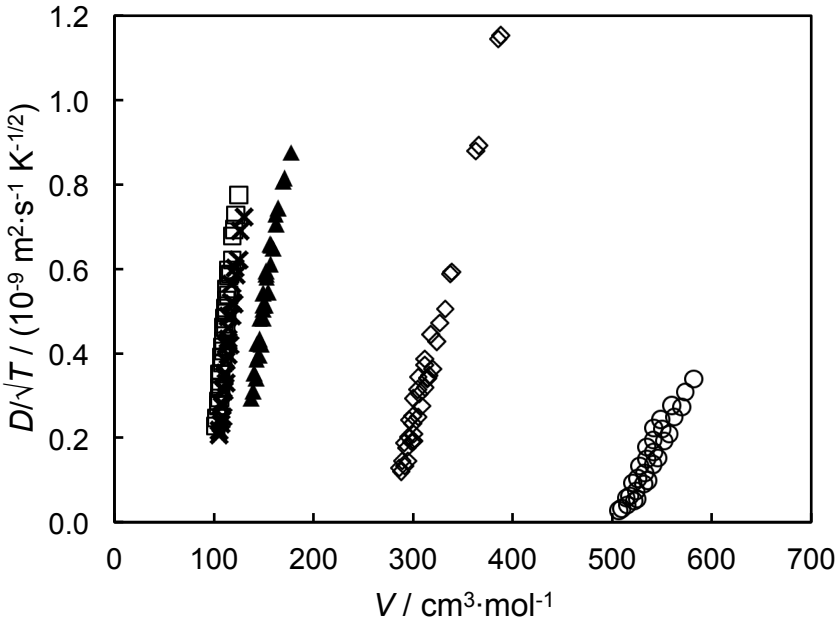

Figure 5-14. CO_2 diffusion coefficients in hydrocarbons divided by $T^{0.5}$ plotted against the solvent molar volume.
The solvents were: ▲, heptane; ◇, hexadecane; O, squalane; ×, cyclohexane and □, toluene.

Correlations for the close packed molar volume of hexadecane, squalane, heptane and toluene were taken from literature sources [5, 10, 16, 17]. The close packed volume of CO_2 was also taken from the literature [5].

No literature close packed molar volume data were found for cyclohexane. Data for the viscosity of cyclohexane over a range of temperature and pressure [8, 18-20] was used to extract and correlate this parameter. The correlation obtained for the close packed volume was as follows;

$$V_0 / (\mathrm{cm}^3 \cdot \mathrm{mol}) = 84.939 - 7.9182\left(T / 300\ \mathrm{K}\right) \qquad (5\text{-}7)$$

The roughness factor for viscosity was 0.96 and the fit quality was excellent; AAD = 0.8%, MAD = 2.5%. However, the experimental data only covered the temperature range up to 348 K and so extrapolation to higher temperatures may introdue uncertainties.

As the core diameter of the solute and the solvent are also weak functions of temperature a correction, Λ, was added in terms of the close-packed volume. The product of Eq. (5-6) and Eq. (5-8) yielded $D/\sqrt{T}$.

$$\Lambda = \frac{2\left(V_{0,2}^{T} + V_{0,CO_2}^{T}\right) - \left(V_{0,2}^{298K} + V_{0,CO_2}^{298K}\right)}{V_{0,2}^{298K} + V_{0,CO_2}^{298K}} \tag{5-8}$$

The superscript *T* denotes the close packed volume at the temperature the diffusion coefficient is measured at while the superscript 298K denotes the close packed volume at T = 298 K. The subscript 2 denotes the respective solvent. This correction is small, less than 3.5%, but not insignificant. This treatment results in two parameters, b and β, to be fitted.

Figure 5-15 to Figure 5-18 show the agreement between the experimental data and the correlation proposed. The fitted parameters for this correlation are tabulated in Appendix 5.

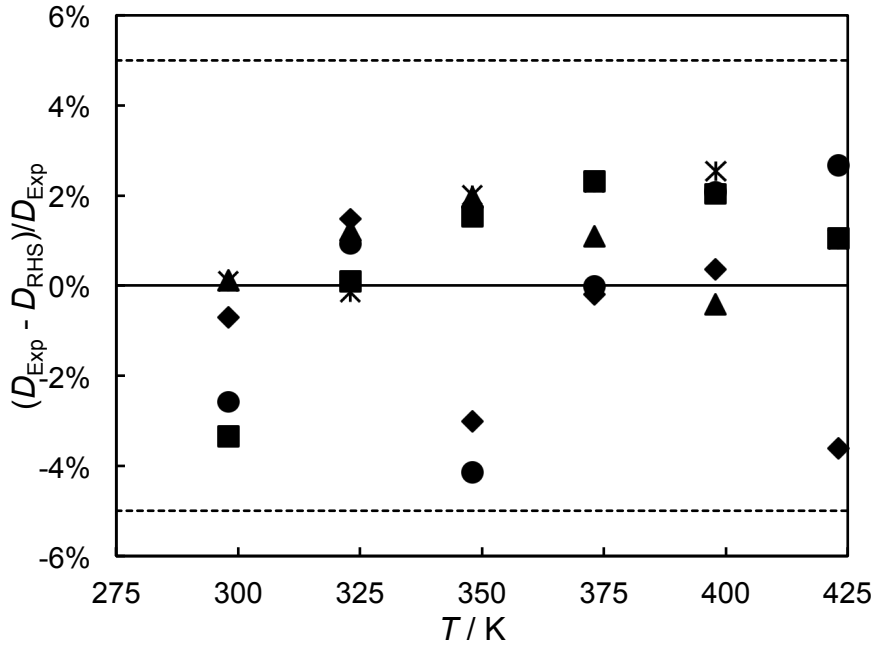

Figure 5-15. Deviation between the measured and correlated diffusivity for CO_2 in heptane.
Measurements were performed at: ▲, p = 1 MPa; ◆, p = 10 MPa; ■, p = 30 MPa; ●, p = 50 MPa; ✱, p = 69 MPa. The dashed lines represent twice the standard deviation from the correlation.
$\beta = 1.34 \times 10^{-12}$ ($m^2 \cdot s^{-1} \cdot K^{-0.5} \cdot m^{-3} \cdot mol$) and b = 1.24.

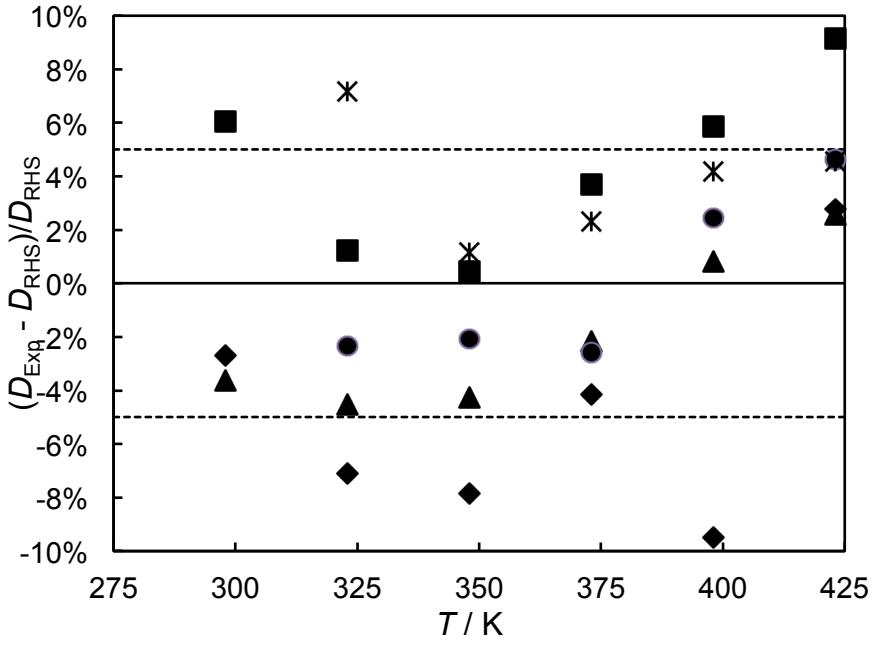

Figure 5-16. Deviation between the measured and correlated diffusivity for CO_2 in hexadecane.
Measurements were performed at: ▲, p = 1 MPa; ◆, p = 10 MPa; ■, p = 30 MPa; ●, p = 50 MPa; ✱, p = 69 MPa. The dashed lines represent twice the standard deviation from the correlation.
$\beta = 5.90 \times 10^{-13}$ ($m^2 \cdot s^{-1} \cdot K^{-0.5} \cdot m^{-3} \cdot mol$) and b = 1.22.

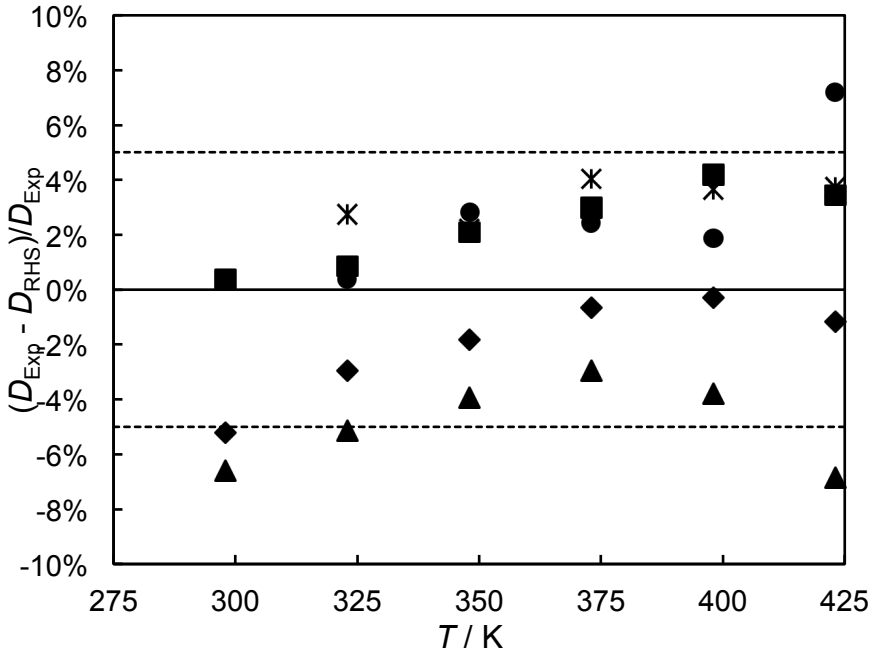

Figure 5-17. Deviation between the measured and correlated diffusivity of CO_2 in cyclohexane.
Measurements were performed at: ▲, p = 1 MPa; ◆, p = 10 MPa; ■, p = 30 MPa; ●, p = 50 MPa; ✱, p = 69 MPa. The dashed lines represent twice the standard deviation from the correlation.
$\beta = 1.87 \times 10^{-12}$ ($m^2 \cdot s^{-1} \cdot K^{-0.5} \cdot m^{-3} \cdot mol$) and b = 1.23.

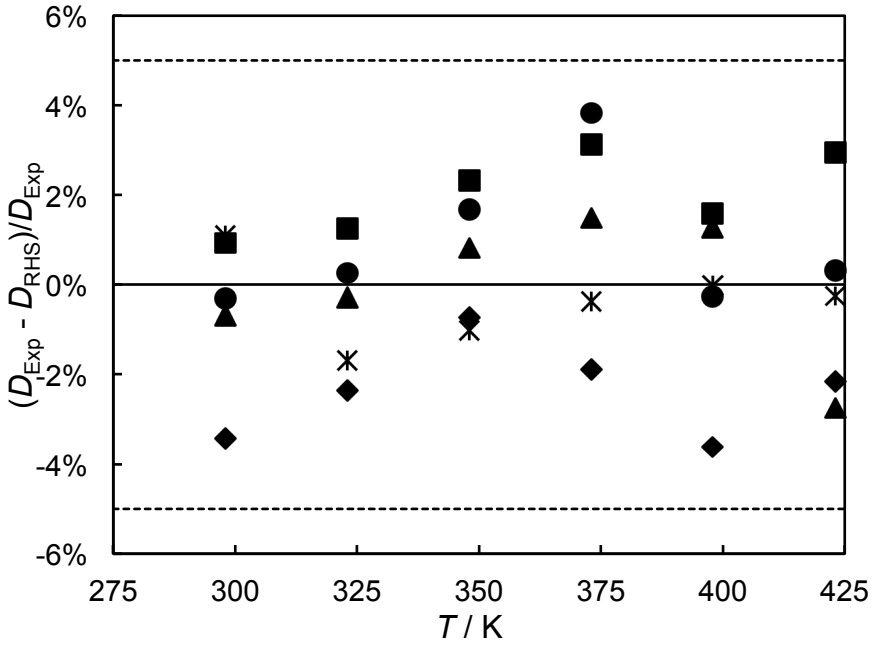

Figure 5-18. Deviation between the measured and correlated diffusivity of CO_2 in toluene.
Measurements were performed at: ▲, p = 1 MPa; ◆, p = 10 MPa; ■, p = 30 MPa; ●, p = 50 MPa; ✱, p = 69 MPa. The dashed lines represent twice the standard deviation from the correlation.
β = 1.98 × 10^{-12} ($m^2 \cdot s^{-1} \cdot K^{-0.5} \cdot m^{-3} \cdot mol$) and b = 1.27.

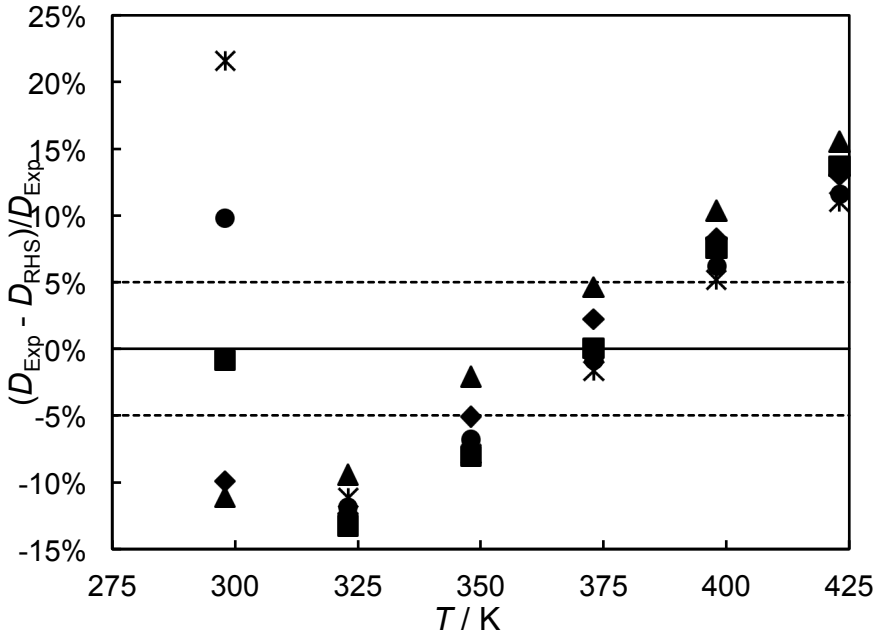

Figure 5-19. Deviation between the measured and correlated diffusivity for CO_2 in squalane.
Measurements were performed at: ▲, p = 1 MPa; ◆, p = 10 MPa; ■, p = 30 MPa; ●, p = 50 MPa; ✱, p = 69 MPa. The dashed lines represent twice the standard deviation from the correlation.
β = 2.10 × 10^{-13} ($m^2 \cdot s^{-1} \cdot K^{-0.5} \cdot m^{-3} \cdot mol$) and b = 1.16.

The value for *b* was relatively constant at approximately 1.23, with the exception of squalane. However, the solute-solvent specific parameter *β* varied more noticeably. With the exception of squalane the proposed treatment correlates the data satisfactorily, to within ± 2.5%. The predicted values for the (CO_2 + squalane) system are least satisfactory at T = 298 K. It is believed this is due to the proximity of V to V_0. The results from the (CO_2 + squalane) system were correlated again without including the results at T = 298 K in the fitting procedure. As can be seen in Figure 5-20, while a systematic error remains using this process, the quality of fit is greatly increased.

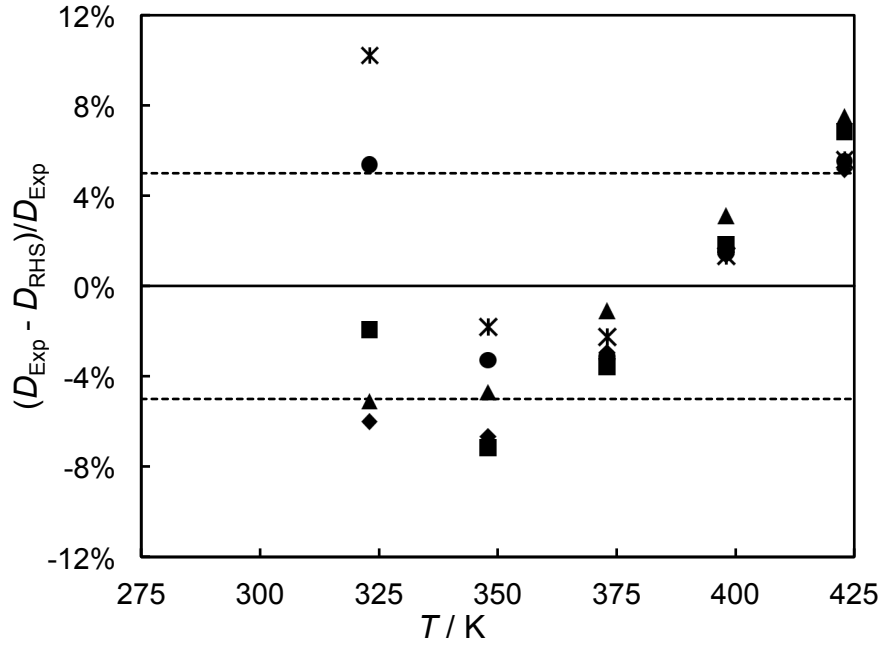

Figure 5-20. Deviation between the measured and correlated diffusivity for CO_2 in squalane where values obtained at T = 298 K omitted.
Measurements were performed at: ▲, p = 1 MPa; ◆, p = 10 MPa; ■, p = 30 MPa; ●, p = 50 MPa; ✱, p = 69 MPa. The dashed lines represent twice the standard deviation from the correlation.
$\beta = 2.49 \times 10^{-13}$ ($m^2 \cdot s^{-1} \cdot K^{-0.5} \cdot m^{-3} \cdot mol$) and b = 1.1835.

Diffusion of CO_2 in a Hydrocarbon Mixture

Results

Figure 5-21 and Figure 5-22 show the measured refractive index corresponding to the injection of CO_2 and a (CO_2 + heptane) mixture into a 50:50 mole mixture of heptane and hexadecane, respectively, plotted against the time elapsed since the injection was performed. The deviation between the experimental data and the Taylor-Aris model of dispersion (as per Eq. (3-2) to Eq. (3-4)) treating the system as a pseudo-binary solution, is shown below the solute dispersion curves.

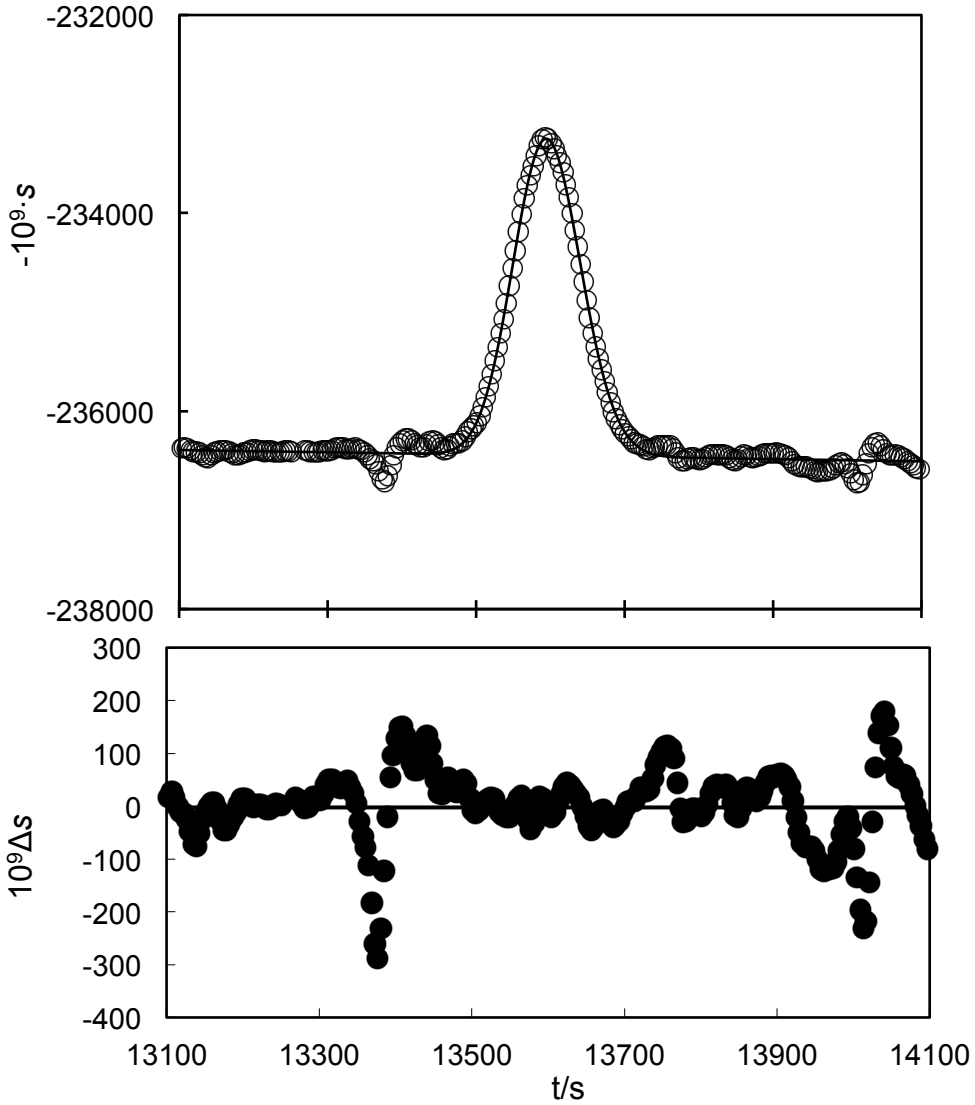

Figure 5-21: (top) Dispersion curve $s(t)$ for an injection of excess CO_2, in an equimolar solution of heptane and hexadecane.
This experiment was performed at T = 423 K and p = 49.5 MPa.
The solid line shows the values predicted by the Taylor-Aris model for a single solute in a single solvent.
(bottom) Deviations Δs between the experimental data and the fitted model.

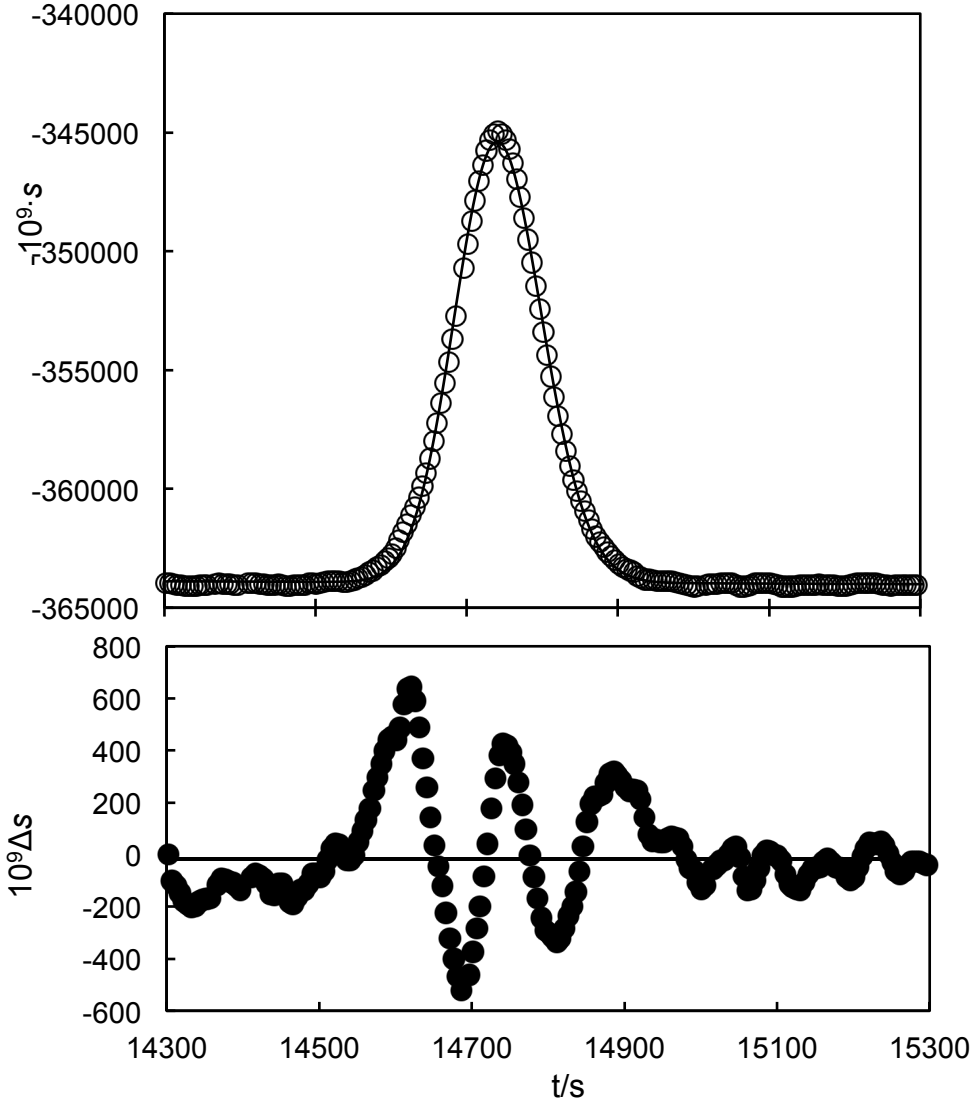

Figure 5-22. (top) Dispersion curve $s(t)$ for an injection of excess CO_2 and heptane, in an equimolar solution of heptane and hexadecane.
This measurement was performed at T =423 K and p = 51.3 MPa plotted against time since the injection was performed.
The solid line shows the values predicted by the Taylor-Aris model for a single solute in a single solvent.
(bottom) Deviations Δs between the experimental data and the fitted model.

The observed behaviour shown in Figure 5-22 appears essentially Gaussian, however, when compared to the working equation a noticeable and systematic deviation between the experimental data and fitted model is noted.

Discussion

The diffusion coefficients as calculated from the classical Taylor-Aris model for binary diffusion are shown in Figure 5-23 and Figure 5-24.

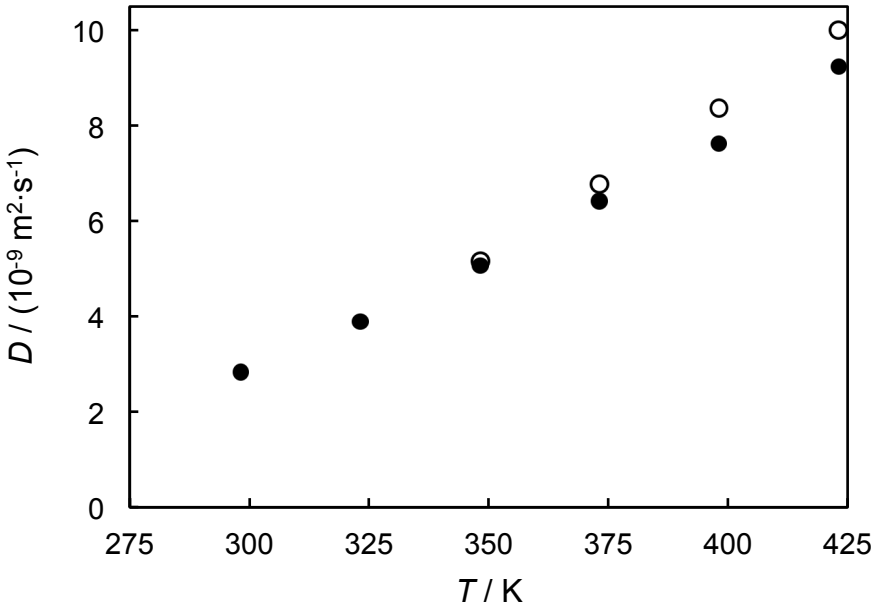

Figure 5-23. Pseudo-binary diffusion coefficient of CO_2 in an equimolar solution of heptane and hexadecane plotted against temperature. Measurements were carried out at: ○, p = 30 MPa and ●, p = 50 MPa.

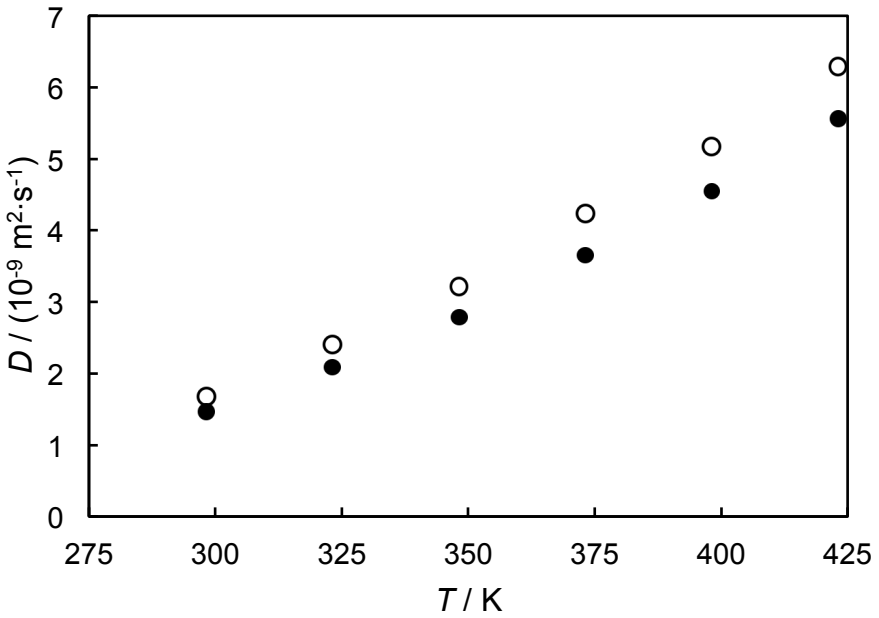

Figure 5-24. Pseudo-binary diffusion coefficient of CO_2 and heptane in an equimolar solution of heptane and hexadecane plotted against temperature. Measurements were carried out at: ○, p = 30 MPa and ●, p = 50 MPa.

This pseudo-binary diffusivity follows the expected trend with temperature. There is a marked reduction in the pseudo-binary diffusion coefficients for the system in which excess CO_2 and heptane were added (see Figure 5-24) compared to the system in which only excess CO_2 was added (see Figure 5-23). As with the binary systems, there is a reduction in the magnitude of the diffusion coefficient with increasing pressure. The scale of this reduction is less pronounced for the case where the perturbation to the mobile phase was the addition of excess CO_2.

The values associated with Figure 5-23 do not correspond to an arithmetic mean of the diffusion coefficients of CO_2 in pure heptane and CO_2 in pure hexadecane.

As previously discussed, to accurately describe the diffusive behaviour of a system of three or more species, a collection of binary diffusion coefficients does not typically suffice. Under certain assumptions a ternary system can be treated as a binary system as previously discussed. However, in the investigated ternary hydrocarbon system two species are present in considerable amounts. The data were therefore analysed using a recently developed method to model Taylor dispersion of ternary systems (as per Eq. (3-6) to Eq. (3-8)) [22, 23]. An example is shown in Figure 5-25.

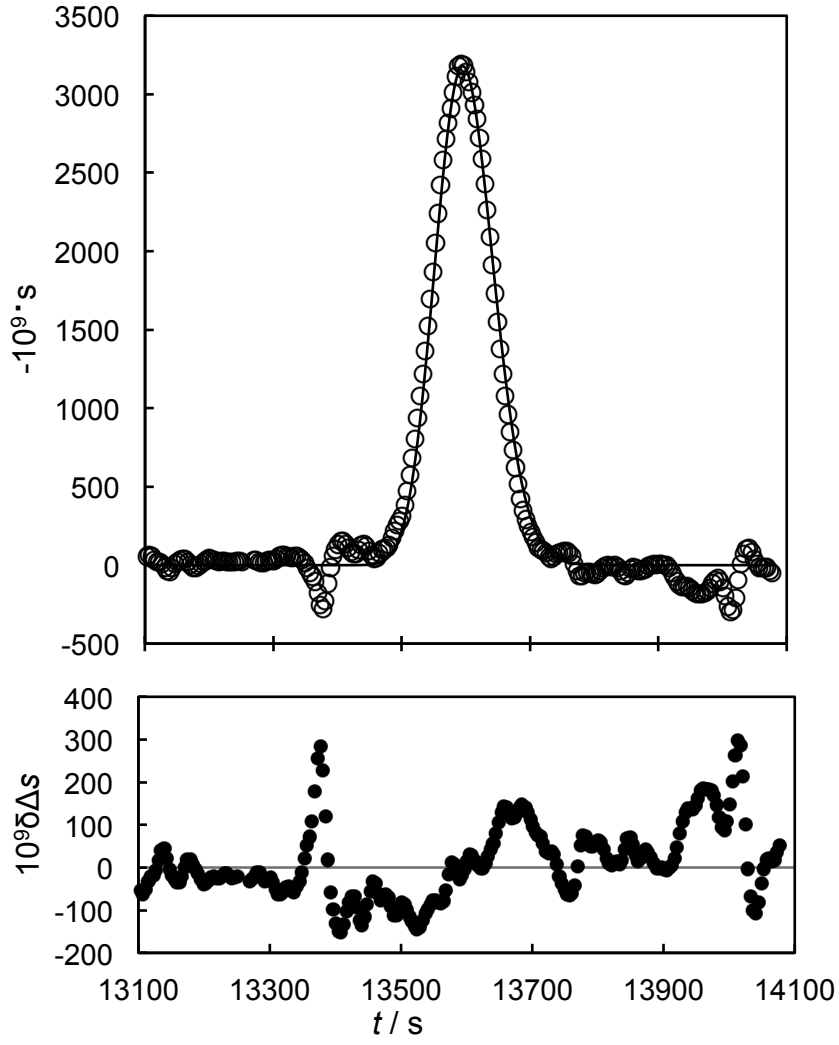

Figure 5-25. (top) Dispersion curve $s(t)$ for an injection of excess CO_2, in a equimolar solution of heptane and hexadecane.
The measurement was performed at T =423 K and p = 51.3 MPa plotted against time since the injection was performed.
The solid line shows the values predicted by the Taylor-Aris model for a ternary system.
(bottom) Deviations Δs between the experimental data and the fitted model.

The deviation between the experimental data and the predictions for the Taylor-Aris model for ternary systems (Figure 5-25 – (bottom)) is not significantly better than the deviation between the experimental data and the Taylor-Aris model for a binary system (Figure 5-21 – (bottom)).

The diffusion results obtained, at temperatures between (298 and 423) K and at pressures of (30 and 50) MPa, are illustrated in Figure 5-26.

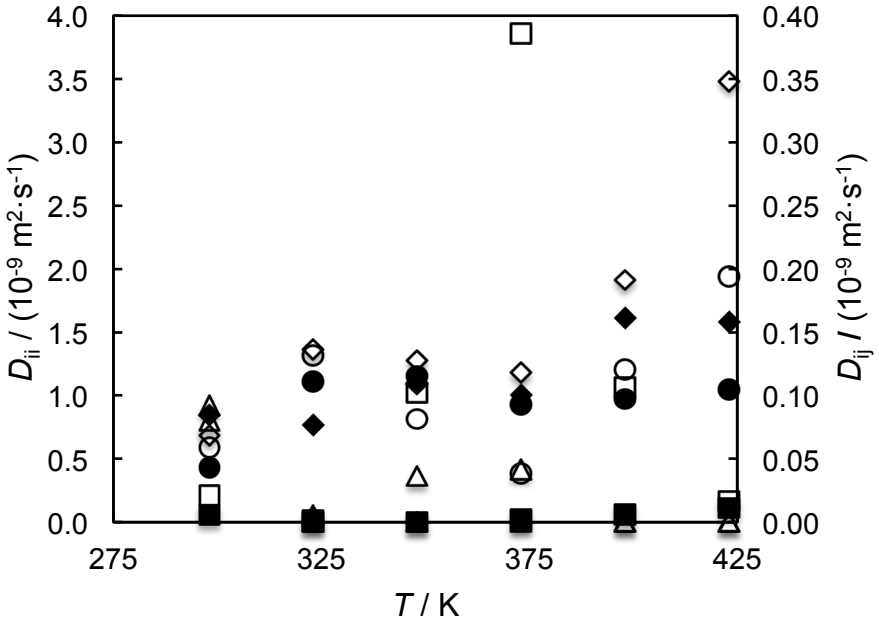

Figure 5-26. Diffusion coefficient matrix for the (CO_2 (1) + heptane (2) + hexadecane) system obtained by using the Taylor-Aris model for a ternary system.
◇, D_{11}; □, D_{12}; △, D_{21}; ○, D_{22}. Empty symbols denote measurement performed at p = 30 MPa and filled symbols denote p = 50 MPa.

It was noted that the diffusion coefficients obtained were more sensitive to the initial guess used in the fitting procedure than the binary diffusion coefficients reported in this and the previous chapter. It is possible that this is due to the fact four parameters are being fitted to only four dispersion profiles.

The results obtained are unconvincing and the behaviour observed is far more complicated than the behaviour of the binary systems. The main diffusion terms, D_{11} and D_{22}, are the dominant terms and do not change appreciably with the initial guesses even when the cross diffusion terms, D_{12} and D_{21}, are set to zero. However, as opposed to binary systems where the diffusivity increases uniformly with temperature the main diffusion terms in Figure 5-26 are relatively insensitive to tempreature. While more complicated behaviour is expected from multi-component systems the trend indicated here is difficult to rationalise and it is possible experimental uncertainty is affecting the results obtained.

Conclusions

The diffusivity of CO_2 in a hydrocarbon is a function of pressure. A decrease in diffusivity of approximately 45% at a given temperature was common over the pressure range investigated. Correlations based on the Stokes-Einstein equation and rough hard sphere theory were not suitable to calculate the diffusion coefficient in these mixtures *ab intio*, but proved adequate to correlate the results for the smaller hydrocarbons. These correlations were unable to predict the diffusivity of the (CO_2 + squalane) system to within 15%. Previously reported values for the diffusion coefficient of CO_2 in n-hexadecane [21] were compared to the values predicted by the rough hard sphere based correlation of the values obtained in this work. The data was found to agree with the current work to within 5% between T = (323 and 443) K, within 10% at T = 513 K, and with a maximum deviation of 19% at T = 564 K.

A ternary system, compromised of CO_2, heptane, and hexadecane was investigated. It was expected the dependence of the four diffusion coefficients relevant to this ternary system on temperature and pressure would be more complicated that that of binary diffusivities. However, the trends observed were even more difficult to rationalise than expected. The measurements were also interpreted by treating the problem as CO_2 diffusing in essentially a pure solvent, i.e. a binary system. The results obtained when an excess of CO_2 was added to the solvent were markedly different from those obtained when and excess of CO_2 and heptane were added.

References

[1] D.G. Leaist, Ternary Diffusion Coefficients of 18-Crown-6 Ether–KCl–Water by Direct Least-Squares Analysis of Taylor Dispersion Measurements, J. Chem. Soc., Faraday Trans. 87 (1991) 597-601.

[2] M. Jamialahmadi, M. Emadi, H. Müller-Steinhagen, Diffusion coefficients of methane in liquid hydrocarbons at high pressure and temperature, J. Pet. Sci. Eng. 53 (2006) 47-60.

[3] T.A. Renner, Measurement and Correlation of Diffusion Coefficients for CO_2 and Rich-Gas Applications, SPE Reservoir Engineering 3 (1988) 517-523.

[4] M.R. Riazi, A new method for experimental measurement of diffusion coefficients in reservoir fluids, J. Pet. Sci. Eng. 14 (1996) 235-250.

[5] F. Ciotta, G. Maitland, M. Smietana, J.P.M. Trusler, V. Vesovic, Viscosity and Density of Carbon Dioxide+ 2, 6, 10, 15, 19, 23-Hexamethyltetracosane (Squalane), J. Chem. Eng. Data 54 (2009) 2436-2443.

[6] R. Span, W. Wagner, Equations of State for Technical Applications. II. Results for Nonpolar Fluids, Int. J. Thermophys. 24 (2003) 41-109.

[7] E.W. Lemmon, R. Span, Short Fundamental Equations of State for 20 Industrial Fluids, J. Chem. Eng. Data 51 (2006) 785-850.

[8] M.L. Huber, A. Laesecke, R.A. Perkins, Model for the Viscosity and Thermal Conductivity of Refrigerants, Including a New Correlation for the Viscosity of R134a, Ind. Eng. Chem. Res. 42 (2003) 3163-3178.

[9] S.G. Penoncello, R.T. Jacobsen, A.R.H. Goodwin, A Thermodynamic Property Formulation for Cyclohexane, Int. J. Thermophys. 16 (1995) 519-531.

[10] F. Ciotta, J.P.M. Trusler, V. Vesovic, Extended hard-sphere model for the viscosity of dense fluids, Fluid Phase Equilib. 363 (2014) 239-247.

[11] B.A. Kowert, M.B. Watson, Diffusion of organic solutes in squalane, J. Phys. Chem. 115 (2011) 9687-9694.

[12] P. Han, D.M. Bartels, Temperature dependence of oxygen diffusion in H_2O and D_2O, J. Phys. Chem. 100 (1996) 5597-5602.

[13] E.L. Cussler, Diffusion: Mass Transfer in Fluid Systems, Cambridge University 2009.

[14] R. Zwanzig, A.K. Harrison, Modifications of the Stokes–Einstein formula, J. Chem. Phys. 83 (1985) 5861-5862.

[15] G.L. Pollack, J.J. Enyeart, Atomic test of the Stokes-Einstein law. II. Diffusion of Xe through liquid hydrocarbons, Phys. Rev. A 31 (1985) 980.

[16] M.J. Assael, J.P.M. Trusler, T.F. Tsolakis, Thermophysical Properties of Fluids, World Scientific 1996.
[17] M.J. Assael, H.M.T. Avelino, N.K. Dalaouti, J.M.N.A. Fareleira, K.R. Harris, Reference Correlation for the Viscosity of Liquid Toluene from 213 to 373 K at Pressures to 250 MPa, Int. J. Thermophys. 22 (2001) 789 - 799.
[18] Y. Tanaka, H. Hosokawa, H. Kubota, T. Makita, Viscosity and density of binary mixtures of cyclohexane with n-octane, n-dodecane, and n-hexadecane under high pressures, Int. J. Thermophys. 12 (1991) 245-264.
[19] T. Aminabhavi, V. Patil, M. Aralaguppi, H. Phayde, Density, viscosity, and refractive index of the binary mixtures of cyclohexane with hexane, heptane, octane, nonane, and decane at (298.15, 303.15, and 308.15) K, J. Chem. Eng. Data 41 (1996) 521-525.
[20] A.A.H. Pádua, J.M.N.A. Fareleira, J.C.G. Calado, W.A. Wakeham, Validation of an accurate vibrating-wire densimeter: Density and viscosity of liquids over wide ranges of temperature and pressure, Int. J. Thermophys. 17 (1996) 781-802.
[21] M.A. Matthews, J.B. Rodden, A. Akgerman, High-Temperature Diffusion, Viscosity, and Density Measurements in n-Hexadecane, J. Chem. Eng. Data 32 (1987) 317-319.
[22] W.E. Price, Theory of the Taylor Dispersion Technique for Three-component-system Diffusion Measurements, J. Chem. Soc. Faraday Trans. 1, 84 (1988) 2431-2439.
[23] L. Chen, D.G. Leaist, Multicomponent Taylor Dispersion Coefficients, J. Solution Chem. 1-14.

6. Conclusion

"*Science is always wrong… [It] can never solve one problem without raising ten more problems*."

George Bernard Shaw
Speech at the Einstein Dinner, Savoy Hotel, London (28 Oct 1930)

The objective of this work was to extend previous measurements of limiting diffusion coefficients of CO_2 in water, brines and hydrocarbons where available, and produce new measurements where not. As these parameters are required for the accurate modelling of CCUS and EOR processes, measurements were performed over a wide range of temperatures (< 423 K) and pressures (<69 MPa). The results obtained for the (CO_2 + heptane), (CO_2 + hexadecane), and (CO_2 + toluene) systems extended the range of pressures for which data was available. Such data had previously only been reported at atmospheric or near-atmospheric pressure. New results were obtained for the diffusion coefficients of CO_2 in brine solutions, cyclohexane and squalane.

The Taylor dispersion apparatus, TDA, inherited from a previous study, was successfully modified to allow injections of gas-saturated solvent using a gas saturation chamber designed and fabricated in house. A program in Agilent VEE™ was written to allow the experiment to be essentially fully automated. The TDA required further modification, i.e. the addition of heat tracing to all elements of the apparatus not housed in the heating bath, to allow measurements of the diffusion coefficients of the (CO_2 + hexadecane) and (CO_2 + cyclohexane) systems to be performed.

Despite notable challenges in measuring the diffusion coefficient of CO_2 in water substantial data has been obtained and the results are believed to be reliable. While the root cause of the anomalous signals obtained for this system was not determined, modification of the operating procedure to use higher experimental flow rates incorporating a generalization of the working equation permitted these measurements. Diffusion coefficients of CO_2 in several hydrocarbons were also measured using the TDA. However, to study the (CO_2 + brine) systems an alternative method was needed and pulsed field gradient NMR was selected. While this method

did not allow the measurement of diffusivities at high pressure or temperature, reliable data was obtained for several brine systems at T = 298 K and p = 0.1 MPa.

Summary of Major Conclusions

The diffusivity of infinitely dilute CO_2 in liquids is a function of temperature and the density of the liquid at the respective state point. In the case of aqueous systems, this density dependence is incorporated through the solution viscosity. Over the temperature range investigated, (298 to 423) K, there was an order of magnitude increase in the diffusivity. The effect of higher density, as accounted for in aqueous systems through the solvent viscosity, resulted in a lower diffusion coefficient.

A model based on the Stokes-Einstein equation was used to correlate the diffusivities measured for the aqueous solutions of CO_2. This model was compared to the diffusion coefficients of CO_2 in brine solutions measured at T = 298 K. It was found the model agreed well with the measured diffusivities. However, for systems of CO_2 in hydrocarbons, where the solvents compressibility is much greater, it was found that a correlation based on the rough-hard sphere theory of transport properties was more appropriate.

The tracer diffusion of CO_2 in water was found to be essentially independent of pressure over the range investigated. Once the effect of the addition of salt was accounted for in terms of the increased solution viscosity there was no apparent effect of the ionic strength of the solution on the diffusivity of CO_2.

The diffusion coefficient of CO_2 in hydrocarbons was found to be a function of pressure in addition to temperature. The diffusivity of infinitely dilute CO_2 in a single hydrocarbon has been rigorously shown to decrease with increasing pressure. This is contrary to some of the available literature, which reports that CO_2 diffusivity in hydrocarbons increases with pressure [1-3]. The determination of the diffusivity of CO_2 in large hydrocarbons is less satisfactorily accounted for. The results obtained in this work broadly agree with previously published findings on the suitability of correlating diffusivity with the solvents molar volume [4] and the use of a simplified rough-hard sphere treatment, based on the free molar volume, looks promising.

Implications

The well-founded but simple correlative models developed based on the results obtained in this work can be used to reliably estimate the diffusion coefficients of CO_2 (and nitrogen, N_2, [5]) in brines over a range of conditions. As N_2 is often present as an impurity in CO_2 captured from power plants, the knowledge of its diffusivity in saline fluids is also important in the context of CCUS.

The fitted parameters obtained for the rough-hard sphere based model of diffusion coefficients of CO_2 in hydrocarbons suggest that a predictive model for diffusivities in hydrocarbons in terms of temperature, density and carbon number is possible. This could be used in scenarios where an oil is modelled as a normal linear alkane. The treatment of large branched hydrocarbons, e.g. squalane, needs further investigation.

A sensitivity analysis has been performed for the effect of diffusivity on the onset time of convective flow in carbon sequestration [6]. Onset time is the amount of time taken for the fluid to begin to move due to buoyant forces. It was found that the onset time was approximately linear with respect to the diffusion coefficient. An increase in the diffusion coefficient of 50% can result in the onset time increasing 2.3 times. Conversely, if the diffusion coefficient is underestimated by 20%, the onset time of convective flow could be underestimated by approximately 10%. As the literature available for the diffusivity of CO_2 in hydrocarbons is especially ambiguous, great care should be taken in the value of the diffusion coefficient used.

The rate of absorption of CO_2 into reservoir fluids, as mentioned earlier, is often governed by the rate of diffusion. There is ambiguity in the literature as to the effect of pressure on the diffusion coefficient of CO_2 in hydrocarbons and, perhaps ironically, depending on the method employed to model such systems for EOR both values, i.e. the true binary diffusion coefficient or the diffusion coefficient taken from absorption rate experiments, may prove to be a better match for observations in the field. If the penertration theory of gas absorption is used and the effect of pressure is not included in assigning a value to D the rate of absorption may be underestimated by 6.5%. This value is based on a 40% reduction in diffusivity over the pressure range (1 to 69) MPa. This magnitude of decrease is reflective of the values obtained in the current work.

Future Work

Methods

The origin of the “pre-peak” observed during analysis of the (CO_2 + H_2O) system remains the subject of uncertainty. The two most likely hypotheses are the formation of carbonate due to the dissociation of CO_2 in H_2O and the proximity of the solution to zero refractive index difference. There are several studies that could be undertaken to address this finding.

The use of another type of detector would be the favoured approach. A pH or conductivity detector could be a promising method. This detector could be used in conjunction with the current refractive index detector. The use of such a configuration has been previously used to investigate the (KCl + KI + H_2O) and the (methanol + acetone +water) systems [7,8]. The pH of solutions of CO_2 has been well studied [9]. If the “pre-peak” is solely due to the proximity of the refractive index of the solution to zero, this effect would not be observed whilst monitoring the pH of the eluent. The use of other types of detectors, with the same intention, could also help identify whether or not the observed behaviour can be rationalised due to the type of detector used.

Another possible methodology would be adjusting the pH of the system. The extent of dissociation reactions is based on the pH of the system. While this approach could illuminate the effect of carbonate formation it would be unsuitable as a method for continuing measurements of CO_2 diffusion in water as this would be a multicomponent system where it could be imagined cross diffusion terms would play a prominent role. However, in an essentially binary system, i.e. CO_2 in a HCl solution added to a HCl solvent, the absence of a noticeable pre-peak in the data would corroborate the hypothesis that dissociated CO_2 was the cause of the pre-peak.

Nuclear magnetic resonance is a promising technique for the determination of not only diffusion coefficients but also other thermodynamic properties, e.g. vapour-liquid equilibria, and transport properties, e.g. viscosity. These techniques and data sets can be used to further develop the measurements NMR can provide, as in the case of magnetic resonance imaging. The implementation of this technology is an exciting technical development [10], NMR is used in not only the biological and chemical research sector, but also in the oil and gas industry in field exploration, the medical sciences [11], process engineering [12] and the food industry. Due to its versatility it is an attractive multi-purpose tool in research [13], including in the measurement of diffusion coefficients. The use of NMR cells capable of maintaining elevated pressure

[14] would not only allow measurements of systems under pressure but also allow, due to an increased possible saturation pressure of CO_2, analysis of systems where CO_2 is only sparingly soluble, due to the higher signal to noise ratio achievable.

Systems

Some brines and groundwater also contains appreciable amounts of bicarbonate ions. It would be interesting to investigate CO_2 diffusion with chemical exchange between CO_2 and HCO_3- species.

Due to the salting out effect the solubility of CO_2 in typical (CO_2 + brine) systems is low, less than 2% on a mole basis. As discussed previously, assuming that due to the low solubility of CO_2 in water and brines diffusion coefficients need only be measured at infinite dilution is an accurate assumption in these systems. However, for hydrocarbon systems the effect of concentration on the diffusion coefficients should be investigated. The Taylor dispersion method is suitable for such measurements [15]. The device used in the current work would require only a modification to the glass cell in the refractive index detector. Cells, of the correct dimensions, capable of operating at pressures up to 9 MPa are commercially available. This would also circumvent the need for a restriction tube between the diffusion column and detector used in the current work. It would also be advisable to measure the viscosity and density of the corresponding mixtures. These results are necessary to correlate the close packed molar volume and molar volume, respectively. Based on the understanding obtained from treating the data using the Stokes-Einstein methodology, it is predicted the diffusion coefficient will increase as the concentration of the CO_2 increases. The argument for this is based on the reduction of the viscosity caused by the addition of CO_2.

Crude oil is a complex mixture of many components. The diffusion in such a system is highly non-ideal. An initial study in which this mixture is treated as pseudo-binary would be the first step in a study of this system. The phase behaviour of a CO_2 and synthetic crude oil has been studied systematically and this is one strong example of the quality of work that is required to tackle this complicated problem [16]. This oil consisted of at least 17 components, equivalent to 256 Fickian diffusion coefficients. Using a Taylor dispersion apparatus to measure these diffusivities would require at least 512 different experiments at each state point. This, of course, is an impractical number of experiments and would require ever-greater experimental precision. It

may be necessary, with our current understanding of diffusion, to even further lump mixed systems.

While for a N component system, $(N\text{-}1)^2$ Fickian diffusion coefficients are required, only $(N^2 - N)/2$ Maxwell-Stefan diffusion coefficients are needed (see Figure 6-1). The experimental barrier to measuring M-S diffusivities is the fact chemical potentials cannot be measured directly.

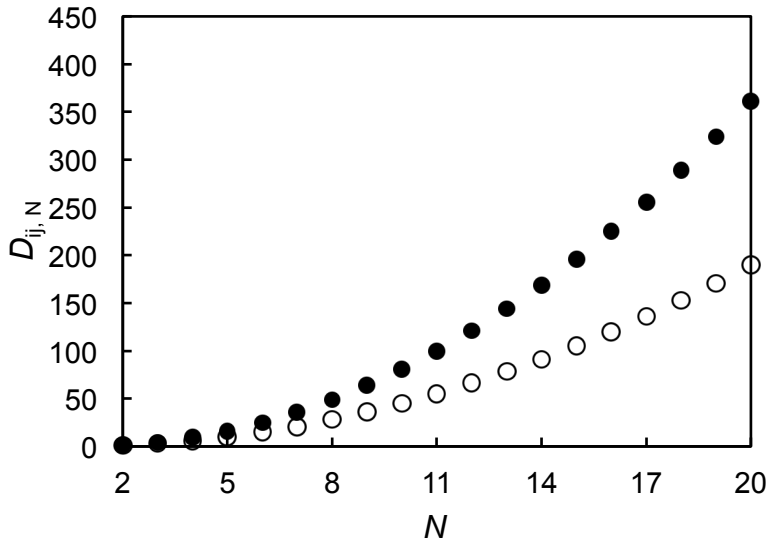

Figure 6-1. Illustration of the increase in diffusion coefficients, $D_{ij,N}$, as the number of components in the mixture, N, increases.
The number of Fickian diffusion coefficients, ●, increases at a far greater rate than that of the Maxwell-Stefan diffusion coefficients, ○.

Theory

A systematic study of other hydrocarbon systems with a view to interpreting the data obtained using the reduced rough-hard sphere theory would be advisable. It could be envisaged that b and β could be shown to be a simple function of carbon number in a homologous series of alkanes. Determining a trend for β along a homologous series with a fixed solvent could be the first step in determining a more general trend for an arbitrary solute-solvent system.

Furthermore, the extension of this theory to fluids in which the attractive potential between molecules cannot be ignored, e.g. the long-range attractive potential present in hydrogen bonding fluids, could be investigated. For example, the statistical associating fluid theory, while initially largely used in the study of non-polar fluids, has been developed as a predictive method for polar liquids such as water and electrolyte solutions [17]. Interestingly, Figure 6-2 indicates that the close-packed molar volume of water, where the data would intersect the abscissa were it to

continue to follow a linear trend, changes with pressure. There is also a clear non-linear trend in the data.

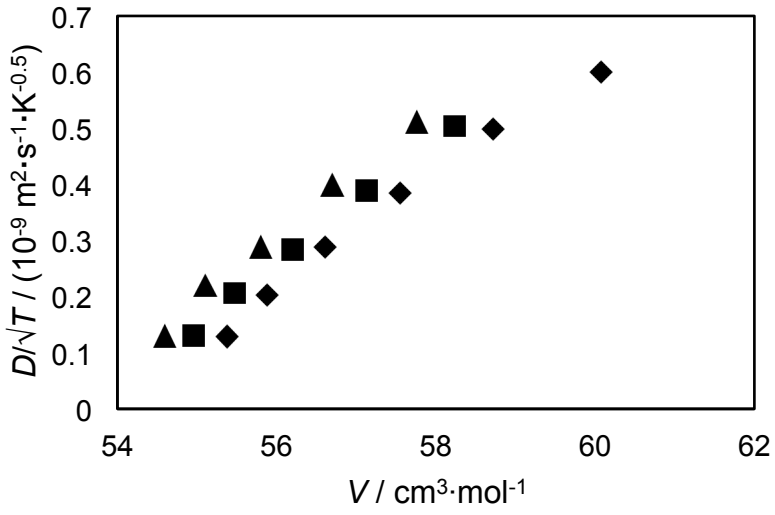

Figure 6-2. Diffusion coefficient of CO_2 in H_2O divided by the square root of the temperature plotted against the molar volume of H_2O at that state point. Measurements were performed at pressures of; ◆, p = 10 MPa; ■, p = 30 MPa; and ▲, p = 45 MPa.

Finally, most systems of interest in the life sciences and engineering are multicomponent by nature. Due to the complicated mathematical nature of the treatment of these system however, full descriptions of the diffusivity of the components are frequently ignored. In the case of dilute systems the mass transfer calculations can be sufficient, however where more than one solute is present in relatively large quantities these models may break down. If the elements of a matrix of diffusion coefficients is considered to denote the effective binary diffusion coefficient between a pair of molecules in the system then it may be possible to estimate such a matrix for the contributions of these individual diffusivities calculated from a rigorous approach.

References:

[1] A.K. Tharanivasan, C. Yang, Y. Gu, Measurements of Molecular Diffusion Coefficients of Carbon Dioxide, Methane, and Propane in a Heavy Oil Under Reservoir Conditions, Energy Fuel. 20 (2006) 2509-2517.

[2] P. Guo, Z. Wang, P. Shen, J. Du, Molecular Diffusion Coefficients of the Multicomponent Gas-Crude Oil Systems under High Temperature and Pressure, Ind. Eng. Chem. Res. 48 (2009) 9023-9027.

[3] L.-S. Wang, C.-Y. Sun, Diffusion of Carbon Dioxide in Tetradecane, J. Chem. Eng. Data 42 (1997) 1181-1186.

[4] M.A. Matthews, J.B. Rodden, A. Akgerman, High-Temperature Diffusion of Hydrogen, Carbon Monoxide, and Carbon Dioxide in Liquid n-Heptane, n-Dodecane, and n-Hexadecane, J. Chem. Eng. Data 32 (1987) 319-322.

[5] S.P. Cadogan, G.C. Maitland, J.P.M. Trusler, Diffusion Coefficients of CO_2 and N_2 in Water at Temperatures between 298.15 K and 423.15 K at Pressures up to 45 MPa. J. Chem. Eng. Data 59 (2014) 519-525.

[6] R. Allen, S. Sun, Carbon Dioxide Sequestration: Modeling the Diffusive and Convective Transport under a CO_2 Cap, SPE Saudi Arabia Section Technical Symposium and Exhibition. Society of Petroleum Engineers, 2012.

[7] H. Lü, D.G. Leaist, Ternary Diffusion Coefficients for the Ill-conditioned Systems KCl-KI-H2O and NaCl-NaI-H2O measured by a Two-detector Taylor Dispersion Method, J. Chem. Soc. Faraday Trans. 87 (1991) 3667-3670.

[8] I.M.J.J. van der Ven-Lucassen, M.F. Kemmere, P.J.A.M. Kerkhof, Complications in the Use of the Taylor Dispersion Method for Ternary Diffusion Measurements: Methanol + Acetone + Water Mixtures, J. Solution Chem. 26 (1997) 1145-1167.

[9] C. Peng, J.P. Crawshaw, G.C. Maitland, J.P.M. Trusler, D. Vega-Maza, The pH of CO_2-saturated water at temperatures between 308 K and 423 K at pressures up to 15 MPa, J. Supercrit. Fluids 82 (2013) 129-137.

[10] L.F. Gladden, Magnetic Resonance: Ongoing and Future Role in Chemical Engineering Research, AIChE J. 49 (2003) 2-9.

[11] D. Le Bihan, Molecular Diffusion Nuclear Magnetic Resonance Imaging, Magn. Reson. Quart. 7 (1991) 1-30.

[12] J. Mitchell, L.F. Gladden, T.C. Chandrasekera, E.J. Fordham, Low-field permanent magnets for industrial process and quality control, Prog. Nucl. Magn. Reson. Spectrosc. 76 (2014) 1-60.

[13] J. Guzmán, L. Garrido, Determination of Carbon Dioxide Transport Coefficients in Liquids and Polymers by NMR Spectroscopy, J. Phys. Chem. 116 (2012) 6050-6058.

[14] W.A. Wakeham, A. Nagashima, J. Sengers, Measurement of the Transport Properties of Fluids, Blackwell Science, 1991.

[15] A.A. Alizadeh, W.A. Wakeham, Mutual Diffusion Coefficients for Binary Mixtures of Normal Alkanes, Int. J. Thermophys. 3 (1982) 307-323.

[16] S.Z. Al Ghafri, G.C. Maitland, J.P.M. Trusler, Experimental and modeling study of the phase behaviour of synthetic crude oil + CO_2, Fluid Phase Equilib. 365 (2014) 20-40.

[17] A. Galindo, A. Gil-Villegas, G. Jackson, A.N. Burgess, SAFT-VRE: Phase Behavior of Electrolyte Solutions with the Statistical Associating Fluid Theory for Potentials of Variable Range, J. Phys. Chem. B, 103 (1999) 10272-10281.

Appendices

Appendix 1A: Reported Values for Diffusion Coefficients of CO_2 in H_2O

Literature values for the infinitely dilute diffusion coefficient of CO_2 in H_2O, D, using the respective experimental technique at a given temperature T with the experimental uncertainty, u, if reported. All experiments were performed at p = 0.1 MPa unless indicated otherwise.

Method	T / K	D / (10^{-9} $m^2 \cdot s^{-1}$)	u / %
(Quiescent) Absorption Tube [1]	298.0	1.86	-
	302.9	2.10	-
Diffusion Cell [2]	283.5	1.50	-
	288.8	1.65	-
	293.7	1.84	-
(Quiescent) Absorption Tube [3]	283.0	1.25	-
	290.5	1.50	-
	297.7	1.79	-
Ringbom Apparatus [4]	303.2	2.18	-
[5]	303.2	2.30	-
(Quiescent) Absorption Tube [6]	296.2	2.35	
	302.2	2.71	
	310.2	3.13	
Laminar Jet [7]	283.2	1.17	-
	288.2	1.39	-
	293.2	1.62	-
	298.2	1.90	-
	303.2	2.25	-
[8]	298.2	1.87	-
Laminar Jet [9]	293.2	1.69	-
	292.7	1.70	-
	279.4	1.08	-
	283.4	1.30	-
	289.0	1.49	-
	293.2	1.69	-
	298.0	1.94	-
	303.2	2.26	-
Laminar Jet [10]	293.2	1.77	-
[11]	298.2	1.95	-
Capillary Method [12]	303.2	2.15	-
[13]	293.2	1.63	-
Diaphragm Cell [14]	298.2	2.00	3.5

Method	T / K	D / (10^{-9} $m^2 \cdot s^{-1}$)	u / %
Laminar Jet [15]	279.7	1.15	-
	298.2	1.85	-
	308.2	2.18	-
	325.2	3.61	-
	338.2	4.30	-
Laminar Jet [16]	298.2	2.05	-
Liquid Jet [17]	298.2	1.91	-
	298.2	1.92	-
	298.2	1.92	-
	298.2	1.92	-
	298.2	1.91	-
	298.2	1.94	-
	298.2	1.92	-
	298.2	1.92	-
	298.2	1.91	-
	298.2	1.91	-
	298.2	1.90	-
	298.2	1.90	-
	298.2	1.86	-
	298.2	1.89	-
	298.2	1.93	-
Laminar Jet [18]	291.7	1.65	-
	298.2	1.95	-
	307.9	2.41	-
	318.4	3.03	-
	328.1	3.68	-
	338.2	4.40	-
	348.3	5.40	-
Taylor Dispersion [19]	298.2	1.92	-
Diaphragm Cell [20]	313.2	2.81	3.6
	333.2	4.15	5.8
Laminar Jet [21]	298.2	1.98	-
	313.2	2.80	-
Constant Bubble Size Method [22]	298.2	1.99	-
Inverted Tube Method [23]	273.0	1.00	-
	278.0	1.16	-
	283.0	1.32	-
	288.0	1.52	-
	293.0	1.74	-
	298.2	1.85	-
	303.0	2.19	-
	308.0	2.41	-

Method	*T* / K	*D* / (10^{-9} $m^2 \cdot s^{-1}$)	*u* / %
Taylor Dispersion [24]	290.0	1.47	-
	291.2	1.61	-
	297.7	1.90	-
Wetted Wall [25]	*293.2*	*1.69*	-
	293.2	*1.73*	-
	293.2	*1.68*	-
Inverse Open Capilary Method [26]	298.2	2.11	
Laminar Film [27]	298.2	1.88	7.8
Wetted Wall [28]	298.2	1.81	-
Laminar Jet [29]	298.2	1.98	
Barrer Method [30]	278.2	1.07	-
	288.2	1.45	-
	298.2	1.91	-
	308.2	2.43	-
Laminar Jet [31]	298.2	1.98	
(Quiescent) Absorption Cell [32]	291.2	1.61	6
	297.7	1.9	6
Wetted Wall [33]	303.2	2.18	
Wetted Sphere [34]	293.0	1.76	-
	298.2	1.94	-
	303.0	2.20	-
	313.0	2.93	-
	333.0	4.38	-
	353.0	6.58	-
	368.0	8.20	-
Taylor Dispersion [35]	298.0	1.98	
Taylor Dispersion [36]	298.2	1.97	-
	308.0	2.49	-
	318.0	3.07	-
	328.0	3.67	-
(Quiescent) Inverted Tube Method [37]	298.0	2.03	
Optical (Laser Induced Fluorescence) [38]	286.0[aa]	1.27	-
	286.0[ab]	1.41	-
Wetted Sphere [39]	298.2	1.88	
	325.2	3.45	
Wetted Wall [40]	298.0	1.71	4
	298.0	1.9	4
	303.0	2.13	4
	308.0	2.47	4
	313.0	2.86	4

Method	T / K	D / (10^{-9} $m^2 \cdot s^{-1}$)	u / %
Optical (Ramann Spectroscope) [41]	393.2[ba]	8.12	1
	268.2[bb]	0.76	3
	273.2[bb]	0.91	1
	278.2[bb]	1.12	3
	298.2[bb]	1.91	1
	313.2[bb]	2.65	1
	323.2[bb]	3.21	1
	353.2[bb]	5.30	2
	373.2[bb]	6.43	2
	393.2[bb]	8.13	1
	433.2[bb]	11.77	3
	313.2[bc]	2.42	2
	353.2[bc]	5.44	5
	393.2[bc]	7.89	1
	393.2[bd]	7.80	3

aa, p = 29.4 MPa; ab, p = 39.2 MPa. ba, p = 10 MPa; bb, p = 20 MPa; bc, p = 30 MPa; bd, p = 45 MPa.

References:

[1] J. Stefan, Über die diffusion der kohlensaure durch wasser und alcohol, S. B. Akad. Wiss. Wien. Math Naturwiss. Kl. Abt. 77 (1878) 371-409..

[2] G. Hufner, Über die bestimmung der diffusion-coefficienten einiger gase für wasser, Ann. Phys. Chem. 60 (1897) 134.

[3] J. Tammann, V. Jessen, Über die diffusionkoeffizienten von gasen in wasser und ihre temperaturabhängigkeit, Z. Anorg. Allegm. Chem. 179 (1929) 125-144.

[4] A. Ringbom, Über die bestimmung der diffusionskoeffizienten von gasen in flüssigkeiten, Z. Anorg. Allgem. Chem. 238 (1938) 94-102.

[5] D.W. Peaceman, Liquid-side resistance in gas absorption with and without chemical reaction, Ph.D. Dissertation: Massachusetts Institute of Technology (1952)

[6] K.H. Gertz, H.H. Loeschcke, Bestimmung des Diffusionskoeffizienten von CO_2 in Wasser, Z. Naturforsch. 11b (1956) 61-64.

[7] E.J. Cullen, J.F. Davidson, Absorption of gases in liquid jets, Trans. Faraday Soc. 52 (1956) 113-120.

[8] L.E. Scriven, Interfacial resistance in gas absorption, Ph.D. Dissertation: Univ. of Delaware (1956)

[9] R.A.T.O. Nijsing, R.H. Hendriksz, H. Kramers, Absorption of CO_2 jets and falling films of electrolyte solutions, with and without chemical reaction, Chem. Eng. Sci. 10 (1959) 88-104.

[10] K. Onda, T. Okamoto, Y. Yamaji, Measurement of the diffusivities of CO_2 in liquids by liquid jets, Kagaku Kogaku 24 (1960) 918-925.

[11] D.R. Woods, Mass transfer between a liquid jet and a countercurrent gas stream, Ph.D. Dissertation: Univ. of Wisconsin-Madison (1961)

[12] L.H. Bodnar, D.M. Himmelblau, Continuous measurement of the diffusion coefficients of gases in liquids using glass scintillators, Int. J. Appl. Radia. Isotopes, 13 (1962) 1-6.

[13] W.S. Norman, F.Y.Y. Sammak, Gas absorption in a packed column – Part 1: The effect of liquid viscosity on the mass transfer coefficient, Trans. Inst. Chem. Engrs. 41 (1963) 109-116.
[14] J.E. Vivian, C.J. King, Diffusivities of slightly soluble gases in water, AIChE J. 10 (1964) 220-221.
[15] A.A. Unver, D.M. Himmelblau, Diffusion coefficients of CO_2, C_2H_4, C_3H_6, and C_4H_8 in water from 6 to 65 ^oC, J. Chem. Eng. Data 9, (1964) 428-431.
[16] J.K.A. Clarke, Kinetics of Absorption of Carbon Dioxide in Monoethanolamine Solutions at Short Contact Times, Am. Chem. Soc. 3 (1964) 239-245.
[17] Y.P. Tang, D.M. Himmelblau, Effect of solute concentration on the diffusivity of carbon dioxide in water, Chem. Eng. Sci. 20 (1965) 7-14.
[18] W.J. Thomas, M.J. Adams, Measurement of the diffusion coefficients of carbon dioxide and nitrous oxide in water and aqueous solutions of glycerol, Trans. Farad. Soc. 61 (1965) 668-673.
[19] R.T. Ferrell, D.M. Himmelblau, Diffusion coefficients of nitrogen and oxygen in water, J. Chem. Eng. Data, 12 (1967) 111-115.
[20] M.J. Tham, K.K. Bhatia, K.E. Gubbins, Steady-state method for studying diffusion of gases in liquids, Chem. Eng. Sci. 22 (1967) 309-311.
[21] J.L. Duda, J.S. Vrentas, Laminar liquid jet diffusion studies, AIChE J. 14 (1968) 286-294.
[22] W.Y. Ng, J. Walkley, Diffusion of gases in liquids: the constant bubble size method, Can. J. Chem. 47 (1969) 1075-1077.
[23] D.M. Maharajh, D.J. Walkley, The temperature dependence of the diffusion coefficients of Ar, CO_2, CH_4, CH_3Cl, CH_3Br and $CHCl_2F$ in water, Can. J. Chem. 51 (1973) 944-952.
[24] K.C. Pratt, D.H. Slatter, W.A. Wakeham, A rapid method for the determination of diffusion coefficients of gases in liquids, Chem. Eng. Sci. 28 (1973) 1901-1903.
[25] H. Sovona, J. Prochazka, A new method of measurement of diffusivities of gases in liquids, Chem. Eng. Sci. 31 (1976) 1091-1097.
[26] F.C. Tse, O.C. Sandall, DIFFUSION COEFFICIENTS FOR OXYGEN AND CARBON DIOXIDE IN WATER AT 25^{o}C BY UNSTEADY STATE DESORPTION FROM A QUIESCENT LIQUID, Chem. Eng. Comm. 3 (1979) 147-153.
[27] A.F. Mazarei, O.C. Sandall, Diffusion coefficients for helium, hydrogen, and carbon dioxide in water at 25 ^{o}C, AIChE J. 26 (1980) 154-157.
[28] E.A. Brignole, R. Echarte, Mass transfer in laminar liquid jets: measurement of diffusion coefficients, Chem. Eng. Sci. 36 (1981) 695-703.
[29] A. Tang, O.C. Sandall, Diffusion Coefficient of Chlorine in Water at 25-60^{o}C, J. Chem. Eng. Data, 30 (1985) 189-191.
[30] B. Jahne, G. Heinz, W. Dietrich, Measurement of the diffusion coefficients of sparingly soluble gases in water, J. Geophys. Res. 92 (1987) 10767-10776.
[31] J.M. Diaz, A. Vega, J. Coca, Diffusivities of CO_2 and N_2O in Aqueous Alcohol Solutions, J. Chem. Eng. Data, 33 (1988) 10-12.
[32] K.K. Tan, R.B. Thorpe, Gas diffusivities into viscous and non-newtonian liquids, Chem. Eng. Sci. 13 (1992) 3565-3572.
[33] A.K. Saha, S.S. Bandyopadhyay, A.K. Biswas, Solubility and Diffusivity of N_2O and CO_2 in Aqueous Solutions of 2-Amino-2-methyl-1-propanol, J. Chem. Eng. Data, 38 (1993) 78-82.
[34] A. Tamimi, E.B. Rinker, O.C. Sandall, Diffusion coefficients for hydrogen sulfide, carbon dioxide, and nitrous oxide in water over the temperature range 293 – 368 K, J. Chem. Eng. Data 39 (1994) 330-332.
[35] E.D. Snijder, M.J.M. te Riele, G.F. Versteeg, W.P.M. van Swaaij, Diffusion Coefficients of CO, CO_2, N_2O, and N_2 in Ethanol and Toluene, J. Chem. Eng. Data, 40 (1995) 37-39.

[36] M.J.W. Frank, J.A.M. Kuipers, W.P.M. van Swaaij, Diffusion coefficients and viscosities of CO_2+H_2O, CO_2+CH_3OH, NH_3+H_2O, and NH_3+CH_3OH liquid mixtures, J. Chem. Eng. Data 41 (1996) 297-302.

[37] R.L. Rowley, M.E. Adams, T.L. Marshall, J.L. Oscarson, W.V. Wilding, D.J. Anderson, Measurement of Diffusion Coefficients Important in Modeling the Absorption Rate of Carbon Dioxide into Aqueous N-Methyldiethanolamine, J. Chem. Eng. Data 42 (1997) 310-317.

[38] S. Hirai, K. Okazaki, H. Yazawa, H. Ito, Y. Tabe, K. Hijakata, Measurement of CO_2 diffusion coefficient and application of LIF in pressurized water, Energy, 22 (1997) 363-367.

[39] M.K. Abu-Arabi, A.M. Al-Jarrah, M. El-Eideh, Physical Solubility and Diffusivity of CO_2 in Aqueous Diethanolamine Solutions, J. Chem. Eng. Data, 46 (2001) 516-521.

[40] B.P. Mandal, M. Kundu, N.U. Padhiyar, S.S. Bandyopadhyay, Physical solubility and diffusivity of N_2O and CO_2 into aqueous solutions of (2-amino-2-methyl-1-propanol + diethanolamine) and (N-methyldiethanolamine + diethanolamine), J. Chem. Eng. Data, 49 (2004) 264-270.

[41] W. Lu, H. Guo, I. Chou, R. Burrus, L. Li, Determination of diffusion coefficients of carbon dioxide in water between 268 and 473 K in a high-pressure capillary optical cell with in situ Raman spectroscopic measurements, Geochim. Cosmochim. Acta 115 (2013) 183-204.

Appendix 1B: Reported Values for Diffusion Coefficients of CO_2 in n-Hexadecane

Literature values for the diffusion coefficient of CO_2 in hexadecane, D, at a given temperature T and pressure p with the relative uncertainty, σ_D [1].

T / K	p / MPa	D / (10^{-9} m^2·s^{-1})	$10^2\sigma_D$
323	1.42	3.48	0.9
323	3.46	3.47	2.6
371	1.40	6.57	0.2
371	3.44	6.53	1.8
443	1.40	23.5	0.8
443	3.43	12.4	0.8
513	1.41	20.2	1.0
513	3.43	19.9	0.5
564	1.40	27.4	0.4
564	3.41	27.2	1.5

[1] M.A. Matthews, J.B. Rodden, A. Akgerman, High-Temperature Diffusion of Hydrogen, Carbon Monoxide and Carbon-Dioxide in Liquid n-Heptane, n-Dodecane, and n-Hexadecane, J. Chem. Eng. Data 32 (1987) 319

Appendix 2: Tabulated Results for Diffusion Coefficients of CO_2 in H_2O

Diffusion coefficients D and standard deviations σ_D for CO_2 in water at temperatures T and pressure p determined from N repeated injections at mean solvent flow speed v, together with the maximum relative standard deviation $(\sigma_s/s_{max})_{max}$ of the RID signal $s(t)$, where s_{max} is the maximum value of s. [a]

T / K	p / MPa	v / ($m \cdot s^{-1}$)	D / (10^{-9} $m^2 \cdot s^{-1}$)	N	$10^2\sigma_D$	$10^2(\sigma_s/s_{max})_{max}$
298	14.0	0.305[b]	2.23	4	1.8	1.3
298	31.6	0.305[c]	2.26	5	3.2	1.8
298	47.7	0.305[d]	2.22	5	1.4	0.8
323	14.2	0.315[b]	3.64	4	1.4	1.4
323	31.8	0.315[c]	3.72	6	1.6	2.0
323	48.6	0.315[d]	3.94	4	2.3	2.4
348	14.9	0.325[b]	5.39	4	1.3	1.8
348	31.8	0.325[c]	5.31	5	1.8	2.6
348	49.3	0.325[d]	5.37	6	2.0	2.3
373	14.9	0.325[b]	7.42	5	0.8	1.8
373	31.0	0.325[c]	7.52	5	4.0	2.3
373	48.5	0.325[d]	7.68	5	1.6	2.8
398	14.3	0.325[b]	9.95	5	3.3	1.7
398	30.9	0.325[c]	10.1	4	1.6	2.3
398	48.0	0.325[d]	10.2	6	3.1	2.3
423	14.3	0.325[b]	12.3	4	1.7	1.3
423	48.0	0.325[d]	12.2	5	1.6	2.4

[a] standard uncertainties are $u(T) = 0.01$ K and $u(p) = 0.0025 \cdot p$

[b] 50 µm i.d. x 500 mm long restriction tube used

[c] 25 µm i.d. x 50 mm long restriction tube used

[d] 25 µm i.d. x 100 mm long restriction tube used

Appendix 3: Tabulated Results for Diffusion Coefficients of CO_2 in Brines

Diffusion coefficients D and standard deviations σ_D for CO_2 in brines of molality m and viscosity η at a temperature of 298 K and atmospheric pressure.

Salt	m / mol·kg^{-1}	η / mPa·s	D / (10^{-9} m^2·s^{-1})	$10^2\sigma_D$
n/a	0.0	0.891	2.13	1.3
NaCl	1.0	0.972	2.06	1.5
	2.5	1.14	1.70	2.1
	5.0	1.53	1.29	7.7
$CaCl_2$	1.0	1.25	1.60	1.4
	2.5	2.01	1.25	6.8
Na_2SO_4	1.0	1.37	1.48	8.6
Prototype	1.9	1.09	1.78	3.2

Appendix 4A: Tabulated Results for Diffusion Coefficients of CO_2 in Heptane

Diffusion coefficients D and standard deviation σ_D for CO_2 in heptane at temperatures T and pressure p determined from at least 5 repeated injections. [a]

T / K	p / MPa	D / (10^{-9} m^2·s^{-1})	$10^2\sigma_D$
298	1.0[b]	7.28	1.3
298	10[c]	6.82	1.2
298	31[d]	5.90	1.9
298	50[e]	5.37	0.8
298	68[e]	5.06	2.4
323	1.0[b]	9.25	1.0
323	10[c]	8.72	0.3
323	30[d]	7.64	0.9
323	51[e]	6.95	0.3
323	68[e]	6.37	1.1
348	1.0[b]	11.4	1.2
348	10[c]	10.2	0.8
348	30[d]	9.40	0.5
348	48[e]	8.10	1.6
348	67[e]	7.89	1.4
373	1.0[b]	13.7	0.9
373	10[c]	12.5	0.6
373	30[d]	11.2	0.6
373	49[e]	9.95	1.5
373	68[e]	9.32	1.5
398	1.0[b]	16.1	1.6
398	10[c]	14.9	1.1
398	30[d]	13.1	0.8
398	50[e]	11.7	1.0
398	68[e]	10.9	1.1
423	1.0[b]	18.0	0.6
423	10[c]	16.8	1.1
423	30[d]	15.0	1.3
423	50[e]	13.6	0.7
423	68[e]	12.3	1.1

[a] standard uncertainties are $u(T) = 0.01$ K and $u(p) = 0.0025 \cdot p$

[b] 50 µm i.d. x 50 mm long restriction tube used

[c] 25 µm i.d. x 100 mm long restriction tube used

[d] 25 µm i.d. x 200 mm long restriction tube used

[e] 25 µm i.d. x 500 mm long restriction tube used

Appendix 4B: Tabulated Results for Diffusion Coefficients of CO_2 in Hexadecane

Diffusion coefficients D and standard deviations σ_D for CO_2 in hexadecane at temperatures T and pressure p determined from at least 5 repeated injections. [a]

T / K	p / MPa	D / (10^{-9} m^2·s^{-1})	$10^2\sigma_D$
298	1.0[b]	2.49	0.5
298	10[c]	2.31	0.6
298	30[d]	2.07	3.0
323	1.1[b]	3.75	0.5
323	10[c]	3.41	2.9
323	30[d]	3.16	4.0
323	51[e]	2.65	9.3
323	69[e]	2.50	3.7
348	1.0[b]	5.13	0.4
348	10[c]	4.64	2.9
348	30[d]	4.28	2.1
348	50[e]	3.83	1.2
348	67[e]	3.48	0.9
373	1.1[b]	6.72	1.2
373	10[c]	6.17	4.5
373	30[d]	5.86	3.1
373	52[e]	5.00	0.9
373	67[e]	4.66	0.9
398	1.1[b]	8.53	0.4
398	10[c]	7.24	1.8
398	29[d]	7.39	1.5
398	53[e]	6.24	2.0
398	69	5.84	1.1
423	1.1[b]	10.41	1.0
423	10[c]	9.72	2.2
423	29[d]	9.15	1.5
423	45[e]	7.92	0.8
423	69[e]	7.03	1.5

[a] standard uncertainties are $u(T) = 0.01$ K and $u(p) = 0.0025 \cdot p$

[b] 0.01” i.d. x 53 mm long restriction tube used

[c] 50 µm i.d. x 100 mm long restriction tube used

[d] 50 µm i.d. x 500 mm long restriction tube used

[e] 25 µm i.d. x 200 mm long restriction tube used

Appendix 4C: Tabulated Results for Diffusion Coefficients of CO_2 in Squalane

Diffusion coefficients D and standard deviations σ_D for CO_2 in squalane at temperatures T and pressure p determined from at least 5 repeated injections. [a]

T / K	p / MPa	D / (10^{-9} m^2·s^{-1})	$10^2\sigma_D$
298	1.1[b]	0.955	1.5
298	10[c]	0.861	0.3
298	32[d]	0.693	4.3
298	52[d]	0.556	2.5
298	66[d]	0.487	0.5
323	1.1[b]	1.78	0.6
323	10[c]	1.61	0.6
323	30[d]	1.35	0.6
323	52[d]	1.14	1.5
323	64[d]	1.02	0.9
348	1.0[b]	2.83	0.8
348	11[c]	2.57	1.0
348	31[d]	2.18	0.4
348	50[d]	1.94	1.5
348	67[d]	1.73	0.9
373	1.0[b]	4.06	0.8
373	10[c]	3.72	4.5
373	30[d]	3.21	0.7
373	47[d]	2.88	1.9
373	66[d]	2.58	0.8
398	1.0[b]	5.45	1.1
398	11[c]	4.98	1.1
398	31[d]	4.38	1.0
398	50[d]	3.89	0.7
398	66[d]	3.55	0.5
423	1.0[b]	7.01	0.9
423	11[c]	6.36	2.6
423	30[d]	5.69	1.8
423	50[d]	5.00	0.8
423	67[d]	4.60	2.3

[a] standard uncertainties are $u(T)$ = 0.01 K and $u(p) = 0.0025 \cdot p$

[b] no restriction tube used

[c] 50 µm i.d. x 50 mm long restriction tube used

[d] 50 µm i.d. x 100 mm long restriction tube used

Appendix 4D: Tabulated Results for Diffusion Coefficients of CO_2 in Cyclohexane

Diffusion coefficients D and standard deviations σ_D for CO_2 in cyclohexane at temperatures T and pressure p determined from at least 5 repeated injections. [a]

T / K	p / MPa	D / (10^{-9} m^2·s^{-1})	$10^2\sigma_D$
298	1.1[b]	4.29	1.0
298	10[c]	4.02	0.7
298	31[d]	3.57	0.6
323	1.0[b]	5.93	0.4
323	10[c]	5.61	0.6
323	31[d]	4.94	0.9
323	49[e]	4.35	4.4
348	1.1[b]	7.84	1.0
348	10[c]	7.40	0.3
348	30[d]	6.58	0.4
348	48[e]	5.90	0.4
348	65[f]	5.27	0.8
373	1.1[b]	10.0	0.9
373	10[c]	9.45	0.5
373	30[d]	8.4	0.2
373	49[e]	7.41	1.8
373	68[f]	6.69	0.4
398	1.1[b]	12.4	0.7
398	10[c]	11.7	0.3
398	30[d]	10.4	0.3
398	47[e]	9.16	1.8
398	65[f]	8.36	0.5
423	1.1[b]	14.9	1.0
423	10[c]	14.2	0.4
423	30[d]	12.4	1.3
423	47[e]	11.60	1.3
423	68[f]	10.0	2.9

[a] standard uncertainties are $u(T) = 0.01$ K and $u(p) = 0.0025 \cdot p$

[b] 50 µm i.d. x 50 mm long restriction tube used

[c] 25 µm i.d. x 50 mm long restriction tube used

[d] 25 µm i.d. x 150 mm long restriction tube used

[e] 25 µm i.d. x 200 mm long restriction tube used

[f] 25 µm i.d. x 500 mm long restriction tube used

Appendix 4E: Tabulated Results for Diffusion Coefficients of CO_2 in Toluene

Diffusion coefficients D and standard deviations σ_D for CO_2 in toluene at temperatures T and pressure p determined from at least 5 repeated injections. [a]

T / K	p / MPa	D / (10^{-9} m^2·s^{-1})	$10^2\sigma_D$
298	1.0[b]	5.53	1.1
298	11[c]	5.09	0.7
298	30[d]	4.77	0.6
298	48[e]	4.28	0.4
298	68[e]	3.92	0.6
323	1.0[b]	7.28	0.8
323	10[c]	6.78	0.7
323	30[d]	6.32	0.6
323	49[e]	5.70	0.4
323	66[e]	5.17	0.2
348	1.0[b]	9.26	0.7
348	11[c]	8.62	0.5
348	30[d]	8.02	0.2
348	48[e]	7.31	0.5
348	67[e]	6.54	0.5
373	1.0[b]	11.4	0.7
373	10[c]	10.4	0.6
373	30[d]	9.81	0.7
373	51[e]	8.94	0.8
373	67[e]	8.00	0.8
398	1.0[b]	13.8	1.0
398	10[c]	12.4	4.3
398	30[d]	11.7	0.5
398	48[e]	10.5	0.8
398	68[e]	9.6	0.8
423	1.1[b]	16.0	0.4
423	10[c]	15.0	0.4
423	30[d]	14.0	0.6
423	50[e]	12.3	0.5
423	67[e]	11.4	0.4

[a] standard uncertainties are $u(T)$ = 0.01 K and $u(p) = 0.0025 \cdot p$

[b] 50 µm i.d. x 50 mm long restriction tube used

[c] 25 µm i.d. x 150 mm long restriction tube used

[d] 25 µm i.d. x 200 mm long restriction tube used

[e] 25 µm i.d. x 500 mm long restriction tube used

Appendix 5: Tabulated Coefficients for Correlations of CO_2 Diffusion Coefficients

Stokes-Einstein Model:

The diffusion coefficient of CO_2 or N_2 in an aqueous solvent can be determined from;

$$D = kT \Big/ 4\pi \left\{ a_{298\mathrm{K}} \left(1 + \alpha_s \left(T/\mathrm{K} - 298 \right) \right) \right\} \eta$$

For CO_2 in hydrocarbons;

$$D = kT \Big/ 4\pi \left(\alpha_s \rho_m + c \right) \eta$$

$$\alpha_s = \sum_{i=0}^{2} A_i \left(T/K \right)^i$$

$$c = \sum_{i=0}^{2} C_i \left(T/K \right)^i$$

Coefficients for the correlation of the hydrodynamic radius of CO_2/N_2 in various solvents.

				CO_2			N_2
	H_2O	*n*-C_7H_{16}	*n*-$C_{16}H_{34}$	$C_{30}H_{74}$	C_6H_{12}	C_7H_8	H_2O
$a_{298\ \mathrm{K}}$ / nm	0.168						0.190
α_a	0.0020						0.0022
A_0		-0.0625	-0.0764	-20.32	-0.0438	-0.0334	
A_1				0.0941			
A_2				-1.11×10^{-4}			
C_0		0.5416	0.3073	42.06	0.4846	0.4222	
C_1				-0.1953			
C_2				2.31×10^{-4}			

O

Fitted Rough-Hard Sphere Parameters:

$$D = \beta\left(V - bV_0\right)\sqrt{T} \div \frac{2\left(V_0^T + V_{0,CO_2}^T\right) - \left(V_0^{298K} + V_{0,CO_2}^{298K}\right)}{\left(V_0^{298K} + V_{0,CO_2}^{298K}\right)}$$

	n-C_7H_{16}	n-$C_{16}H_{34}$	$C_{30}H_{74}$	C_6H_{12}	C_7H_8
$10^{12}\cdot\beta$ / ($m^2\cdot s^{-1}\cdot K^{-0.5}\cdot m^{-3}\cdot mol$)	1.34	0.59	0.21	1.87	1.98
$10^{12}\cdot\beta^{\dagger}$ / ($m^2\cdot s^{-1}\cdot K^{-0.5}\cdot m^{-3}\cdot mol$)	1.96	0.83	0.43	2.55	2.58
$10^{12}\cdot\beta^{\dagger\dagger}$ / ($m^2\cdot s^{-1}\cdot K^{-0.5}\cdot m^{-3}\cdot mol$)	2.04	0.92	0.51	2.91	2.84
b	1.24	1.22	1.16	1.23	1.27
$b^{\dagger *}$	1.41	1.32	1.19	1.24	1.38
$10^3\cdot V_D^{\dagger}$ / ($m^3\cdot mol^{-1}$)	132	290	507	95.4	97.9
$10^3\cdot V_{0,298\,K}$ / ($m^3\cdot mol^{-1}$)	93.3	220	427	77.1	71.0

† M.A. Matthews, A. Akgerman, Hard-sphere theory for correlation of tracer diffusion of gases and liquids in alkanes, J. Chem. Phys. 87 (1987) 2285-2291.
†† M.A. Matthews, A. Akgerman, Diffusion Coefficients for Binary Alkane Mixtures to 573 K and 3.5 MPa, AIChE J. 33 (1987) 881-885.

As the literature sources provide correlations for V_D, i.e. bV_0, the values of V_D, provided by the correlations, were divided by the close-packed molar volume at 298 K, $V_{o,\,298\,K}$ to allow for comparison.

Appendix 6: Tabulated Results for TDA Tubing Dimensions

Section		Radius / mm		Length / m
Inlet	R_i	0.392	L_i	0.3
Column	R_c	0.541	L_c	4.518
Outlet	R_o	0.127	L_o	0.58
RID inlet path	R_d	0.224	L_d	0.39

Appendix 7: CO_2 Saturation Vessel

Figure 1: Pressure Vessel Lid

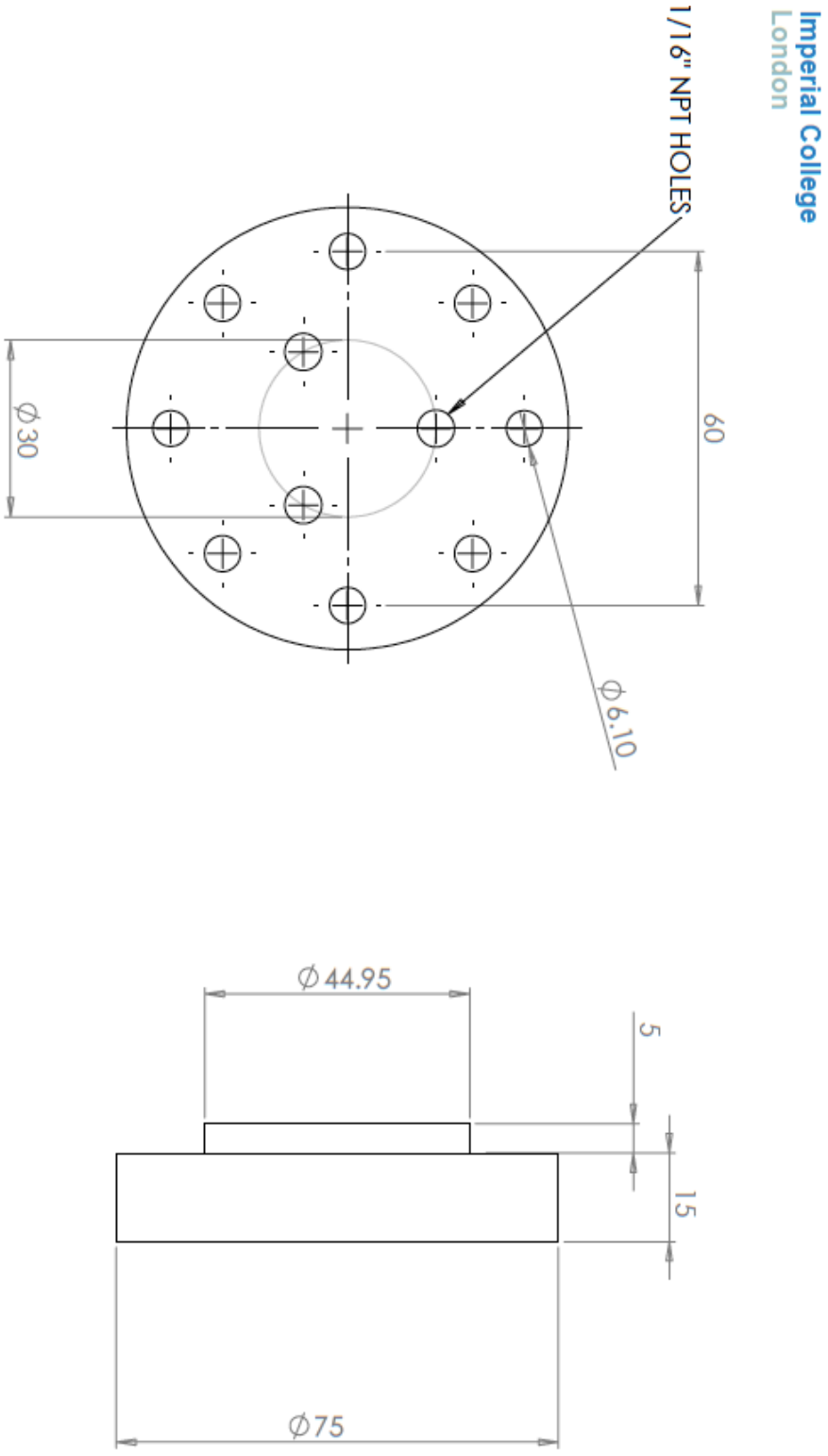

R

Figure 2: Pressure Vessel Body

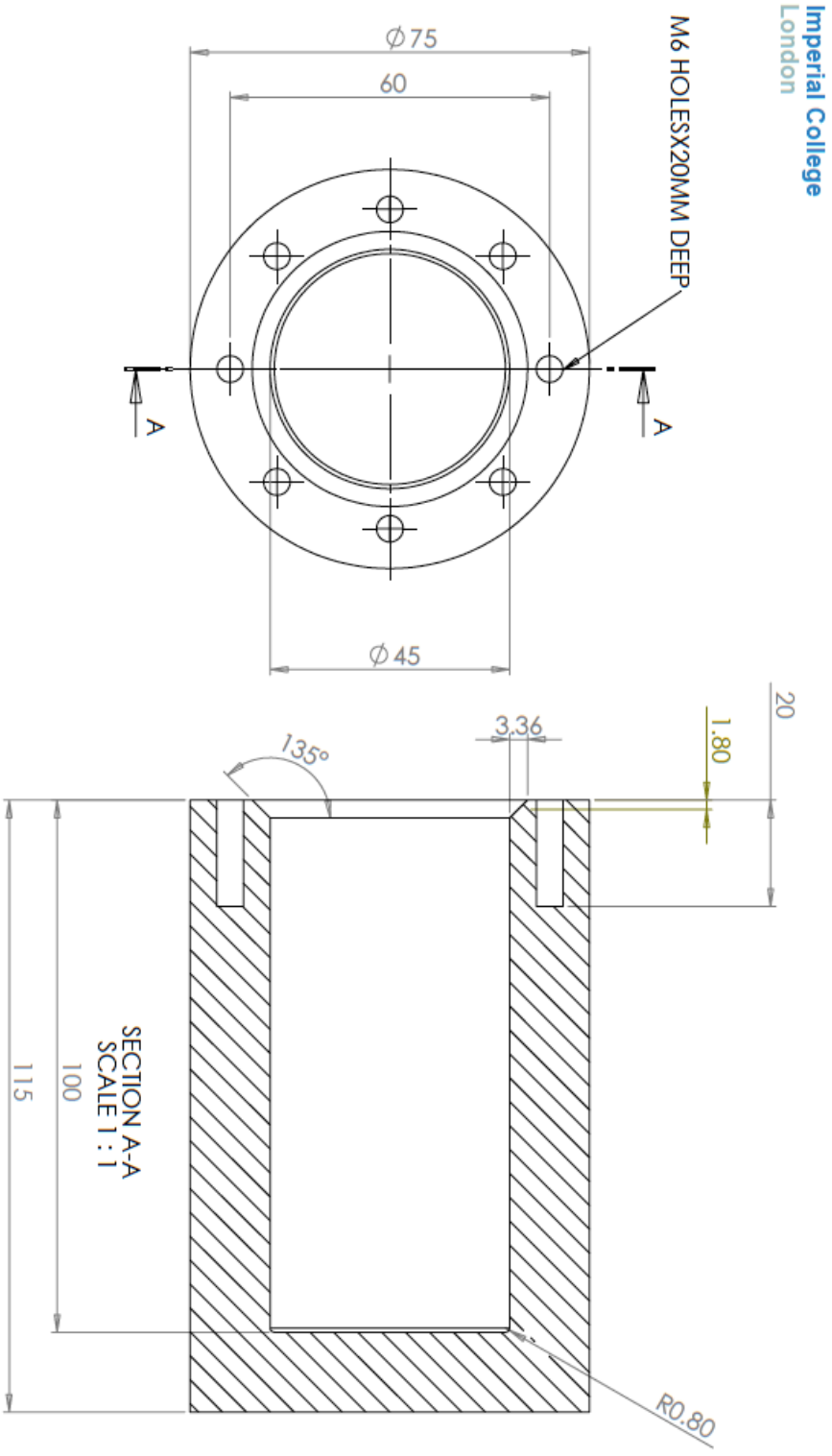

S